Doctoral Thesis ETH No. 16942

A Modular Approach to Functional Self-Assembled Monolayers

A dissertation submitted to the

SWISS FEDERAL INSTITUTE OF TECHNOLOGY ZURICH

for the degree of

Doctor of Sciences

presented by

Firat Durmaz

Dipl. Chemiker. ETH

born on April 6, 1974

citizen of Turkey

accepted on the recommendation of

Prof. Dr. Nicholas D. Spencer, examiner

Prof. Dr. A. Dieter Schlüter, co-examiner

Dr. Stefan Zürcher, co-examiner

Zürich, November 2006

For My Family

ANYTHING CAN BE MADE TO WORK IF YOU FIDDLE WITH IT LONG ENOUGH.

MURPHY'S LAW

Abstract

"Self-Assembled Monolayers" (SAMs) represent a type of structure that is using molecular self-assembly to build structure and function on the nanometer scale. Self-assembled monolayers, which have desired control on the molecular level, should be considered as a potential technique for the construction of more highly ordered materials. Monolayers on substrates formed by self-assembly technique can be used as surface modification, to adjust the physicochemical property of the outermost surface of a material.

The aim of this project is to demonstrate a modular approach to the synthesis of new functionalized molecules for self-assembly. In this way we can create a library of molecules which can be used to pass the desired chemical or physical properties to surfaces. In the same strategy, we include a reactive group that can be used to polymerize the molecules once they have self-assembled on the surface or in solution. This is intended to increase the final stability of the films by multi-site attachment and is expected to eliminate the two main disadvantages of the simple alkane phosph(on)ate SAMs, their inferior stability in aqueous solutions and the difficulty of introducing reactive functionalities for the attachment of biomolecules.

Starting from 3-bromophenol (**1**) and 12-iodododecylphosphonic acid (**12a**), compounds 12-(4-amino-3-vinylphenoxy)dodecylphosphonic acid (**14**) and 12-(4-acetamido-3-vinylphenoxy) dodecylphosphonic acid (**21**) were designed and new procedures have been developed. Polymerization and solvolysis of compound tert-butyl-4-(12-(diethoxyphosphoryl)dodecyloxy)-2-vinylphenylcarbamate (**16**) gave poly-2-ethyl-4-(12-phosphonododecyloxy)benzenaminium bromide (**26**). Copolymerization of **16** with styrene gave poly-(2-isopropyl-4-(12-phosphonododecyloxy)benzenaminium bromide)-co-styrene (**28**). All compounds were fully characterized by NMR spectroscopy, elemental analysis and when pos-

sible, melting points and molecular weight distribution were investigated for the polymers.

SAMs were prepared with the synthesized monomers and polymers. The substrates are dipped in a solution containing the adhesion promoter, until highly organized and densely packed molecular layers were formed on the substrate. The formation of SAM is driven by a strong interaction between the substrate and the anchoring group of the adhesion promoter, e.g. phosphonic acid and metal oxide surface.

The modified surfaces were characterized by variable angle spectroscopic ellipsometer (VASE), X-ray photoelectron spectroscopy (XPS), and Infrared spectroscopy (PM-IRRAS).

Zusammenfassung

Selbstorganisierende monomolekulare Schichten, sogenannte SAMs, können dazu verwendet werden die Struktur und Funktion einer Oberfläche im Nanometerbereich zu verändern. Wird der Aufbau auf der molekularen Ebene kontrolliert, können solche SAMs als mögliche Bausteine zur Herstellung von höhergeordneten Materialien dienen. Ausserdem können die physikochemischen Eigenschaften einer Oberfläche durch solche monomolekulare Schichten angepasst werden.

Dieses Projekt soll zeigen, dass es möglich ist mit einem modularen Ansatz funktionalisierte Moleküle zu synthetisieren. So kann eine systematische Zusammenstellung von Molekülen hergestellt werden, welche es ermöglicht die chemischen und physikalischen Eigenschaften der Oberfläche in der gewünschten Weise zu verändern. Mit demselben Ansatz soll eine reaktive Gruppe ins Molekül eingebaut werden, welche eine Polymerisation erlaubt, sobald sich die Moleküle auf der Oberfläche oder in Lösung angeordnet haben. Durch diese Polymerisation und das Verwenden von multiplen Bindungsstellen auf der Oberfläche wird die Stabilität des Films erhöht. Diese Modifikation sollte die zwei Hauptnachteile von einfachen Alkanphosphat-SAMs eliminieren, das heisst die verminderte Stabilität in wässriger Lösung und die Schwierigkeit reaktive Gruppen anzubringen, welche das Funktionalisieren mit Biomolekülen ermöglicht.

12-(4-amino-3-vinylphenoxy)dodecylphosphonic acid (**14**) und 12-(4-acetamido-3-vinylphenoxy) dodecylphosphonic acid (**21**) wurden ausgehend von 3-bromophenol (**1**) und 12-iodododecylphosphonic acid (**12a**) hergestellt, wobei neue Vorgehensweisen entwickelt werden mussten. Die Polymerisation und Solvolyse von tert-butyl-4-(12-(diethoxyphosphoryl)dodecyloxy)-2-vinylphenyl-carbamate (**16**) ergab die Verbindungen poly-2-ethyl-4-(12-phosphonododecyloxy)benzenaminium bromide (**26**). Durch die Copolymerisation von **16** mit Styrol entstand poly-(2-isopropyl-4-(12-

phosphonododecyloxy)benzenaminium bromide)-co-styrene (**28**). Alle Komponenten wurden mit NMR Spektroskopie und Elementaranalyse charakterisiert und wenn möglich wurden die Schmelzpunkte und Molekulargewichts-verteilungen bestimmt.

Die synthetisierten Monomere und Polymere wurden dazu verwendet selbstorganisierende Schichten herzustellen. Dazu wurden die Substrate in eine Lösung synthetisierter Moleküle getaucht bis organisierte und dichtgepackte monomolekulare Schichten entstanden. Die starke Wechselwirkung zwischen Substrat und Ankergruppe des synthetisierten Moleküls, in diesem Fall zwischen Metalloxid und Phosphonsäure, begünstigt dabei die Bildung des SAMs.

Alle modifizierten Oberflächen wurden mit Röntgenphotoemissions Spektroskopie (XPS), spektroskopischer Ellipsometrie (VASE) und Infrarot Spektroskopie (PM-IRRAS) charakterisiert.

Contents

Introduction and Scientific Background

1.1 Background of Self-Assembled Monolayers (SAMS)

1.1.1 Definition of Self-Assembly

An organized self-assembled monolayer (SAM) is a single layer of molecules on a substrate in which the molecules exhibit a high degree of orientation, molecular order and packing. There are two common methods for depositing such a monolayer, namely, Langmuir-Blodgett deposition and self-assembly technique.

The three different definitions of self-assembly are as follows:

1) In chemical solutions, self-assembly (also called Brownian assembly) results from the random motion of molecules and the affinity of their binding sites for one another. Also, it refers to the joining of complementary surfaces via nano-molecular interactions [1].

2) A method of integration in which the components spontaneously assemble, typically by bouncing around in a solution or gas phase until a stable structure of minimum energy is reached [2].

3) Self-assembly is the process by which a system of non-living chemical components has become a living, biological system [3].

These three definitions highlight the problem of defining self-assembly. Today, self-assembly is one of the most interesting topics in science, and governments are

investing enormous amounts of money into related projects. As the number of publications on SAMs is increasing tremendously (273 in 1996, 562 in 1998, 721 in 2000 and 946 in 2002), new applications are likely to be developed.

SAMs are ordered molecular assemblies formed by the spontaneous adsorption of an active surfactant on a solid surface from solution or a gas phase (Fig. 1.1). Here the surfactant consists of a surface active head-group, a spacer, usually with an alkyl group, and a reactive tail group. The assembly into these two-dimensional systems is produced by a spontaneous chemical reaction at the interface, as the system approaches equilibrium. The degree of order in these systems is largely determined by the alkyl chain length; SAMs prepared by using molecules with short alkyl chains (fewer than 10 carbons) apparently lack suffcient attractive interactions between alkyl chains to produce well-ordered monolayers [4]. Although there is a limitation in using long-chain molecules, SAMs of functionalized long-chain hydrocarbons are most frequently used as building blocks of supermolecular structures which show new functions that can not be exhibited by the isolated monomer. The interactions between subunits are non-covalent such as hydrogen bonds, electrostatic and van der Waals forces.

An appropriate choice of the building groups will contribute to the optimal design of the SAMs. Deposition of SAMs is done by either liquid-phase or vapor-phase deposition. Liquid-phase deposition is a very convenient, fast, and easy process. Vapor-phase deposition, on the other hand, requires a specially constructed reactor and gas flow lines, but can overcome the limitations of liquid-phase deposition, such as difficulty in the transport of reactive species, non-uniform distribution of reactants, and incomplete coverage of surfaces, but it is limited to volatile, low-molecular-weight adsorbates.

This simple process makes SAMs inherently manufacturable and thus technologically attractive for surface engineering and the building of superlattices. One advantage of using SAMs is that the alkane chain length can also be easily modified, thus creating films of variable thickness. Longer alkane chains with methyl or trifloromethyl end groups will have greater dispersion interactions than shorter chains, thus leading to a lower free energy and a more ordered monolayer [6].
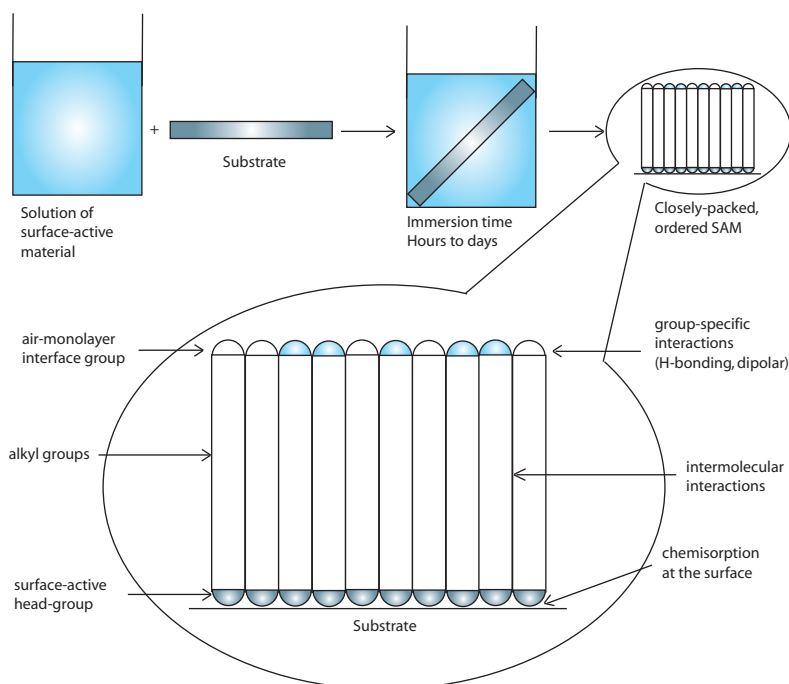
Figure 1.1: Self-assembled monolayers are formed by simply immersing a substrate into a solution of the surface-active compound. The driving force for the spontaneous formation of the 2D assembly includes chemical bond formation of molecules with the surface and intermolecular interactions [5].

1.1.2   History of Self-Assembly

In the past decade, self-assembled monolayers (SAMs) have been extensively studied due to their well-defined structures that can be fabricated by a simple dipping process [5]. These organized, surface-confined monolayers are commonly used to impart the desired chemical or physical properties to surfaces.

It is interesting to comment on the modest beginning of self assembly and on important milestones. The field really has begun much earlier than is often recognized. In 1946, Zisman and his coworkers published the preparation of a monomolecular layer by adsorption (self-assembly) of a surfactant onto a clean metal surface [7]. At that time, the potential of self assembly was not recognized, and this publication initiated only a limited level of interest. In the late 1970s Sagiv [8] successfully adsorbed trichlorosilanes onto silicon oxide. Nuzzo & Allara [9] showed in the early 1980s that thiols on gold SAMs can be prepared by the adsorption of di-n-alkyl disulfides from dilute solutions, which were to become the most popular SAM system and brought SAMs into the popular scientific consciousness. Interest in these monolayer films has tremendously increased since that time, and the development

and application of surface-sensitive experimental techniques (e.g. scanning probe microscopy, and infrared spectroscopy and X-ray photoelectron spectroscopy) have resulted in an improved understanding of the film structure and growth process. Ulman's book [10] serves as a useful introduction to SAMs and thin organic films in general.

1.1.3 Ultrathin Films; Langmuir-Blodgett versus SAM Techniques

Studies of monolayers have been motivated by their relevance to a variety of heterogeneous phenomena including solid-state microelectronics, electrochemistry, catalysis and biology. One route to the preparation of such structures is via the classical Langmuir-Blodgett monolayer transfer technique [11] [12]. The area of Langmuir-Blodgett films, monolayer structures transferred from a water surface to a substrate has received a great deal of attention [13]. These films are effective for study because of the simple manner in which a single monolayer or multilayers can be deposited. This powerful approach unfortunately suffers from several drawbacks, most important being the requirement for planar substrates, the sensitivity to environmental contaminants and the large number of mechanical manipulations required to produce complex structures. These problems arise from the fact that LB films are metastable structures and prepared via transfer of preassembled monolayers to the substrate [11]. Sagiv and coworkers have demonstrated that the adsorption of a stable monolayer, followed by alternate chemical activation and adsorption steps, can yield organized multilayer structures without the need of monolayer transfer techniques. Unfortunately, the α-chlorosilane-ω-alkene system, which they chose to illustrate this concept, does not permit stacking of more than 2-3 layers before structural defects occur in the film [14].

There are two main aims in the preparation of organic thin layers on solid surfaces. One is the modification of the surface properties of the solids. Physicochemical properties, such as the stability and wettability of solid surfaces, can be altered by the adsorption of ultrathin organic layers. Both modified and unmodified surfaces provide new paths for chemical reactions and selective guest binding. The other aim is the construction of novel supramolecular assemblies on solid surfaces. The distribution, orientation and diffusion of adsorbed species on solid surfaces have

been controlled by the interactions between the surface of inorganic solids and the adsorbed species, the intermolecular interactions between adsorbed species, and the presence of co-adsorbed species. Consequently, novel controlled microstructures can be achieved by the choice of host (solid surface) and guest species. The reactions of adsorbed species at solid surfaces can often generate desirable features that are not available in homogeneous media.

Typical LB films are prepared by transferring monolayers of amphiphilic molecules at the air-water interface onto solid substrates. The amphiphilic molecule is a molecule with one end that is hydrophilic, and, therefore, is preferentially immersed in water, and the other end that is hydrophobic, and preferentially resides in air (or in the nonpolar solvent). The amphiphilic molecules are first dissolved in an organic solvent that is immiscible with water, spread on the water surface, and compressed by decreasing the area in which the molecules are confined, to form a monolayer at the air-water interface, at the same time as the solvent evaporates. Then the monolayer is transferred onto a solid substrate, either by dipping the substrate through the interface or by touching it to the interface. The procedure can be used to obtain ultrathin films with the structure and thickness (monolayer or multilayer) controlled at molecular level. Three possible structures produced by LB technique are shown in Fig. 1.2.
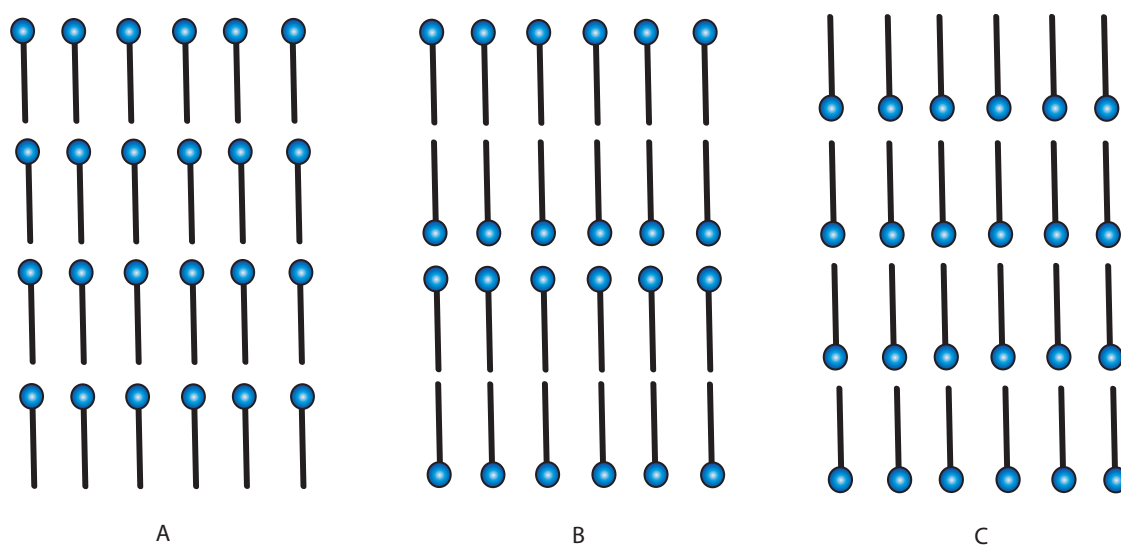
Figure 1.2: A, B and C- mode in Langmuir-Blodgett film deposition.

1.2 Substrates for SAMs

SAMs provide a convenient, flexible and simple system with which to tailor the interfacial properties of metals, metal oxides and semiconductors. The molecules that form SAMs have a chemical functionality, or headgroup, with a specific affinity for a substrate, the headgroup has a high affinity for the surface and displaces adsorbed organic materials from the surface. There are a number of headgroups that bind to specific metals and metal oxides (Table 1).

1.3 Investigated SAM Systems

Many studies have been carried out to clarify the monolayer structures using various surface probes such as X-ray photoelectron spectroscopy [43], grazing incidence infrared reflection absorption spectroscopy (IR-RAS) [44], ellipsometry [45], surface plasmon resonance spectroscopy (SPR) [46], or atomic force microscopy (AFM) [6].

The monolayer self-assembly technique is based on a reasonable choice of both the adsorption chemistry and the molecular shape of the adsorbate. By choosing an adsorption chemistry, which is selective but stable, a large variety of functional groups can be incorporated into the adsorbed molecule without disrupting the expected connectivity with the substrate. By choosing an appropriate set of molecular shapes, dense crystalline-like packings can be achieved. In favorable cases, one can achieve a unique and well-defined monolayer structure. Today, monolayer self-assembly chemistries include thiols [47], disulfides [48] and sulfides [48] on gold; fatty acids [49] and phosph(on)ates on metal oxides [50]; silanes on silicon dioxide [51] and hydroxy functionalized surfaces [52]; and isonitriles on platinum [53]. Many more are certainly possible, such as the recently published catechol derivative anachelin on TiO_2 surfaces [54].

1.3.1 Thiols, Sulfides, Disulfides

In the self-assembly method, alkanethiols, $SH(CH_2)_nX$, usually in the form of thiols, disulfides, or sulfides are spontaneously assembled onto gold or other precious metals upon exposure of the metal surface. Solution adsorption of sulfides onto zerovalent gold substrates are preferred because of their inertness toward corrosion or oxidation.

Table 1.1: Combinations of headgroups and substrates used in forming SAMs on metals and metal oxides [15]

Amphiphiles	Substrates	References [15]
ROH	Fe_xO_y	[16]
	Si-H	[17]
	Si	[18]
$RCOO^-$/RCOOH	α-Al_2O_3	[19]
	Fe_xO_y	[20]
	Ni	[21]
	Ti/TiO_2	[22]
RCOO-OOCR	Si(111):H	[23]
	Si(100):H	[23]
RNH_2	FeS_2	[24]
	Mica	[25]
	Stainless Steel	[26]
RCN	Ag	[27]
	Au	[27]
RNC	Pt	[28]
RSH	Au	[29]
	Stainless Steel	[26]
RSR	Au	[30]
RSSR	Au	[9]
R_3P	Au	[31]
R_3P=O	Co	[32]
$RPO_3{}^{2-}$/RP(O)(OH)$_2$	Al	[33]
	Indium tin oxide	[34]
	Mica	[35]
	TiO_2	[36]
	ZrO_2	[37]
$RPO_4{}^{2-}$/RPO_4H_2	Al	[38]
	Nb_2O_3	[38]
	Ta_2O_3	[4]
$RSiX_3$ X = H, Cl, OCH_2CH_3	HfO_2	[39]
	Indium tin oxide	[40]
	PtO	[41]
	TiO_2	[39]
	ZrO_2	[42]

Such SAMs can be simply prepared that are highly stable, densely packed and ordered.

These SAMs remain the most popular system despite being limited to noble metals. The selective binding of thiols to gold, as well as the absence of a stable gold oxide surface layer, allows for the incorporation of a wide range of functional groups (Fig. 1.3). The structure of a self-assembled monolayer depends on the morphology of the metal and characteristic of the molecules such as size, head- and tail-group.
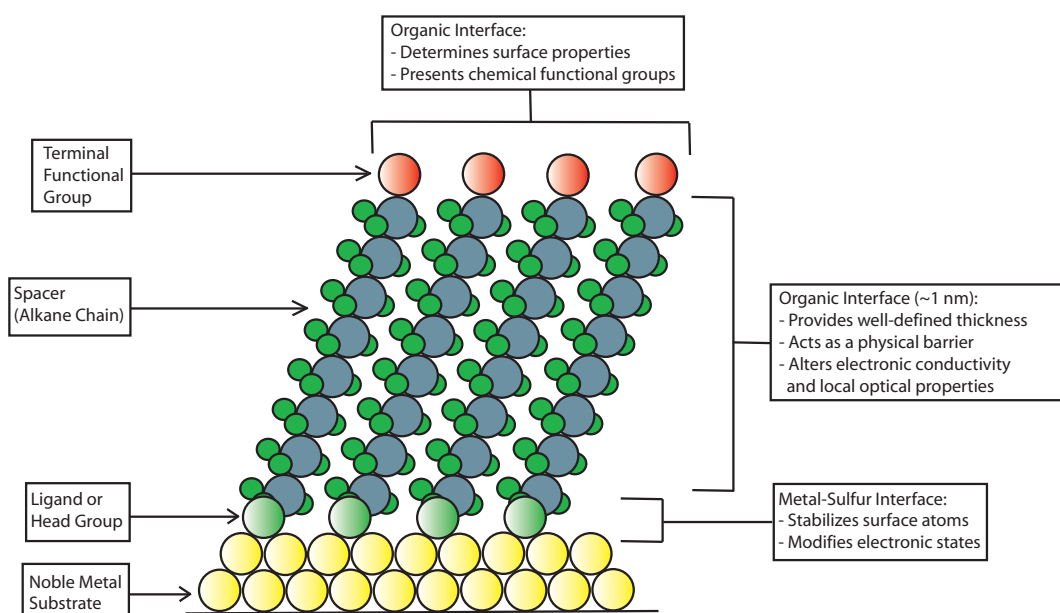
Figure 1.3: Schematic diagram of an ideal, single-crystalline SAM of alkanethiolates supported on a gold surface with a (111) texture.

1.3.2 Silanes

Trichlorosilanes are known for their excellent grafting to silica surfaces. Substrates such as Si/SiO_2 can react with trichlorosilanes resulting in a three-dimensional network of reactive Si-OH groups and Si-O-Si bonds. The organosilane derivatives $RSiX_3$, R_2SiX_2 or R_3SiX, where X is a chloride or alkoxy group and R is an organic group that can carry different functionalities, are known to react with hydroxylated surfaces to form monolayers. In a typical procedure, a hydroxylated surface
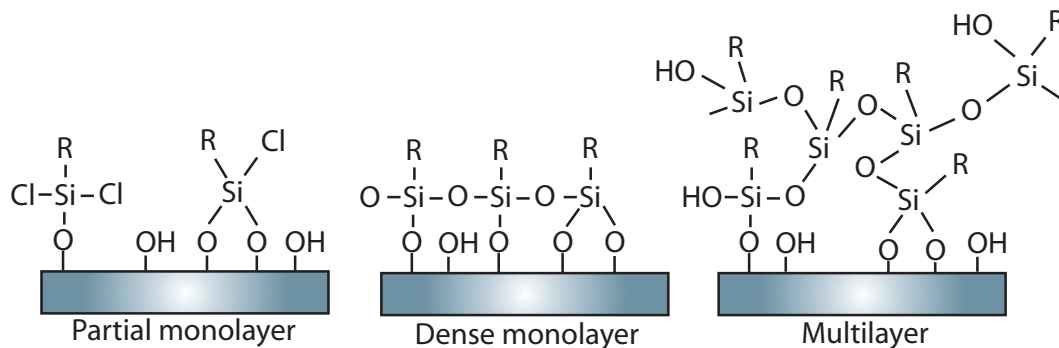
Figure 1.4: Schematic diagram of surface modification of an oxide surface by octadecyltrichlorosilane [56].

is introduced into a solution of alkyltrichlorosilane in an organic solvent. When alkyltrichlorosilane is used, Si-Cl bonds react with the OH groups present on the surface of the substrate to form a siloxane network.

Silane chemistry has also been used for covalent multilayer growth [55], but this chemistry can be difficult to control and it is susceptible to unwanted polymerization reactions, preventing the ability to create uniform, layered interfaces (Fig. 1.4).

1.3.3 General Overview of Phosphate and Phosphonate SAMs

As an important class of self-assembled organic molecules, phosphonic acids, are somewhat less often characterized compared to silanes and thiols, but are the becoming of great practical interest because of their ability to produce SAMs on a range of metal oxide surfaces [33].

Organophosphonates and organophosphates are structurally similar. An organophosphate has 4 oxygens with an alkyl group connected via a phosphoester bond. Phosphonates have 3 oxygens with a carbon attached directly to phosphorus (Fig. 1.5). The lack of a hydrolyzable P-O-C linkage makes phosphonate compounds more stable in aqueous solution and easier to make SAMs with than organophosphate compounds.
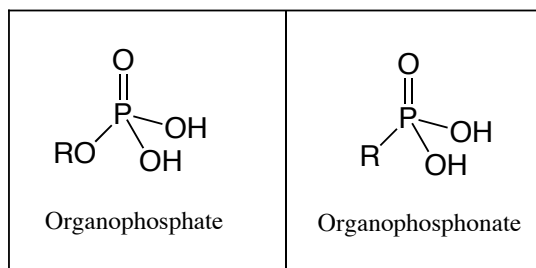
Scheme 1.1: Structure of organophosphate and phosphonate compounds.

The reaction of long-chain alkylphosphonic acids with metal oxide supports leads to dense, well-ordered SAMs [37] [57] [36] that can find applications in a wide range of fields such as catalysis, corrosion resistance, microelectronics, and chemical sensors [5].

Organophosphorus compounds have attracted interest as an alternative to organosilane compounds in the functionalization of inorganic surfaces due to their characteristic features such as a large number of available organophosphorus functional molecules and the difference in surface reaction mechanisms between phosphorus- and silane-compounds. Many metal oxides, including metal oxides of titanium, aluminum, iron, steel, and copper, have been used as a substrate organophosphorus compound-involved surface modification because they are not water sensitive [58]. The binding mode of organophosphorus molecules has been proposed to be mono-, bi-, and tridentate (Fig. 1.6) this being a property of both the surface and the nature of the organophosphorus compounds. Surface modification of TiO_2 with phosph(on)ates or phosphoric acids is an attractive topic because of the altered catalytic function of the transition metal oxide surface [59]. Phosphonates and phosphonic acids form SAMs on TiO_2 surfaces by the formation of Ti-O-P bonds. Textor et. al. [56] [60] [61] [62] have extensively studied alkyl phosphate-SAM formation on TiO_2, Ni_2O_5, Ta_2O_5 of alkyl phosphates. X-ray photoelectron spectroscopy (XPS) and time-of-flight secondary ion mass spectroscopy (TOF-SIMS) were employed to study the binding of alkyl phosphates to TiO_2.

Transition metal oxides such as tantalum oxide (Ta_2O_5), niobium oxide (Ni_2O_5), and titanium oxide (TiO_2), in particular, are known to interact strongly with phosph(on)ates and to form relatively stable interfacial bonds. Like thiol on gold, phosph(on)ate-metal oxide SAMs form monolayers with a "tail-up" orientation and a tilt angle of the hydrocarbon chains of about 30° with respect to the surface nor-
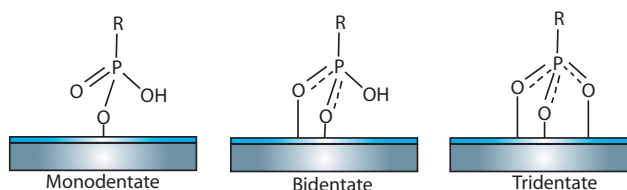
Figure 1.5: Different bonding modes of a phosphonate unit to a metal oxide surface [56].

mal [63] [64]. The use of organic solvents in the deposition process has three main disadvantages compared to water:

(1) Organic solvent molecules may be trapped within the adlayer and reduce the order of the SAMs.

(2) For the formation of mixed adlayer systems, it can be difficult to find an organic solvent that is suitable for both components.

(3) On an industrial scale, organic solvents are increasingly disfavored because of both environmental emission and disposal issues.

Moreover, for applications in areas such as medical devices and implants, the presence of even minor organic solvent residues in the adlayers cannot be tolerated, in view of potential cell-toxicity effects and other biological risks. On the other hand, SAMs, in particular of molecules with functional groups, are of great interest for the modification and functionalization of biomaterials and medical devices. Therefore, a technique based on the deposition of SAMs from aqueous alkyl phosphate solutions has been developed and successfully applied to a variety of metal oxide substrates [56]. Textor et. al. [56] [60] [61] [62] have studied alkyl phosphate-SAM formation on TiO_2 with an agressive solution of a dodecyl phosphate ammonium salt. They showed that self-assembly process from aqueous solution onto titanium oxide surface allows the wettability of the surface to be tailored, not only in the case of smooth surfaces but also for high-surface-area materials, such as a sandblasted and acid etched (SLA) dental implant surface.

Lightweight, strong titanium metal is of increasing importance in fields as diverse as aviation and aerospace [65], high-performance sports equipment [66], and medical implants [67] [68] [69]. Titanium metal readily surface oxidizes [70], but the native oxide coating is generally resistant to further chemical reaction, which makes coating with organics problematic. Alkanephosphonic acids are common coatings [71] for

native oxide surfaces of metals or alloys such as tin [72] [73], iron [74] [75], steel [73] [75], aluminum [75] or copper [76] [74] or for bulk oxides such as mica [77]. Indeed, even though phosphonic acids react strongly with ZrO_2 from hot solution, the comparable reaction with TiO_2 is poor [57]. Schwartz and co-workers have reported that self-assembly of alkanephosphonates on the native oxide surface of Ti can be effected by a simple procedure of aerosol deposition followed by solvent evaporation; subsequent warming gives a strongly surface-bound, ordered films of the alkanephosphonate species, which resist removal by solvent washing or mechanical peel testing [78].

The adsorption of octadecyl phosphate from organic solvent onto oxide surfaces of tantalum, titanium, niobium, and aluminum was studied with different surface analytical tools. The molecules were found to form densely packed SAMs if prepared from a heptane/2-propanol solution. The packing density is comparable to that of alkanethiols on gold, resulting in a similar inclination of the alkane chains from the surface normal. However the average size of regular two dimensional structures is smaller (< 2 nm x 2 nm) than those of thiols on polycrystalline gold (> 10 nm) due to the nanocrystalline to amorphous character of the oxide surface. Zwahlen et. al. [79] found that dodecyl phosphate adsorbed from aqueous solution formed self-assembled films of comparable quality to those of the longer octadecyl phosphate prepared from organic solvent and those of a similar thiol/gold systems.

Octadecyl phosphoric acid ester on metal oxide has been found by contact angle, optical waveguide lightmode spectroscopy (OWLS), near-edge X-ray absorption fine structure spectroscopy (NEXAFS) and X-ray photoelecrtron spectroscopy (XPS) measurements [4] to closely resemble those from the corresponding alkane thiol-gold systems, with respect to packing density, inclination and order. The system shows promise as an approach to functionalizing oxide surfaces with well-ordered organic layers with potential applications in the fields of biochemical analysis and sensors. Spencer and coworkers have described for the first time a self-assembly technique that employs alkyl phosphoric acid esters to produce dense, highly ordered monolayers in a "tails-up" configuration, on a Ta_2O_5 surface. Tantalum oxide was chosen because of its high refractive index, which makes it possible for application in a planar-waveguide-based bioaffinity sensor [80]. Upon appropriate ω-functionalization, alkanephosphate-based SAMs have the potential to be used as the interface that anchors active sensing elements or as the basis of passive, biomolecule-resistant regions on the sensor surface.

Textor et. al. [63] have focused on the structural chemistry at the phosphate oxide interface. By the help of three complementary surface analytical techniques (angle-dependent X-ray photoelectron spectroscopy, time-of-flight secondary ion mass spectroscopy, and atomic force microscopy in lateral force mode) they showed that a 2.2 nm thick "tails-up"-oriented adlayer is formed, which displays local near-hexagonal order, strong P-O-Ta bonding, and the presence of $(-P-O-)_2Ta$ species. They proposed a model for the binding and the structural organization of the octadecly phosphate molecules on the tantalum oxide surface involving direct coordination of the terminal phosphate head-group to Ta(V) cations forming a strong complexation bond, two types of bonding of the octadecyl phosphate with both monodentate and bidentate phosphate-Ta(V) coordinative interactions.

Hofer et. al. [56] have demostrated that both pure and mixed alkyl phosphates with different terminal functionalities can be deposited from aqueous solution by converting the free (water-insoluble) alkyl phosphoric acid into the corresponding water-soluble salts . They described two novel approaches to modifying metal oxide surfaces: use of aqueous solutions of alkane phosphates in the self-assembly process and the tailoring of surface wettability based on mixed alkane phosphate/hydroxy-terminated alkane phosphate SAMs. Mixed SAMs on metal oxide surfaces are of particular interest to the biosensor and biomaterial field, because they allow surface properties such as wettability, polarity, surface charge, and so forth to be tailored in a precise manner. Such surface tailoring may prove to be highly relevant for controlling the interaction between the SAM-modified surface and biological systems, such as proteins, antibodies, and cells.

Tosatti et. al. [60] continued with SAMs of dodecyl and hydroxy-dodecyl phosphates on both smooth and rough titanium and titanium oxide surfaces. They performed the deposition and characterization of monolayers of dodecyl and hydroxy-dodecyl phosphates and a mixture of the two from aqueous solutions of their ammonium salts onto three different substrates: titanium oxide and titanium metal films, deposited by physical vapor deposition onto glass and silicon substrates (serving as smooth, flat model surfaces), and a special titanium dental implant surface with a rough, highly corrugated surface. This study describes the physicochemical and structural properties of the single-component and mixed SAMs on titanium and tests the feasibility of using alkyl phosphate based SAMs to tailor the surface properties of titanium medical devices.

It is well established that thiols are strongly adsorbed on gold and silver, carboxylic acids adhere to aluminum oxide surfaces, and nitriles and amines bind to platinum [81]. There is very little reported in the literature about surfactants with phosphonate or phosphate headgroups as protecting agents. In one such piece of work, Maoz and Sagiv, reported that C_{18} phosphates form robust self-assembled monolayers on polar surfaces such as glass and ZnSe [55][75], unlike surfactants with -OH and -COOH terminal functional groups. Consequently, alkyl phosphates or phosphonates should be considered for applications where strong binding of organic molecules to surfaces is needed. As for the adsorption of phosphonates or phosphates ontp nanoparticle surfaces, the literature is extremely sparse. In one such work, Gedanken et. al. [82] studied the adsorption of alkanesulfonic and alkanephosphonic acids on the surface of amorphous ferric oxide particles and proposed two possible bonding schemes for the phosphonate ions on Fe^{3+}, i.e., one Oxygen or two Oxygen atoms of the phosphonate group binding onto the surface. The possibility of using alkyl phosphonate and phosphate surfactants as efficient binding ligands on metal oxide nanoparticle surfaces has motivated others; Sahoo et. al. [83] showed the surface derivatization of magnetite (Fe_3O_4) by oleic acid (OA), lauric acid (LA), dodeclyphosphonic acid (DDP), hexadecylphosphonic acid (HDP), and dihexadecyl phosphate (DHDP). They compare properties of carboxylic acid coated particles to colloidal nanoparticles coated with phosphonate or phosphate ligands. They found that alkyl phosph(on)ates could be used for obtaining thermodynamically stable dispersions of magnetic ferrite nanoparticles. The good biocompatibility of phosph(on)ate ligands may advance the utilization of encapsulated magnetic nanoparticles in medical applications such as magnetic resonance imaging and other biophysical purposes. Besides alkyl phosph(on)ates bind efficiently to iron oxide particle surfaces and can serve, in general, as potential alternatives to fatty acids as coating agents for oxide nanoparticles.

Zr Complex-Modified Surfaces, Multilayers

While alkanethiols on gold have been investigated extensively, the opportunity to form complex interfacial structures, e.g. multilayers, is limited unless specially functionalized molecules are used in the formation of the initial layer [44] [84] [85] [86]. For alkanethiols, terminal methyl groups effectively prevent chemical addition beyond the first layer so alternative chemistries that allow for the simple formation

of multiple layers had to be developed to avoid this problem. Metal-phosphonate chemistries have proven to be a remarkably effective and robust route to the formation of multilayer assemblies. Layered metal phosphonates are attractive materials for several reasons. Synthesis of the layered assemblies is simple, involving an immersion of a primed substrate into alternating metal ion and α, ω-biphosphonate solutions. The low solubility of the complex formed between phosphonates and several metal ions makes the structures especially robust, in contrast to Langmuir-Blodgett layers, which are characterized by weak interlayer associations. Zirconium phosphonate layered complexes are most common, but other metal ions like iron have been used as well [75] [87] [88]. The structures are built up one layer at a time with control over the specific molecular identity of each layer, which allows for a fine control over the chemical, electrical, or optical properties of each layer and, consequently, of the entire film.

Alkanethiols do not form strongly bound monolayers on native metal oxide surfaces [89] [90], and siloxanes can be unstable to hydrolysis under physiological conditions [91] [92]. Schwartz and co-workers have reported that self-assembled monolayers of phosphonates can be strongly bonded to Ti or Ti alloy surfaces via reaction of phosphonic acid with their native oxides [78] [92] [93], but attempts to make sterically controlled films of two different phosphonates on the same substrate have not been succesful, mixing of the precursor phosphonic acids on the surface is apparently faster than their bonding to that surface. They further reported that α, ω-diphosphonic acids can form hydrolytically stable, strongly bound films of the corresponding phosphonates directly on the native oxide surfaces of Ti and Ti-6Al-4V. These films can be activated in a way that is, in principle, accessible to patterning. This method gives a new type of compound interface between a surface and a biomolecule. In particular, they found that zirconium tetra-(tert-butoxide) can react rapidly with these films, either across the entire surface or at determined places by controlled deposition. These surface-bound alkoxides can be further derivatized to bind a biomolecule to the surface. Derivatized Zr complex-modified surfaces are hydrolytically stable, and they can retain the high mechanical shear strength of parent diphosphonate film-metal oxide surface interfaces [94].

Mallouk et al [95] [96] have reported a multilayer synthesis based on the sequential adsorption of components of ZDBP, $Zr(O_3PC_{10}H_{20}PO_3)$. They selected this compound because like many transition-metal phosphonates, it spontaneously

crystallizes as a layered compound when solutions of the appropriate metal salt and phosphonic acids are mixed.

When considering the possible structures that may result from a particular surfactant/substrate combination, it is useful to examine the bulk state analogues. A wide range of layered metal carboxyalkylphosphonates have been synthesized to investigate their potential use as ion exchangers, proton conductors, catalyst and host materials. Divalent metals such as Zn and Fe can form structures where the carbonyl group is connected to the metal center. In the case of tetravalent metals (Zr, Ti) only the phosphonic acid groups coordinate with the metal. The resulting lamellar $Zr[O_3P(CH_2)_nCO_2H]_2$ structures consist of planes of metal atoms linked together by phosphonate groups with the organic groups lying above and below the inorganic layer. The pendant acid groups form strong interlayer hydrogen bonds, associating as interlayer dimers. Interesting even/odd effects have been observed for the reactivity of $Zr[O_3P(CH_2)_nCO_2H]_2$ toward guest molecules which was attributed to changes in the orientation of pendant carboxylic acid groups with the numbers of methylene groups [97]. Given these results, it is not unreasonable to expect that carboxyalkylphosphonic acids will form carboxylic acid terminated surfaces on ZrO_2 and TiO_2 [37].

1.4 Applications of SAMs

Self-organized molecular monolayers at interfaces have been intensively studied in recent years for a variety of scientific and technological reasons [98]. Monolayers of insoluble amphiphiles deposited at the water/air interface, known as Langmuir monolayers (LMs), provide insight into fundamental issues of two-dimensional physics. They are also model systems for studies of structure and dynamics in membranes. SAMs represent a particular flexibility of surface modification and are believed to hold promise in a variety of technologies, including corrosion resistance, catalysis, prevention of bio-fouling, chemical sensing, and microelectronics [5]. Sophisticated surface analytical and structural techniques have led to a detailed understanding of molecular epitaxy and packing in SAMs, particularly in films composed of alkylthiols adsorbed on the Au(111) surface [99].

Self-assembly is one of the few practical strategies for making nanostructured ensembles. Therefore, the field of nanotechnology and robotics will benefit from

self-assembly. It is also common to find self-assembly in more dynamic systems such as smart materials and self-healing structures [3].

SAMs that resist the attachment of protein are being studied for a wide range of applications, from the reduction of biofilms on large ships to the prevention of the foreign body response on implants.

1.4.1 Corrosion Protection

The application of self-assembly for corrosion protection has been recently in the focus of interest. Self-assembling molecules with unique properties, e.g. formation of well-defined dense, ordered and stable layers, are capable to form protective layers with appropriate stability. The design of surface properties became possible in this way.

Although the self-assembling phenomenon is well known, care must be taken during application on commonly used structural metals. There is a significant impact of the structure and composition of the metal surface itself on the self-assembly. Oxide-free metal surfaces and metals covered with stable oxides provide favorable conditions for self-assembly [49]. Some problems arise when molecules are self-assembled on continuously changing surfaces or metals covered with unstable, porous oxides. In this later case, the inhomogenity and instability of the metal substrate result in a disordering of the adsorption layers. SAMs derived from the assembly of n-alkanethiols onto copper have been succesfuly applied for prevention of corrosion of the underlying copper in various conditions [51] [52] [50] [53]. Chemisorption of alkanethiols on a reduced iron surface has been shown to supress iron corrosion by hydrophobic film formation [100] [101]. Another field of application of the assembly process is in the replacement of chromating procedures on reactive metals such as aluminum. Chemical modification of aluminum [102] [103] and zinc [102] surfaces by self-assembled layers of alkanephosphonic and -phosphoric acids can improve the organic coating adhesion and corrosion protection. Self-assembling molecules with two reactive groups, one attached to the metal surface and the other connected to an organic coating, can inhibit electrochemical reactions at the interface and result in very stable bonds between the organic coating and the metal surface.

Corrosion testing of SAMs indicated a higher corrosion resistance for aluminum modified with SAMs of phosphonic acid compared to carboxylic acids. An inelastic

electron tunneling spectroscopy study of the adsorption and structure of alkyl phosphonic and alkyl phosphoric acids suggested that tridentate species were formed with aluminum oxide surfaces [103].

1.4.2   Friction Reduction

Aluminum-coated silicon substrates are commonly used for various micro/nanotechnological systems (MOEMS/NOEMS) including Digital Micromirror Devices (DMD). For efficient and failure proof operation of these devices, ultrathin lubricant films of self-assembled monolayers (SAMs) are increasingly being employed. Fluorinated molecules are known to exhibit a low surface energy, adhesion and friction, which is desirable for tribological applications. Hoffmann and co-workers [104] have investigated contact angle, surface energy, friction, adhesion and wear properties of a perfluoroalkylphosphonate SAM and compared them with those of alkylphosphonate SAMs on Al surfaces. They found that both fluorocarbon and hydrocarbon SAMs showed a reduction in adhesive force, friction force, and coefficient of friction as compared to bare Al. Perfluorophosphonic acid, which has the lowest surface energy, also exhibited a lower adhesive force than decyl- and octadecylphosphonic acid SAMs. At small normal loads, the friction force for fluorocarbon SAMs was lower than for their hydrocarbon counterparts. However, for high loads, the friction force was higher for fluorocarbon compared to hydrocarbon SAMs. From a tribological point of view, it is found that SAMs with compliant and long hydrocarbon backbone chains and those with fluorocarbon backbone chains show a highly desirable behaviour [105].

1.4.3   SAMs for Biomaterials

SAMs help in the development of new biomaterials. They serve as model surfaces for isolating biological interactions (such as cell signaling, cell adhesion, and protein interactions) on the molecular level. A primary advantage of SAMs is that changing as little as one atom of the terminal group can dramatically alter the macroscopic properties of the surface. Such surface properties include wettability, biocompatibility and protein/cellular adhesion.

The use of titanium and its alloys as biomaterials is increasing due to their relatively low modulus and good corrosion resistance [106] [107]. Also, titanium is

remarkably compatible with human tissue in comparison with other metals. Since the biological response to an implanted biomaterial is influenced by the surface properties of the materials at a molecular level [108] [109] [110], the interaction between an implant and its surrounding tissue can often be controlled by modifying the chemical and/or physical properties of the implant surface. This control is achieved in two stages, for example, electropolishing and anodic oxidation of the Ti45Nb alloy provide a surface with a uniform oxide layer that is the mixture of TiO_2 and Nb_2O_5 [111]. SAMs are useful for modifying surface chemistry and/or attaching molecules to surfaces. The SAMs provide chemically and structurally well-defined surfaces that can be manipulated using standard synthetic methodologies [112]. SAM attachment to a metal or alloy surface depends in large part on the composition and reactivity of the surface. It is therefore important to control the surface onto which a SAM will be attached with respect to its chemical composition and microstructure, as they will determine the quality of the SAM in terms of its stability, degree of coverage, and order.

Self-assembled monolayers are finding increasing use to tailor the molecular recognition properties of surfaces used in biosensing. Self-assembled monolayers have been used to control the properties of sensors on the basis of the quartz crystal microbalance [113], acoustic plate modes [114] and surface plasmon resonance [115]. Non-specific adsorption of protein is a common problem with these devices. Ligands immobilized on SAMs terminated in oligo(ethylene glycol) groups provide a route to generate biospecific surfaces with a high control over the properties of the surfaces [116].

High selectivity provided by biomolecules (antibodies, enzymes, nucleic acids) or biological systems (receptors, whole cells) is exploited in biosensors, in which a biological sensing element is integrated with an electrochemical, optical or piezo-electric transducer [117] [118]. Most commonly, the biological component (capture molecule) is immobilised on the surface of the transducer. As a consequence, immobilisation strategies for biomolecules are of importance in order to preserve their biological activity. At biological recognition, i.e. when the immobilised molecule and its ligand (analyte) interact, a signal is generated which is related to the concentration or amount of the analyte in the sample, or bound to the surface.

1.5   Scope of this Thesis

In the past 10 years, organophosphorus compounds have attracted growing interest due to their high affinity toward metal oxides. In our case TiO_2 was chosen because dodecyl phosphate and hydroxy-terminated dodecyl phosphate were shown to spontaneously assemble on smooth titanium oxide [56] and due to its importance related to applications in the fields of medical devices or optical biosensors.

In this work, the self-assembly technique has been used to fabricate monolayers. By using phosphonic acid ester derivatives in establishing monolayers is believed to have potential for designing specific interface architectures in sensor technology, for surface modification of oxide-passivated metallic biomaterials and for composite metal oxide-polymer interfaces.

Most of the SAMs studied so far use the sulfur-gold interaction. Since gold is not a preferred material for large-scale applications and/or transparent optical sensors, a self-assembling system for metal oxide substrates is favored. With this background in mind, this thesis aims at developing "A Modular Approach to Functional SAMs" that takes into account a polymerization on the substrate. A particular objective is to develop a synthetic scheme where we combine a polymerizable center piece with **11** and tail group. To achieve this, several synthetic steps had to be developed, optimized, adapted and finally combined in order to produce densely packed self-assembled monolayers.

The specific tasks comprising this research are as follows:

(1) Synthesis of functionalized alkyl phosphonates.

(2) Self-assembly of phosphonates on TiO_2.

(3) Polymerisation of SAMs on the substrate.

(4) Compare with assembled polymers from the same monomer.

At their fundamental level, living cells self-assemble. Thus, an understanding of the mechanisms behind self-assembly will help to understand life. Beyond this though, self-assembly has countless uses. Among the benefits of self-assembly are:

(1) huge numbers of components can be dealt with

(2) fabrication with (sub)atomic accuracy in the z-direction

(3) patterning a theoretical single molecule resolution

(4) low cost of fabrication

(5) generation of 3D structures is possible

Chapter 2 describes the various surface analytical methods and tools to clean and characterize the modified surface. These techniques include UV-cleaner, oxygen plasma cleaner, contact angle measurement, variable angle spectroscopic ellipsometer (VASE), X-ray photoelectron spectroscopy (XPS).

Chapter 3 describes the design of the adhesion promoter, the formation of the self-assembly monolayer and characterization of the self-assembly layer. 12-(4-amino-3-vinylphenoxy)dodecylphosphonic acid (**14**) respective (**22**), 12-(4-acetamido-3-vinylphenooxy)dodecylphosphonic acid (**21**), poly-2-ethyl-4-(12-phosphonododecyloxy)benzenaminium bromide (**26**) and poly-(2-isopropyl-4-(12-phosphonododecyloxy)benzenaminium bromide-co-styrene) (**28**) are designed as adhesion promoters. This involves the synthesis of compounds **14**, **21**, **26**, and **28**. The most challenging part of the project was to synthesize the above mentioned molecules in a pure form. Until now these compounds have not been described in the literature. Various new procedures have been developed to achieve the monomers and polymers.

Chapter 4 describes analytical methods to characterize synthesized molecules and preparation of surfaces for self-assembly. Synthesis protocols of compounds and characterization results are explained in the last part.

References

[1] http://www.nanotech-now.com/nanotechnology-glossary-S-U.htm.

[2] Gracias, D. H., Tien, J., Breen, T. L. and Hsu, C. Forming Electrical Networks in Three Dimensions by Self-Assembly. *Science*, **289**, 1170–1172, 2000.

[3] Grzybowski, B. A. and Whitesides, G. M. Dynamic aggregation of chiral spinners. *Science*, **295**, 2418–2421, 2002.

[4] Brovelli, D., Hahner, G., Ruiz, L., Hofer, R., Kraus, G., Waldner, A., Schlosser, J., Oroszlan, P., Ehrat, M. and Spencer, N. D. Highly oriented, self-assembled alkanephosphate monolayers on tantalum(V) oxide surfaces. *Langmuir*, **15**(13), 4324–4327, 1999.

[5] Ulman, A. Formation and structure of self-assembled monolayers. *Chemical Reviews*, **96**(4), 1533–1554, 1996.

[6] Schreiber, F. Structure and growth of self-assembling monolayers. *Progress in Surface Science*, **65**(5-8), 151–256, 2000.

[7] Bigelow, W. C., Pickett, D. L. and Zisman, W. A. Oleophobic Monolayers .1. Films Adsorbed from Solution in Non-Polar Liquids. *Journal of Colloid Science*, **1**(6), 513–538, 1946.

[8] Sagiv, J. and Polymeropoulos, E. E. Adsorbed Monolayers - Molecular-Organization and Electrical-Properties. *Berichte Der Bunsen-Gesellschaft-Physical Chemistry Chemical Physics*, **82**(9), 883–883, 1978.

[9] Nuzzo, R. G. and Allara, D. L. Adsorption of Bifunctional Organic Disulfides on Gold Surfaces. *Journal of the American Chemical Society*, **105**(13), 4481–4483, 1983.

[10] Ulman, A. *Organic Thin Films and Surfaces: Directions for the Nienties*, volume 20. Academic Press Boston, 1995.

[11] Blodgett, K. B. Films built by depositing successive monomolecular layers on a solid surface. *Journal of the American Chemical Society*, **57**(1), 1007–1022, 1935.

[12] Blodgett, K. B. Properties of built-up films of barium stearate. *Journal of Physical Chemistry*, **41**(7), 975–984, 1937.

[13] Roberts, G. G. An Applied Science Perspective of Langmuir-Blodgett Films. *Advances in Physics*, **34**(4), 475–512, 1985.

[14] Gun, J., Iscovici, R. and Sagiv, J. On the Formation and Structure of Self-Assembling Monolayers .2. a Comparative-Study of Langmuir-Blodgett and Adsorbed Films Using Ellipsometry and Ir Reflection Absorption-Spectroscopy. *Journal of Colloid and Interface Science*, **101**(1), 201–213, 1984.

[15] Love, J. C., Estroff, L. A., Kriebel, J. K., Nuzzo, R. G. and Whitesides, G. M. Self-assembled monolayers of thiolates on metals as a form of nanotechnology. *Chemical Reviews*, **105**(4), 1103–1169, 2005.

[16] Boal, A. K., Das, K., Gray, M. and Rotello, V. M. Monolayer exchange chemistry of gamma-Fe2O3 nanoparticles. *Chemistry of Materials*, **14**(6), 2628–2636, 2002.

[17] Zharnikov, M., Kuller, A., Shaporenko, A., Schmidt, E. and Eck, W. Aromatic self-assembled monolayers on hydrogenated silicon. *Langmuir*, **19**(11), 4682–4687, 2003.

[18] Niederhauser, T. L., Lua, Y. Y., Jiang, G. L., Davis, S. D., Matheson, R., Hess, D. A., Mowat, I. A. and Linford, M. R. Arrays of chemomechanically patterned patches of homogeneous and mixed monolayers of 1-alkenes and alcohols on single silicon surfaces. *Angewandte Chemie-International Edition*, **41**(13), 2353–2356, 2002.

[19] Taylor, C. E. and Schwartz, D. K. Octadecanoic acid self-assembled monolayer growth at sapphire surfaces. *Langmuir*, **19**(7), 2665–2672, 2003.

[20] Hyeon, T., Lee, S. S., Park, J., Chung, Y. and Bin Na, H. Synthesis of highly crystalline and monodisperse maghemite nanocrystallites without a size-selection process. *Journal of the American Chemical Society*, **123**(51), 12798–12801, 2001.

[21] Salem, A. K., Searson, P. C. and Leong, K. W. Multifunctional nanorods for gene delivery. *Nature Materials*, **2**(10), 668–671, 2003.

[22] Chen, H. G., Wu, X. D., Yu, Q. Q., Yang, S. R., Wang, D. P. and Shen, W. Z. Self-assembled monolayers of n-hexadecanoic acid and alpha-hydroxyl n-hexadecanoic acid on titanium surfaces. *Chinese Journal of Chemistry*, **20**(12), 1467–1471, 2002.

[23] Linford, M. R. and Chidsey, C. E. D. Alkyl Monolayers Covalently Bonded to Silicon Surfaces. *Journal of the American Chemical Society*, **115**(26), 12631–12632, 1993.

[24] Himmel, H. J., Kaschke, M., Harder, P. and Woll, C. Adsorption of organic monolayers on pyrite (FeS2)(100). *Thin Solid Films*, **285**, 275–280, 1996.

[25] Benitez, J. J., Kopta, S., Ogletree, D. F. and Salmeron, M. Preparation and characterization of self-assembled monolayers of octadecylamine on mica using hydrophobic solvents. *Langmuir*, **18**(16), 6096–6100, 2002.

[26] Ruan, C. M., Bayer, T., Meth, S. and Sukenik, C. N. Creation and characterization of n-alkylthiol and n-alkylamine self-assembled monolayers on 316L stainless steel. *Thin Solid Films*, **419**(1-2), 95–104, 2002.

[27] Frey, S., Shaporenko, A., Zharnikov, M., Harder, P. and Allara, D. L. Self-assembled monolayers of nitrile-functionalized alkanethiols on gold and silver substrates. *Journal of Physical Chemistry B*, **107**(31), 7716–7725, 2003.

[28] Hickman, J. J., Laibinis, P. E., Gardner, T. J., Whitesides, G. M. and Wrighton, M. S. Toward Orthogonal Self-Assembly of Redox Active Molecules on Pt and Au - Selective Reaction of Disulfide with Au and Isocyanide with Pt. *Langmuir*, **8**, 357–359, 1992.

[29] Malinsky, M. D., Kelly, K. L., Schatz, G. C. and Van Duyne, R. P. Chain length dependence and sensing capabilities of the localized surface plasmon resonance of silver nanoparticles chemically modified with alkanethiol self-assembled monolayers. *Journal of the American Chemical Society*, **123**(7), 1471–1482, 2001.

[30] Troughton, E. B., Bain, C. D., Whitesides, G. M., Nuzzo, R. G., Allara, D. L. and Porter, M. D. Monolayer Films Prepared by the Spontaneous Self-Assembly of Symmetrical and Unsymmetrical Dialkyl Sulfides from Solution onto Gold Substrates - Structure, Properties, and Reactivity of Constituent Functional-Groups. *Langmuir*, **4**(2), 365–385, 1988.

[31] Weare, W. W., Reed, S. M., Warner, M. G. and Hutchison, J. E. Improved synthesis of small (d(CORE) approximate to 1.5 nm) phosphine-stabilized gold nanoparticles. *Journal of the American Chemical Society*, **122**(51), 12890–12891, 2000.

[32] Puntes, V. F., Zanchet, D., Erdonmez, C. K. and Alivisatos, A. P. Synthesis of hcp-Co nanodisks. *Journal of the American Chemical Society*, **124**(43), 12874–12880, 2002.

[33] Pellerite, M. J., Dunbar, T. D., Boardman, L. D. and Wood, E. J. Effects of fluorination on self-assembled monolayer formation from alkanephosphonic acids on aluminum: Kinetics and structure. *Journal of Physical Chemistry B*, **107**(42), 11726–11736, 2003.

[34] Lewington, T. A., Alexander, M. R., Thompson, G. E. and McAlpine, E. Bodycote Prize Paper Characterisation of alkyl phosphonic acid monolayers self assembled on hydrated surface of aluminium. *Surface Engineering*, **18**(3), 228–232, 2002.

[35] Neves, B. R. A., Salmon, M. E., Russell, P. E. and Troughton, E. B. Spread coating of OPA on mica: From multilayers to self-assembled monolayers. *Langmuir*, **17**(26), 8193–8198, 2001.

[36] Helmy, R. and Fadeev, A. Y. Self-assembled monolayers supported on TiO2: Comparison of C18H37SiX3 (X = H, Cl, OCH3C18H37Si(CH3)2C1, and C18H37PO(OH)(2). *Langmuir*, **18**(23), 8924–8928, 2002.

[37] Pawsey, S., Yach, K. and Reven, L. Self-assembly of carboxyalkylphosphonic acids on metal oxide powders. *Langmuir*, **18**(13), 5205–5212, 2002.

[38] Hahner, G., Hofer, R. and Klingenfuss, I. Order and orientation in self-assembled long chain alkanephosphate monolayers adsorbed on metal oxide surfaces. *Langmuir*, **17**(22), 7047–7052, 2001.

[39] Fadeev, A. Y., Helmy, R. and Marcinko, S. Self-assembled monolayers of organosilicon hydrides supported on titanium, zirconium, and hafnium dioxides. *Langmuir*, **18**(20), 7521–7529, 2002.

[40] Koide, Y., Such, M. W., Basu, R., Evmenenko, G., Cui, J., Dutta, P., Hersam, M. C. and Marks, T. J. Hot microcontact printing for patterning ITO surfaces. Methodology, morphology, microstructure, and OLED charge injection barrier imaging. *Langmuir*, **19**(1), 86–93, 2003.

[41] Long, Y. T., Herrwerth, S., Eck, W. and Grunze, M. Synthesis and characterization of self-assembled monolayers based on redox-active silane compounds on platinum surfaces. *Physical Chemistry Chemical Physics*, **4**(3), 522–526, 2002.

[42] Marcinko, S., Helmy, R. and Fadeev, A. Y. Adsorption properties of SAMs supported on Tio(2) and ZrO2. *Langmuir*, **19**(7), 2752–2755, 2003.

[43] Ishida, T., Hara, M., Kojima, I., Tsuneda, S., Nishida, N., Sasabe, H. and Knoll, W. High resolution x-ray photoelectron spectroscopy measurements of octadecanethiol self-assembled monolayers on Au(111). *Langmuir*, **14**(8), 2092–2096, 1998.

[44] Nuzzo, R. G., Dubois, L. H. and Allara, D. L. Fundamental-Studies of Microscopic Wetting on Organic-Surfaces .1. Formation and Structural Characterization of a Self-Consistent Series of Polyfunctional Organic Monolayers. *Journal of the American Chemical Society*, **112**(2), 558–569, 1990.

[45] Bain, C. D., Troughton, E. B., Tao, Y. T., Evall, J., Whitesides, G. M. and Nuzzo, R. G. Formation of Monolayer Films by the Spontaneous Assembly of Organic Thiols from Solution onto Gold. *Journal of the American Chemical Society*, **111**(1), 321–335, 1989.

[46] Kajikawa, K., Hara, M., Sasabe, H. and Knoll, W. Exchange kinetics of alkanethiol self-assembled monolayers probed by attenuated total reflection with enhancement of surface plasmon resonance. *Japanese Journal of Applied Physics Part 2-Letters*, **36**(8B), L1116–L1119, 1997.

[47] Ginnai, T. M., Oxley, D. P. and Pritchard, R. G. Elastic and Inelastic Tunnelling in Single-Layer Langmuir Films. *Thin Solid Films*, **68**(1), 241–256, 1980.

[48] Vincett, P. S. and Roberts, G. G. Electrical and Photo-Electrical Transport-Properties of Langmuir-Blodgett Films and a Discussion of Possible Device Applications. *Thin Solid Films*, **68**(1), 135–171, 1980.

[49] Rohwerder, M. and Stratmann, M. Surface modification by ordered monolayers: New ways of protecting materials against corrosion. *Mrs Bulletin*, **24**(7), 43–47, 1999.

[50] Itoh, M., Ihara, M., Nishihara, H. and Aramaki, K. Corrosion Inhibition of Cobalt in Some Acid-Solutions by Bismuth(Iii) Chloride. *Journal of the Electrochemical Society*, **141**(2), 352–358, 1994.

[51] Laibinis, P. E. and Whitesides, G. M. Omega-Terminated Alkanethiolate Monolayers on Surfaces of Copper, Silver, and Gold Have Similar Wettabilities. *Journal of the American Chemical Society*, **114**(6), 1990–1995, 1992.

[52] Aramaki, K., Shimizu, K., Sakakibara, M. and Nishihara, H. Corrosion of Iron in Anhydrous Acetonitrile Solutions of Some Carboxylic-Acids. *Journal of the Electrochemical Society*, **140**(6), 1561–1567, 1993.

[53] Laibinis, P. E. and Jennings, G. K. Alkanethiol monolayers on atomically modified gold substrates. *Abstracts of Papers of the American Chemical Society*, **212**, 20–COLL, 1996.

[54] Zurcher, S., Wackerlin, D., Bethuel, Y., Malisova, B., Textor, M., Tosatti, S. and Gademann, K. Biomimetic surface modifications based on the cyanobacterial iron chelator anachelin. *Journal of the American Chemical Society*, **128**(4), 1064–1065, 2006.

[55] Maoz, R. and Sagiv, J. On the Formation and Structure of Self-Assembling Monolayers .1. a Comparative Atr-Wetability Study of Langmuir-Blodgett and Adsorbed Films on Flat Substrates and Glass Microbeads. *Journal of Colloid and Interface Science*, **100**(2), 465–496, 1984.

[56] Hofer, R., Textor, M. and Spencer, N. D. Alkyl phosphate monolayers, self-assembled from aqueous solution onto metal oxide surfaces. *Langmuir*, **17**(13), 4014–4020, 2001.

[57] Gao, W., Dickinson, L., Grozinger, C., Morin, F. G. and Reven, L. Self-assembled monolayers of alkylphosphonic acids on metal oxides. *Langmuir*, **12**(26), 6429–6435, 1996.

[58] Mutin, P. H., Guerrero, G. and Vioux, A. Hybrid materials from organophosphorus coupling molecules. *Journal of Materials Chemistry*, **15**(35-36), 3761–3768, 2005.

[59] Mutin, P. H., Lafond, V., Popa, A. F., Granier, M., Markey, L. and Dereux, A. Selective surface modification of SiO2-TiO2 supports with phosphonic acids. *Chemistry of Materials*, **16**(26), 5670–5675, 2004.

[60] Tosatti, S., Michel, R., Textor, M. and Spencer, N. D. Self-assembled monolayers of dodecyl and hydroxy-dodecyl phosphates on both smooth and rough titanium and titanium oxide surfaces. *Langmuir*, **18**(9), 3537–3548, 2002.

[61] Michel, R., Reviakine, I., Sutherland, D., Fokas, C., Csucs, G., Danuser, G., Spencer, N. D. and Textor, M. A novel approach to produce biologically relevant chemical patterns at the nanometer scale: Selective molecular assembly patterning combined with colloidal lithography. *Langmuir*, **18**(22), 8580–8586, 2002.

[62] Michel, R., Lussi, J. W., Csucs, G., Reviakine, I., Danuser, G., Ketterer, B., Hubbell, J. A., Textor, M. and Spencer, N. D. Selective molecular assembly patterning: A new approach to micro- and nanochemical patterning of surfaces for biological applications. *Langmuir*, **18**(8), 3281–3287, 2002.

[63] Textor, M., Ruiz, L., Hofer, R., Rossi, A., Feldman, K., Hahner, G. and Spencer, N. D. Structural chemistry of self-assembled monolayers of octadecylphosphoric acid on tantalum oxide surfaces. *Langmuir*, **16**(7), 3257–3271, 2000.

[64] Hofer, R. *Surface Modification for Optical Biosensor Applications.* PhD thesis, ETH Zurich, 2000.

[65] Chattopadhyay, A. A. and Zentner, A. A. Aerospace and Aircraft Coating. Technical report, 1990.

[66] Froes, F. H. Is the use of advanced materials in sports equipment unethical? *Jom-Journal of the Minerals Metals & Materials Society*, **49**(2), 15–19, 1997.

[67] Geissler, U., Hempel, U., Wolf, C., Scharnweber, D., Worch, H. and Wenzel, K. W. Collagen type I-coating of Ti6Al4V promotes adhesion of osteoblasts. *Journal of Biomedical Materials Research*, **51**(4), 752–760, 2000.

[68] Oji, M. O., Wood, J. V. and Downes, S. Effects of surface-treated cpTi and Ti6Al4V alloy on the initial attachment of human osteoblast cells. *Journal of Materials Science-Materials in Medicine*, **10**(12), 869–872, 1999.

[69] Anselme, K., Linez, P., Bigerelle, M., Le Maguer, D., Le Maguer, A., Hardouin, P., Hildebrand, H. F., Iost, A. and Leroy, J. M. The relative influence of the topography and chemistry of TiAl6V4 surfaces on osteoblastic cell behaviour. *Biomaterials*, **21**(15), 1567–1577, 2000.

[70] Lu, G., Bernasek, S. L. and Schwartz, J. Oxidation of a polycrystalline titanium surface by oxygen and water. *Surface Science*, **458**(1-3), 80–90, 2000.

[71] Fang, J. L., Wu, N. J., Wang, Z. W. and Li, Y. Xps, Aes and Raman Studies of an Antitarnish Film on Tin. *Corrosion*, **47**(3), 169–173, 1991.

[72] Hibi, T., Marikowa, H., Yamamoto, K., Idea, J. and Tatsumi, K. Daido Chemical Industry Co. Ltd. *Chem. Abst.*, **116**, 109915s, 1992.

[73] Kuznetsov, Y. I. and Raskolnikov, A. F. Inhibition of Iron Corrosion by Nitrilotrimethylphosphonate Complexes. *Protection of Metals*, **28**(2), 186–192, 1992.

[74] Gawalt, E. S., Lu, G., Bernasek, S. L. and Schwartz, J. Enhanced bonding of alkanephosphonic acids to oxidized titanium using surface-bound alkoxyzirconium complex interfaces. *Langmuir*, **15**(26), 8929–8933, 1999.

[75] G. A. Nitowski, L. F. Wiserman, K. W. *Chem. Abst.*, **121**, 20979w, 1994.

[76] Van Alsten, J. G. Self-assembled monolayers on engineering metals: Structure, derivatization, and utility. *Langmuir*, **15**(22), 7605–7614, 1999.

[77] Woodward, J. T. and Schwartz, D. K. In situ observation of self-assembled monolayer growth. *Journal of the American Chemical Society*, **118**(33), 7861–7862, 1996.

[78] Gawalt, E. S., Avaltroni, M. J., Koch, N. and Schwartz, J. Self-assembly and bonding of alkanephosphonic acids on the native oxide surface of titanium. *Langmuir*, **17**(19), 5736–5738, 2001.

[79] Zwahlen, M., Tosatti, S., Textor, M. and Hahner, G. Orientation in methyl- and hydroxyl-terminated self-assembled alkanephosphate monolayers on titanium oxide surfaces investigated with soft X-ray absorption. *Langmuir*, **18**(10), 3957–3962, 2002.

[80] Duveneck, G. L., Pawlak, M., Neuschafer, D., Bar, E., Budach, W. and Pieles, U. Novel bioaffinity sensors for trace analysis based on luminescence excitation by planar waveguides. *Sensors and Actuators B-Chemical*, **38**(1-3), 88–95, 1997.

[81] Colvin, V. L., Goldstein, A. N. and Alivisatos, A. P. Semiconductor Nanocrystals Covalently Bound to Metal-Surfaces with Self-Assembled Monolayers. *Journal of the American Chemical Society*, **114**(13), 5221–5230, 1992.

[82] Kataby, G., Cojocaru, M., Prozorov, R. and Gedanken, A. Coating carboxylic acids on amorphous iron nanoparticles. *Langmuir*, **15**(5), 1703–1708, 1999.

[83] Sahoo, Y., Pizem, H., Fried, T., Golodnitsky, D., Burstein, L., Sukenik, C. N. and Markovich, G. Alkyl phosphonate/phosphate coating on magnetite nanoparticles: A comparison with fatty acids. *Langmuir*, **17**(25), 7907–7911, 2001.

[84] Whitesides, G. M. and Laibinis, P. E. Wet Chemical Approaches to the Characterization of Organic-Surfaces - Self-Assembled Monolayers, Wetting, and the Physical Organic-Chemistry of the Solid Liquid Interface. *Langmuir*, **6**(1), 87–96, 1990.

[85] Frey, B. L., Hanken, D. G. and Corn, R. M. Vibrational Spectroscopic Studies of the Attachment Chemistry for Zirconium Phosphonate Multilayers at Gold and Germanium Surfaces. *Langmuir*, **9**(7), 1815–1820, 1993.

[86] Sun, L., Kepley, L. J. and Crooks, R. M. Molecular-Interactions between Organized, Surface-Confined Monolayers and Vapor-Phase Probe Molecules - Hydrogen-Bonding Interactions. *Langmuir*, **8**(9), 2101–2103, 1992.

[87] Neff, G. A., Mahon, T. M. and Abshere, C. J. *Mater. Res. Symp. Proc.*, **435**, 661, 1996.

[88] Feldheim, D. L. and Mallouk, T. E. Layer-by-layer assembly and intercalation reactions of iron(III) and iron(II) alkanebisphosphonates on gold surfaces. *Chemical Communications*, **x**(22), 2591–2592, 1996.

[89] Laibinis, P. E., Hickman, J. J., Wrighton, M. S. and Whitesides, G. M. Orthogonal Self-Assembled Monolayers - Alkanethiols on Gold and Alkane Carboxylic-Acids on Alumina. *Science*, **245**(4920), 845–847, 1989.

[90] Gardner, T. J., Frisbie, C. D. and Wrighton, M. S. Systems for Orthogonal Self-Assembly of Electroactive Monolayers on Au and Ito - an Approach to Molecular Electronics. *Journal of the American Chemical Society*, **117**(26), 6927–6933, 1995.

[91] Xiao, S. J., Textor, M., Spencer, N. D. and Sigrist, H. Covalent attachment of cell-adhesive, (Arg-Gly-Asp)-containing peptides to titanium surfaces. *Langmuir*, **14**(19), 5507–5516, 1998.

[92] Gawalt, E. S., Avaltroni, M. J., Danahy, M. P., Silverman, B. M., Hanson, E. L., Midwood, K. S., Schwarzbauer, J. E. and Schwartz, J. Bonding organics to Ti alloys: Facilitating human osteoblast attachment and spreading on surgical implant materials. *Langmuir*, **19**(1), 200–204, 2003.

[93] Schwartz, J., Avaltroni, M. J., Danahy, M. P., Silverman, B. M., Hanson, E. L., Schwarzbauer, J. E., Midwood, K. S. and Gawalt, E. S. Cell attachment and spreading on metal implant materials. *Materials Science & Engineering C-Biomimetic and Supramolecular Systems*, **23**(3), 395–400, 2003.

[94] Danahy, M. P., Avaltroni, M. J., Midwood, K. S., Schwarzbauer, J. E. and Schwartz, J. Self-assembled monolayers of alpha,omega-diphosphonic acids on Ti enable complete or spatially controlled surface derivatization. *Langmuir*, **20**(13), 5333–5337, 2004.

[95] Lee, H., Kepley, L. J., Hong, H. G., Akhter, S. and Mallouk, T. E. Adsorption of Ordered Zirconium Phosphonate Multilayer Films on Silicon and Gold Surfaces. *Journal of Physical Chemistry*, **92**(9), 2597–2601, 1988.

[96] Lee, H., Kepley, L. J., Hong, H. G. and Mallouk, T. E. Inorganic Analogs of Langmuir-Blodgett Films - Adsorption of Ordered Zirconium 1,10-Decanebisphosphonate Multilayers on Silicon Surfaces. *Journal of the American Chemical Society*, **110**(2), 618–620, 1988.

[97] Burwell, D. A., Valentine, K. G. and Thompson, M. E. P-31 and C-13 Chemical-Shift Tensors in Zirconium Phosphonates. *Journal of Magnetic Resonance*, **97**(3), 498–510, 1992.

[98] Tredgold, R. H. Cambridge University Press, Cambridge, 1994.

[99] Poirier, G. E. Characterization of organosulfur molecular monolayers on Au(111) using scanning tunneling microscopy. *Chemical Reviews*, **97**(4), 1117–1127, 1997.

[100] Volmeruebing, M., Reynders, B. and Stratmann, M. Binding Behavior of Organic Monomers on Iron Surfaces and Corrosion of the Resultant Chemically Modified Surfaces. *Werkstoffe Und Korrosion-Materials and Corrosion*, **42**(1), 19–34, 1991.

[101] Nozawa, K., Nishihara, H. and Aramaki, K. Chemical modification of alkanethiol monolayers for protecting iron against corrosion. *Corrosion Science*, **39**(9), 1625–1639, 1997.

[102] Stratmann, M., Feser, R. and Leng, A. Corrosion Protection by Organic Films. *Electrochimica Acta*, **39**(8-9), 1207–1214, 1994.

[103] Maege, I., Jaehne, E., Henke, A., Adler, H. J. P., Bram, C., Jung, C. and Stratmann, M. Self-assembling adhesion promoters for corrosion resistant metal polymer interfaces. *Progress in Organic Coatings*, **34**(1-4), 1–12, 1998.

[104] Bhushan, B., Cichomski, M., Hoque, E., DeRose, J. A., Hoffmann, P. and Mathieu, H. J. Nanotribological characterization of perfluoroalkylphosphonate self-assembled monolayers deposited on aluminum-coated silicon substrates. *Microsystem Technologies-Micro-and Nanosystems-Information Storage and Processing Systems*, **12**(6), 588–596, 2006.

[105] Chen, Y. X., Liu, W. M., Ye, C. F., Yu, L. G. and Qi, S. K. Preparation and characterization of self-assembled alkanephosphate monolayers on glass substrate coated with nano- TiO2 thin film. *Materials Research Bulletin*, **36**(15), 2605–2612, 2001.

[106] Rosenberg, R., Starosvetsky, D. and Gotman, I. Surface modification of a low modulus Ti-Nb alloy for use in medical implants. *Journal of Materials Science Letters*, **22**(1), 29–32, 2003.

[107] Godley, R., Starosvetsky, D. and Gotman, I. Bonelike apatite formation on niobium metal treated in aqueous NaOH. *Journal of Materials Science-Materials in Medicine*, **15**(10), 1073–1077, 2004.

[108] Kasemo, B. Biocompatibility of Titanium Implants - Surface Science Aspects. *Journal of Prosthetic Dentistry*, **49**(6), 832–837, 1983.

[109] Ratner, B. D. Surface Characterization of Biomaterials by Electron-Spectroscopy for Chemical-Analysis. *Annals of Biomedical Engineering*, **11**(3-4), 313–336, 1983.

[110] Gristina, A. G. Biomaterial-Centered Infection - Microbial Adhesion Versus Tissue Integration. *Science*, **237**(4822), 1588–1595, 1987.

[111] Zorn, G., Gotman, I., Gutmanas, E. Y., Adadi, R., Salitra, G. and Sukenik, C. N. Surface modification of Ti45Nb alloy with an alkylphosphonic acid self-assembled monolayer. *Chemistry of Materials*, **17**(16), 4218–4226, 2005.

[112] Balachander, N. and Sukenik, C. N. Monolayer Transformation by Nucleophilic-Substitution - Applications to the Creation of New Monolayer Assemblies. *Langmuir*, **6**(11), 1621–1627, 1990.

[113] Ward, M. D. and Buttry, D. A. Insitu Interfacial Mass Detection with Piezoelectric Transducers. *Science*, **249**(4972), 1000–1007, 1990.

[114] Kepley, L. J., Crooks, R. M. and Ricco, A. J. Selective Surface Acoustic Wave-Based Organophosphonate Chemical Sensor Employing a Self-Assembled Composite Monolayer - a New Paradigm for Sensor Design. *Analytical Chemistry*, **64**(24), 3191–3193, 1992.

[115] Mrksich, M., Sigal, G. B. and Whitesides, G. M. Surface-Plasmon Resonance Permits in-Situ Measurement of Protein Adsorption on Self-Assembled Monolayers of Alkanethiolates on Gold. *Langmuir*, **11**(11), 4383–4385, 1995.

[116] Mrksich, M., Grunwell, J. R. and Whitesides, G. M. Biospecific Adsorption of Carbonic-Anhydrase to Self-Assembled Monolayers of Alkanethiolates That Present Benzenesulfonamide Groups on Gold. *Journal of the American Chemical Society*, **117**(48), 12009–12010, 1995.

[117] Turner, A. F. P. *Biosensors: Fundamentals and Applications*, volume V-VIII. Oxford University Press, Oxford, 1987.

[118] Byfield, M. P. and Abuknesha, R. A. Biochemical Aspects of Biosensors. *Biosensors & Bioelectronics*, **9**(4-5), 373–400, 1994.

Instruments

The following instruments were used for specific parts of the work:

2.1   UV-cleaner

An easy method for cleaning substrate surfaces is the treatment in a UV-cleaner for 30 minutes. The mercury vapor lamp that is placed close to the substrate surface transforms ambient oxygen into ozone. Singlet oxygen, ozone and high intensity UV irradiation oxidize traces of organic impurities. However, in some experiments we saw that higher amounts of impurities at the surface cannot be burned away with this method. We used two different UV-cleaners in our experiments: UV-Ozone Cleaner (Model 135500 Boekel Industries; Inc.) in Laminar flow box (Skan USA-180) for surface preparation & UV-Ozone Photoreaktor (Ultra-Violet Products).

2.2   Oxygen plasma cleaner

A related method is oxygen-plasma cleaning. Typical treatment times are a couple of minutes. It has been shown that repetitive cleaning cycles or cleaning for a longer time is not useful to remove contamination and we believe that excessively long radiation may result in surface damage. The apparatus used for the experiments are: Plasma Cleaner/Sterilizer (Harrick) & Plasma Cleaner/Sterilizer (Harrick PDC-32G).

2.3   Contact Angle Mesurement

One of the most sensitive techniques for obtaining surface information is the measurement solid/liquid/vapor contact angle. The basis of the method is related to surface/interface energy and surface tension. When atoms or molecules are exposed at an interface, they are no longer surrounded from every side like molecules in the bulk substance. They either lose some of their interaction energy, in the case of the ideal surface/vacuum interface or share some of the interaction energy with the molecules in the surrounding medium. Hence the tendency of liquids to minimize their surface area or the occurrence of capillary phenomena determines the surface tension (capillarity is the collective name of phenomena occurring on surfaces that are mobile enough to modify their shape according to surface tension requirements [1]

The basis for measuring the instrument of solid surface tension by contact angle is the equilibrium at the three-phase boundary (Fig. 2.1). A drop of a liquid placed on a solid surface will modify its shape due to the different surface/interfacial tensions, until an equilibrium is reached. Thomas Young described the three-phase equilibrium in terms of the vectorial sum shown in Figure 2.1, resulting in the following equation (2.1) or interfacial equilibrium [2] [3].

$$\gamma_{SV} - \gamma_{SL} = \gamma_{LV} \cos\theta \qquad (2.1)$$

Surface wettability was investigated by measuring advancing and receding contact angles in a sessile drop experiment (Ramè-hart, Inc. NRL C.A. Goniometer Model No 100-00-230). All the reported values are the average of advancing contact angles at 5 different spots per sample.

2.4   Variable   Angle   Spectroscopic   Ellipsometer (VASE)

Ellipsometry is an optical technique used for investigation of optical properties and thickness of layered structures. Ellipsometry measures a phase shift and changes in amplitude of polarized light upon reflection at interfaces. Flat reflective surfaces are required.
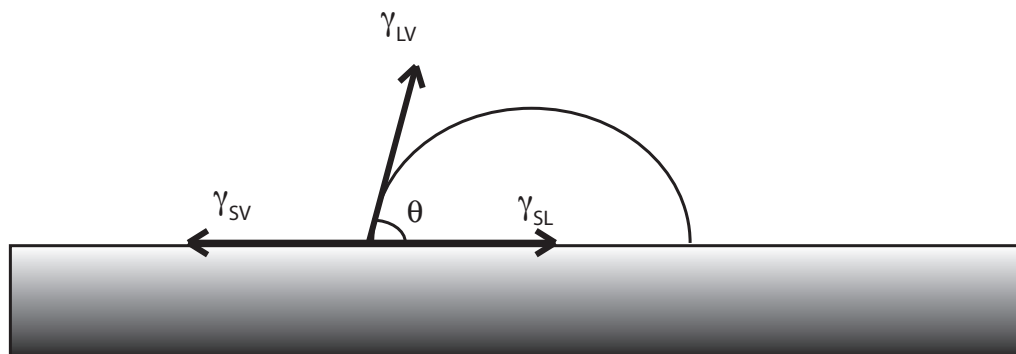
Figure 2.1: Liquid drop on a surface. The resulting interfacial tensions γ_{ij} are related with the contact angle θ through the Young equation 2.1. L = liquid, S = Solid, V = vapour

This technique is based on changes in the polarization due to reflection of a light beam on the sample surface. The amount of change in polarization upon reflection is dependent on the optical properties of the substrate, the surface layer and the ambient [4]. To correlate the measured changes in light polarization with surface properties, a theoretical optical model is needed. With the help of such models it is possible to determine refractive index and thickness of the adsorbed layer by iteration of the ellipsometric angles ψ and Δ. Δ (Delta) is defined as the change of the phase difference between the p- and s-components of the polarized light upon reflection, while ψ (Psi) is the angle whose tangent is the ratio of the magnitudes of the total reflection coefficients of the p- and s- component. The total reflection coefficient is the ratio of the amplitudes of the outgoing wave to the incoming wave. Therefore, the results are highly dependent on the assumption made about the surface properties.

Using a single wavelength ellipsometer, the two ellipsometric angles, ψ and Δ, are measured and the effective refractive index, N= n+ik, obtained by iteration. When a new adlayer is adsorbed, e.g. a protein, the ψ and Δ angles change and three more parameters have to be determined: the adsorbates refractive index (real and imaginary) and its thickness (Fig. 2.2). Since only one equation with three unknown variables is available, two of these three parameters have to be known or assumed within the model. For organic films, which are generally dielectrics, the imaginary part of the refractive index, k, is usually set to zero [4] and therefore the adlayer refractive index can be chosen from a pre-set value, determined with
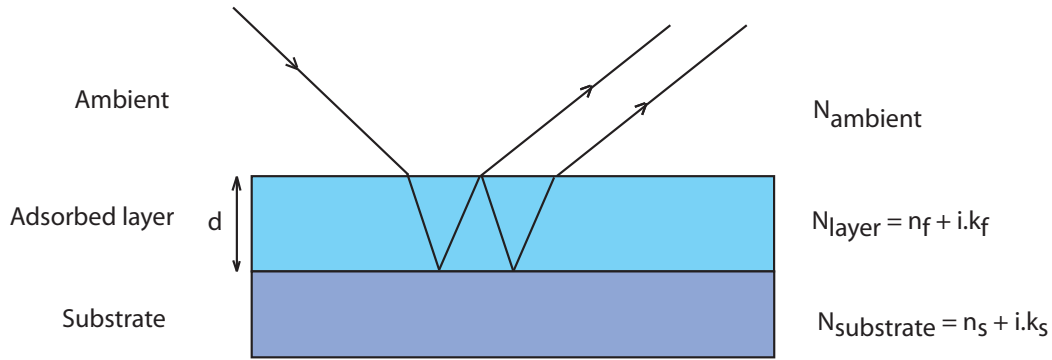
Figure 2.2: Three phase model for ellipsometric measurements [4]

independent methods. This assumption allows the calculation of the film thickness through iteration.

Ellipsometry measures:

$$\Delta = \delta_i - \delta_j \qquad (2.2)$$

$$\tan \psi = \frac{|R^p|}{|R^s|} \qquad (2.3)$$

Δ: phase sensitive parameter

$\delta_{i,r}$: phase difference between s- and p-wave

R^p, R^s: total reflection coefficient

The monolayer thickness was measured, using a VASE (M-2000F, L.O.T. Oriel GmbH, Germany) and data were evaluated using the software WVASE (WexTech Systems, Inc., New York). The samples were measure at different of angles 65°, 70° and 75° immediately before and after monolayer formation. The parameters fort data evaluation are summarized in table 2.1.

Table 2.1: Layer model and parameters for VASE data fitting

Layer description	used layer model	fitting parameters	layer thickness
Alkylphosphonate SAM	Cauchy	d	measured
		$A_n = 1.45$	
		$B_n = 0.01$	
		$C_n = 0.00$	
Titanoxide	$TiO_2 - mat$	$d, n, k \; before$ $adsorption, after$ $adsorption \; fixed$	$10 - 20 nm$
natural Silicon oxide	$SiO_2 - mat$	none	$2.3 \; nm$
Silicon	$Si - jell$	none	$1 \; mm$ $(Substrate)$

Each sample was measured individually before and after adsorption of the SAM due to VASE sensitivity to small deviations in the layer thickness. A cauchy layer was fitted as the difference between these two measurements where d is the layer thickness on TiO_2 / SiO_2 / Si-layer. For the substrate layers which are below the cauchy layer, the parameters have been fitted individually for each sample measured before adsorption and then fixed. The calculated layered thickness are not absolute because the refractive index for the phosphonate SAM is not known.

2.5 X-ray photoelectron spectroscopy (XPS)

X-ray photoelectron spectroscopy makes use of the photo-electric effect to quantitatively measure the chemical composition at the surface of a sample. A heated filament emits an electron current which is directed and accelerated (E_{kin} approx. 15kEV) towards an anode where it evokes both a continuous X-ray spectrum as well as discrete Roentgen lines due to relaxation process (Al K_α 1486.6 eV or Mg K_α 1253.6 eV). Anode materials are chosen in such a manner that they have one dominating X-ray line with an energy that is sufficient to knock electrons out of the inner shells of numerous elements.

On their way to the electron detector, the liberated electrons pass a system of electron lenses and an energy analyzer. The purpose of the lenses is to flexibly alter the kinetic energy of electrons by imposing an electric field. Its form can be adjusted to affect electrons from different spatial regions of emission differently. In the (hemispherical) analyzer the electrons are then deflected by two electrodes. The geometry and construction is such that only electrons entering the analyzer in a

given direction and with a given energy, can reach a fixed electron detector. This
working principle allows the separation of electrons according to their kinetic energy
as well as their point emission (imaging XPS [5]). An XPS measurement hence yields
the number of electrons as a function of their kinetic energy, which can be directly
transformed into a spectrum as a function of the original binding energy:

$$E_{Binding} = h\nu - E_{kin} - \phi \tag{2.4}$$

Where hν is the energy of the incoming photon, E$_{kin}$ stands for the kinetic
energy of the electron and ϕ denotes the work function of the apparatus. In figure
2.3 the survey spectrum of a phosphonate monolayer on titanium oxide is exemplarily
shown. In an XPS spectrum, peaks appear at all those binding energies at which
electrons are bound in the sample. The peak positions are characteristic for the
atomic species which are present in the sample so that the individual peaks can
be attributed to a specific element. The energy resolution of the analyzer is also
sufficient to discriminate between different chemical states of an atomic species (such
as oxygen in **Ti-O, P=O** or **P-O-C** in the case of phosphonate on titanium oxide).
After this initial stage of the analysis, one hence knows the qualitative chemical
composition of the sample. By inclusion of the elemental photon absorption cross-
sections (also known from reference measurements and called "sensitivity factors" in
this specific context) and a consideration of the experimental transmission function,
the significance of an XPS-spectrum strongly rises. Apart from identifying the
different chemical species, an XPS measurement on such a calibrated systems now
also quantifies their proportions (accuracy approx. $\pm 10\%$), assuming a homogeneous
layer.

The XPS method owes its surface sensitivity due to the short mean-free path of
electrons in a solid [6] [7]. Typical electron escape depths range from approximately
0.5-3 nm in the energy region of 10-1000 eV for normal substrates.

XPS is an invaluable surface-analytical technique because of its capability to
quantitatively analyse surface chemistry and its ability to discriminate between dif-
ferent oxidation states and is hence available in most surface science laboratories.
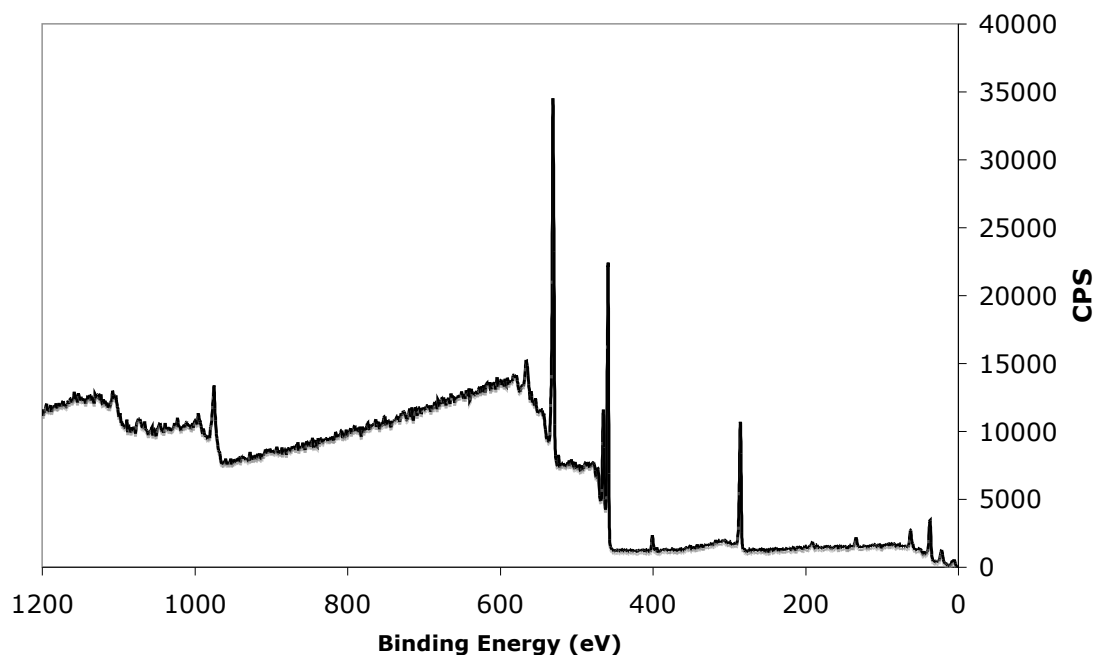
Figure 2.3: Survey spectra of compound **21** on TiO$_2$

2.6 Gel Permeation Chromatography (GPC)

GPC is the only fast technique for characterizing polymer molecular weight distribution. GPC provides key information to predict the processability and material properties of a polymer changing molecules size from 10^3 to 10^7 g/mol^{-1} (Fig. 2.4)

GPC columns perform a separation based on the molecular size of polymer molecules in solution, not molecular weight. Columns are made of cross-linked polystyrene with different pore sizes. Resolution and/or resolving range is increased by use of multiple column systems (Fig. 2.5).

Columns are packed with porous particles of controlled pore and particle size and shape. Columns are produced by slurry packing technique, packed at pressures in excess of 2000psi (140 bar). Column dimensions are typically 7-8 mm in dimension and 250-600 mm in length. It is important to choose the right column before starting measurement. Column selection criteria:
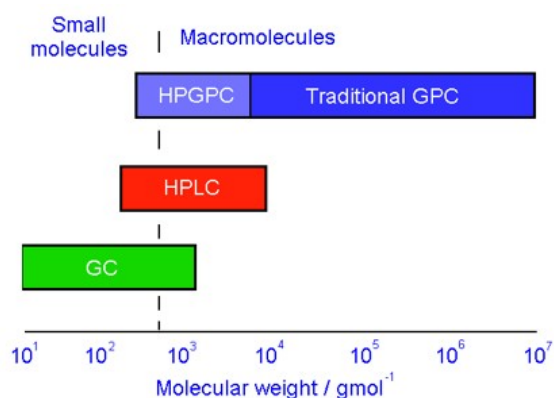
Figure 2.4: Different chromatography methods for different molecule sizes

* Particle size: smaller particles for higher resolution, larger particles to avoid shear degradation of high MW components.

* Pore size: depends on molecular weight range of sample, avoid exclusion of sample components, maximize pore volume in required separation region, individual pore size or mixed gel columns.

Most commonly used polymer calibrants are

- polystyrene in THF, toluene or chloroform

-polymethyl methacrylate in ethyl acetate, acetone or DMF

-polyethylene glycol in aqueous eluents, DMF or DMSO

The sample peak when integrated can be assumed to be a histogram consisting of a number of individual slices. For each slice, i, the molecular weight (M_i) can be derived from the room temperature and the number of molecules (N_i) from detector response Fig(2.6).
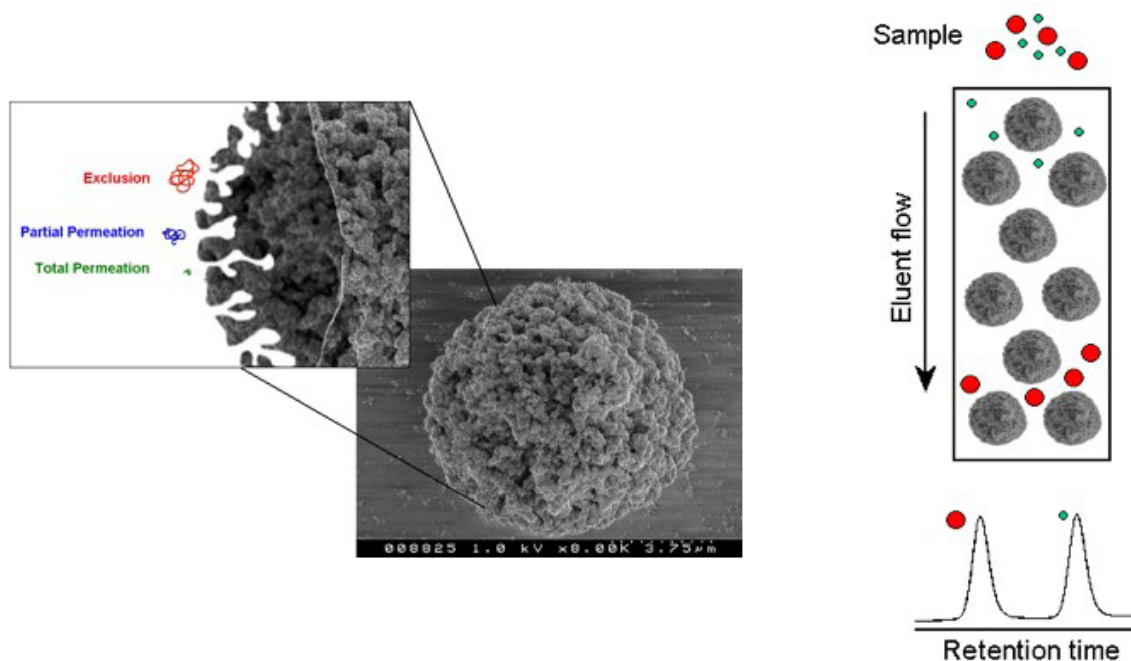
Figure 2.5: Separation based upon size in solution
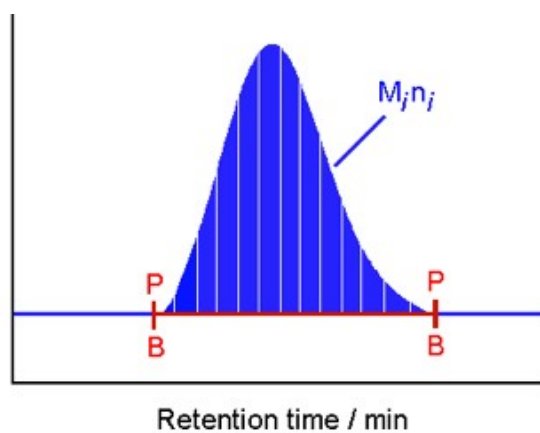
Figure 2.6: Peak-Integration

There are different types of GPC detectors; concentration detectors i.e. differential refractometer (RI), ultraviolet absorbance (UV), Infra-red (IR) and molecular-weight-sensitive detectors i.e. viscometry and light scattering (Table 2.2). This technique has advantages like measuring at the same time M_n, M_w, M_v, M_z and M_w/M_n and up to 20 analysis per day can be performed.

GPC measurements were carried out using PL-GPC 220 instrument with 2x PL-Gel Mix-B LS column set (2x30 cm) equipped with RI (refractive index), viscosity

Table 2.2: Different detection techniques

Method	absolute	relative	Resulting M	Analysis/Day
Light Scattering	X		$\overline{M_w}$	2-3
Osmometry	X		$\overline{M_n}$	1
Ultra Centrifugation	X		$\overline{M_z}$	1-2
Viscometry		X	$\overline{M_v}$	1-2
GPC		X	$\overline{M_n}$, $\overline{M_w}$, $\overline{M_v}$, $\overline{M_z}$	10-20
			and $\overline{M_w}/\overline{M_n}$	

and LS (Light Scattering with 15° and 90° angle) detectors [DMF + 1gL^{-1} LiBr as eluent at 80°C]. Universal calibration was done using PMMA standards in a range of Mp= 2.680.000 to 3.900.000 (Polymer Labs. Ltd., UK).

Calibrations are done with either polyethylene or polystyrene. However, if a calibration of size versus retention time could be generated then one true calibration would hold for all sample types. A universal calibration plot of log[η]M versus RT holds true for all polymer types. By using measured intrinsic viscosity and retention time we can obtatin accurate molecular weights [8]. In figure 2.8 a phosphonic acid styrene copolymer (chapter 3, **27**) was measured with GPC after column was calibrated with polystyrene.
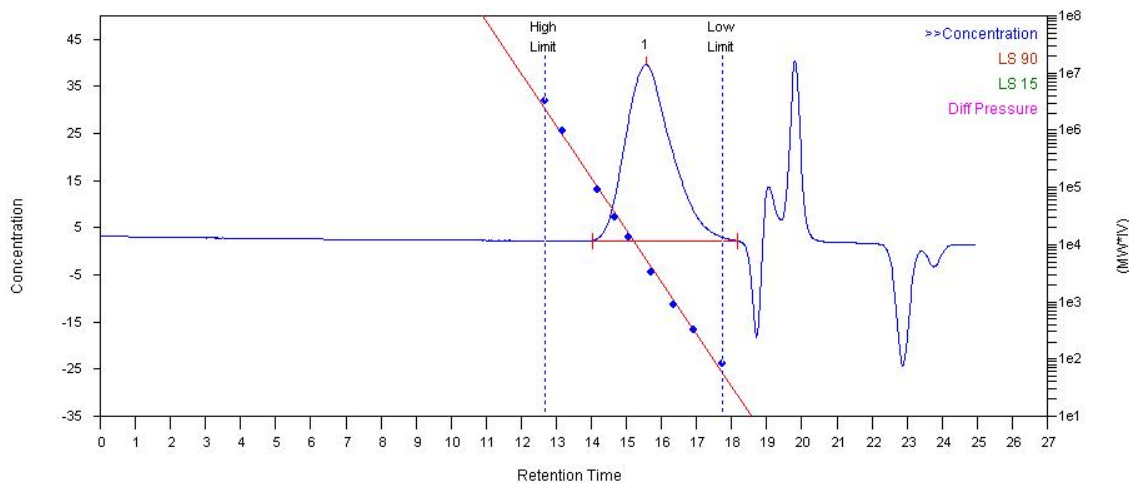
Figure 2.7: A GPC of a compound **27**

References

[1] Holly, F. J. *Physiochemical Aspects of Polymer Surfaces*. Plenum Press, New York, 1983.

[2] Padday, J. F. Effect of Temperature on Wettability of Low-Energy Surfaces. *Journal of Colloid and Interface Science*, **28**(3-4), 557, 1968.

[3] Befay, P. and Petre, G. Dynamic Surface Tension. *Surface Colloid Science*, **3**, 27–80, 1969.

[4] Benesch, J. *Null Ellipsometry and Protein Adsorption to Model Biomaterials*. PhD thesis, Linköpings, 2001.

[5] Briggs, D. and Seah, M. P. *Practicle Surface Analysis Auger and X-Ray Photoelectron Spectroscopy*, volume Volume 1. John Wiley & Sons, Chichester, 1983.

[6] Lindau, I. and Spicer, W. E. Probing Depth in Photoemission and Auger-Electron Spectroscopy. *Journal of Electron Spectroscopy and Related Phenomena*, **3**(5), 409–413, 1974.

[7] Powell, C. J. Attenuation Lengths of Low-Energy Electrons in Solids. *Surface Science*, **44**(1), 29–46, 1974.

[8] Grubisic, Z., Rempp, P. and Benoit, H. A Universal Calibration for Gel Permeation Chromatography. *Journal of Polymer Science Part B-Polymer Letters*, **5**(9PB), 753, 1967.

Results and Discussion

3.1 Synthesis of Monomers

3.1.1 Motivation/ Introduction and Planning of Synthesis

Functionalized self-assembled monolayers (SAMs) are an interesting and simple way to tailor surfaces. As indicated in chapter 1, amphiphilic molecules, building blocks of SAMs, are generally characterized by a carbon chain having a surface-specific and reactive head group at one end and a functional group at the other. The reactive groups react with the solid surface while the functional groups form the outer interface, determining the surface properties of the monolayer. Among all used SAM systems, alkanethiols on gold have been the most extensively investigated [1]. Since gold is not a preferred material for large-scale applications and/or optical sensors, a self-assembling system for metal oxide substrates is favored.

Alkylphosph(on)ates on metal oxide surfaces have been shown to form well-ordered monolayers [2]. The functionalization of these molecules, to use them as docking sites, is possible, but not straightforward [3]. Furthermore the application of simple alkane phosph(on)ate SAMs to produce biointerfaces has proven to have a number of limitations, in particular relating to their stability in aqueous media [4] [5].

The aim of this project is to demonstrate a modular approach to the synthesis of new functionalized molecules for self-assembly. In this way we can create a library of molecules that can be used to pass the desired chemical or physical properties

to surfaces. In the same strategy, we include a reactive group that can be used to polymerize the molecules once they have self-assembled on the surface or in solution. This is intended to increase the final stability of the films by multi-site attachment and is expected to eliminate the two main disadvantages of the simple alkane phosph(on)ate SAMs—their inferior stability in aqueous solutions and the difficulty of introducing reactive functionalities for the attachment of biomolecules.
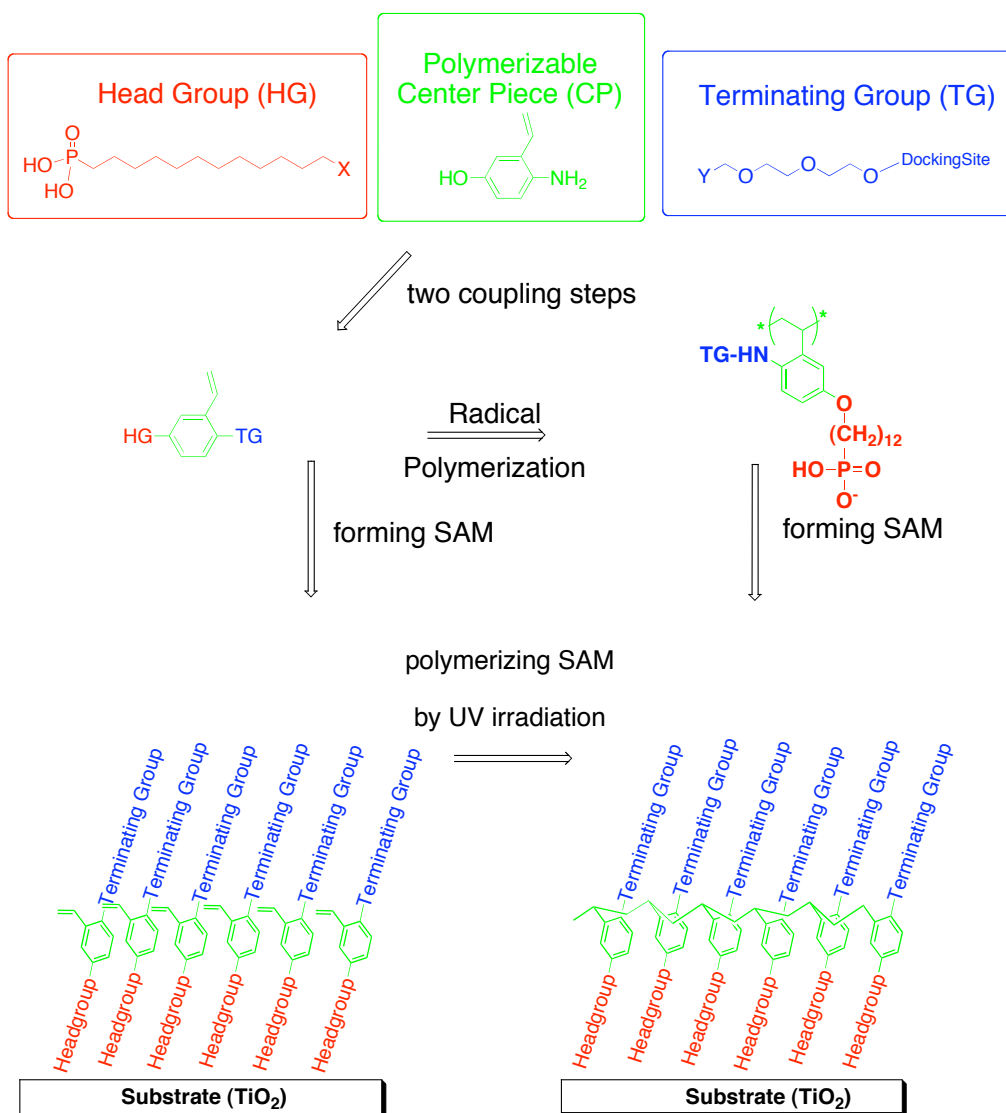
Figure 3.1: Sketch of the modular synthesis of self-assembling functional molecules. Possible heads and tails are depicted.

The modular synthesis of self-assembling functional molecules is summarized in Fig. 3.1. Our approach for the chosen head group (**HG**) consists of an electrophile halogen a Cl or a Br at one end, a 12 carbon-chain in the middle and a phosphonate at the other end which binds to the substrate (TiO_2) surface. The polymerizable center piece (**CP**) has three important groups: the hydroxy group which can be coupled to the **HG**, the vinyl group, which will be the polymerizable group and the amino group, which can be selectively coupled to the end-functionalized terminating groups (**TG**). Using an amino group as the attaching site for the functional end groups makes it theoretically possible to attach up to three equal or different chains in the same molecule. This could be advantageous to increase the density as well as the order of the SAM. For our coupling chemistry we prefer to end up with an amide bond, which we expect to be stable, and where we can rely on mild peptide bond formation chemistry. The other advantage of the amide bond, compared to an amine, is that it will not be protonated at physiological pH and will therefore not carry a positive charge. But it is limiting us to have just one chain, that can be used as a specific docking site. There are different surface properties associated with different tails. For example PEG-based (Figure 3.2) brush surfaces resist non-specific adsorption of proteins, whereas biotin binds specifically to streptavidin which serves as a linker molecule [6].
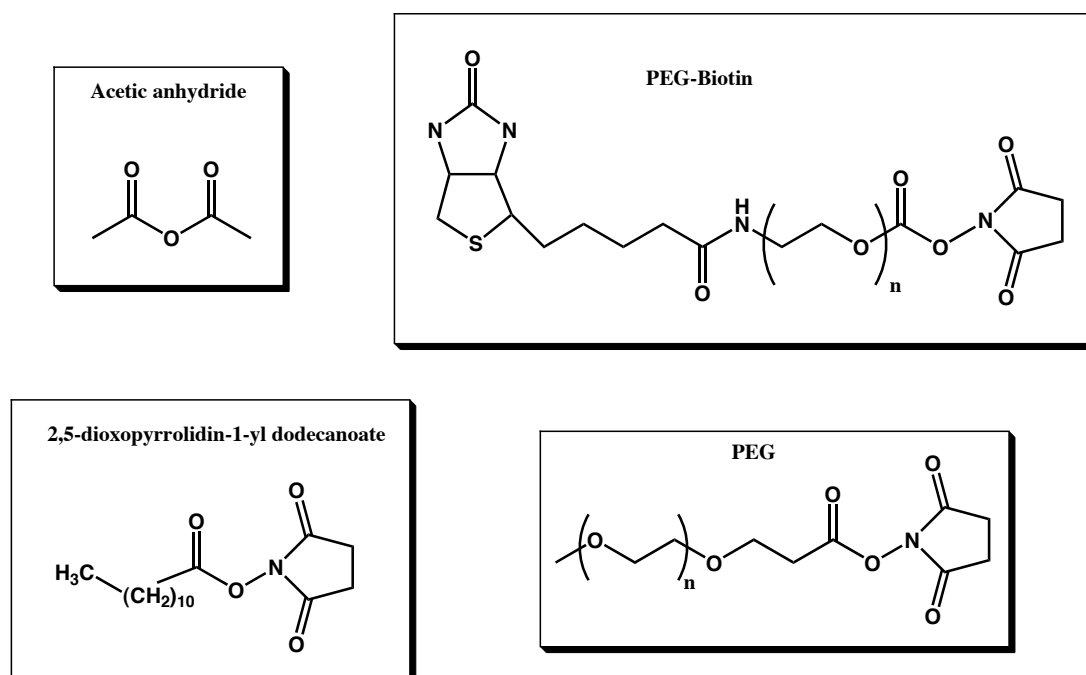
Figure 3.2: Different tails will impart different properties to surfaces. Biotin can be function-alized with streptavidin, PEG coupled surfaces resist non-specific adsorption of proteins and 2,5-dioxopyrrlidin-1-yl dodecanoate can be used to make hydrophobic surfaces.

Following the two coupling steps of the center piece with the head group and terminating group we aim to have the desired monomer. From this point on two different routes have been evaluated; first forming of SAMs on a substrate to yield a flexible film followed by polymerisation by UV irradiation which was supposed to result in a stable two-dimensional structure. The second route is to polymerize the monomer in a reaction flask and to adsorb the polymer onto the substrate by a self-assembly method. Certainly the first route would have advantages in patterning applications due to the relatively small monomer size, in comparison to a big, bulky polymer. In this way small areas (nm range) can be targeted and a higher theoretical resolution can be achieved.

It has been shown that long-chain molecules, particularly those with more than 12 carbon atoms, become more difficult to synthesize and purify [7]. Shorter chains are also more soluble than very long chains and allow a wider range of concentrations and solvents. A chain length of 10-12 carbons seems to be ideal for the preparation of α, ω-functionalized alkyl-phosphonic acids. The preparation of ω-terminated alkyl-

phosphonic acids with more than six carbons is rare in the literature. Mallouk, who pioneered the zirconium diphosphonate multilayers has published a synthesis for long-chain alkyl-diphosphonic acids [7]. We have chosen an analogous approach to produce phosphonic acids via the Michaelis-Arbuzov reaction [8] [9] [10].

3.1.2 Syntheses

Synthesis of Center Piece (CP)

A candidate for the center piece is 4-amino-3-vinyl-phenol **5** (Scheme 3.3). The phenol group can be used to attach the head group, while the aminogroup can be selectively coupled to the end-functionalized terminating groups. The vinyl group will be the polymerizable group. 4-amino-3-vinyl-phenol **5** has only been published as a side product of an electrochemical reaction [11] and in a patent for resists for photolithography [12]. No efficient synthetic protocol has been published for this rather simple compound. The starting compound for our investigated synthetic protocol is 3-bromophenol **1**. This reagent can be coupled selectively in the position 4 with 4-sulfobenzenediazonium to obtain compounds **2a, 2b** [13] [14] in good isolated yields (92%). All byproducts, including starting materials, were removed using column chromotography. We thought that we could use the diazo group as a protecting group for the aniline nitrogen, which can be easily deprotected by a mild reducing agent, e.g. sodium dithionite to **5**. Therefore we tried to directly introduce the vinyl group, using a Pd-catalyzed Suzuki cross-coupling (SCC) reaction [15] [16] [17]. The reagent used to introduce the vinyl group is trivinylboronicacidanhydride-pyridine (scheme 3.1) [18]. Trimethyl borate was added to THF at -78 °C and then vinylmagnesium bromide added under N_2-atmosphere for 1h. The reaction mixture was acidified with 2N HCl at -78 °C. The resulting mixture was extracted first with NaCl and then with diethyl ether and dried over $MgSO_4$. Pyridine was added to the previous mixture and stirred over night at room temperature. Distillation with a HV-pump at 70 °C gave trivinylboronicacidanhydride-pyridine as colorless oil.

The Suzuki protocol makes exclusive use of boronic acids and borates connected to a sp^2-carbon. This mechanism can be understood according to the general catalytic cycle for Pd^0-catalyzed cross-coupling reactions (Scheme 3.2). It consists of oxidative insertion, transmetallation and reductive elimination. The most commonly

used catalyst precursor for palladium-mediated reactions is Pd[PPh$_3$]$_4$, a saturated 18 e-complex.
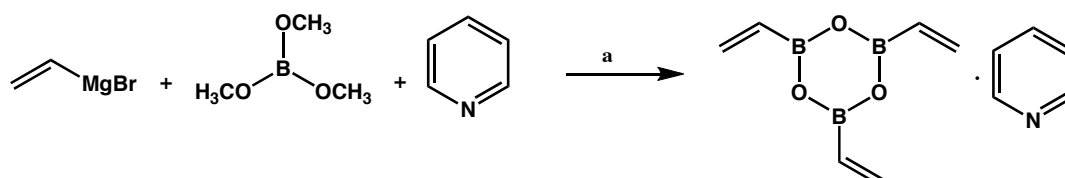
Scheme 3.1: Synthesis of trivinylboronicacidanhydride-pyridine. (a) THF, trimethyl borate, vinylmagnesium bromide, -78 °C, 60 min.; 2N HCl, -78 °C, 30 min.; pyridine, rt, 12 h.
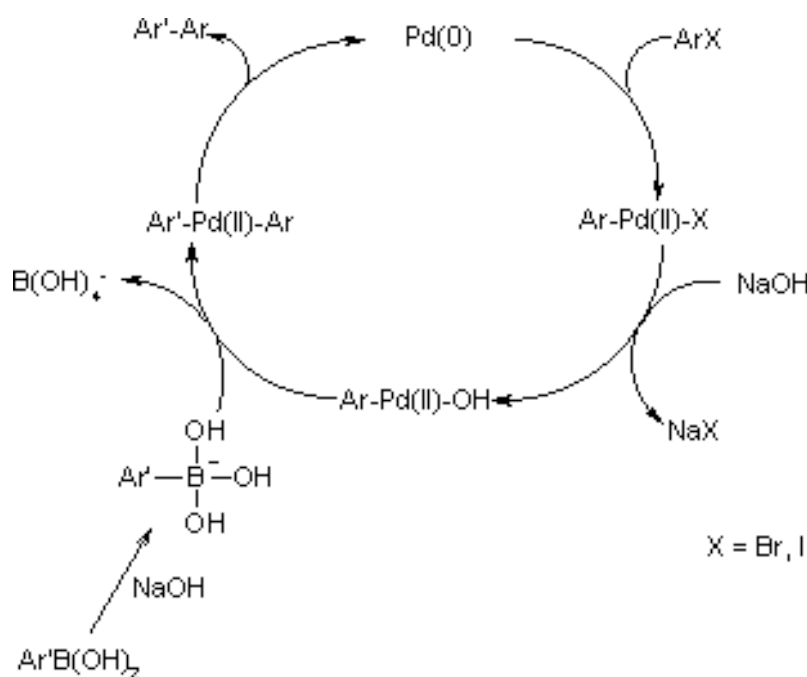
Scheme 3.2: Mechanism of the Suzuki cross-coupling reaction: [19]

Instead of the desired compounds **3a, 3b** we produced a new highly luminescent (cinnoline) diazanaphtalene (Figure 3.3) derivative **4b** (Scheme 3.3). Even though **4b** was not our target, this approach offers easy synthetic access to a class of compounds which has not been studied in detail so far. A small discussion on cinnolines can be found in chapter 3.3.6 and references [20] [21] [22].

As a reference compound and potential spacer molecule, without amino group 12-(3-vinylphenoxy)dodecylphosphonic acid **7** has been synthesized. Under the same conditions (SCC), the vinyl group was introduced to 3-bromophenol **1** and 12-bromododecylphosphonic acid was coupled to 3-vinylphenol **6** in EtOH, K_2CO_3 was used as a base. The obtained colorless oil was recrystallized from hexane at 0 °C to yield 12-(3-vinylphenoxy)dodecylphosphonic acid **7**.
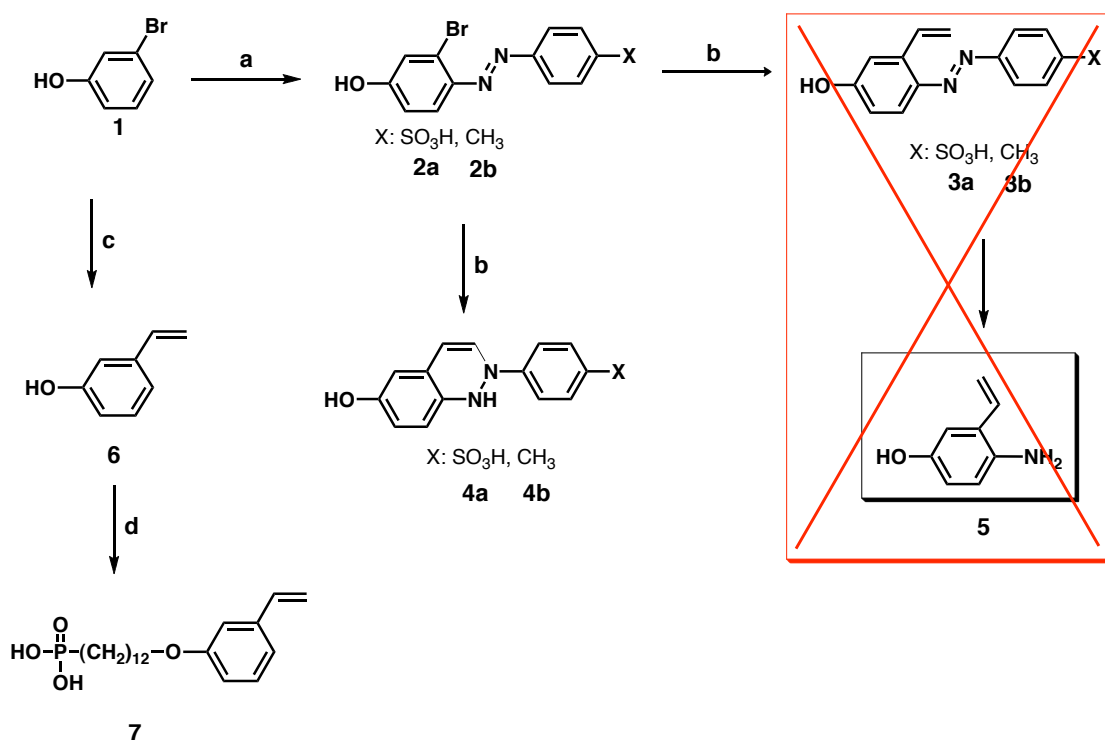
Scheme 3.3: Diazanaphtalene formation **4b**, synthesis of **CP 5**, 3-vinylphenol **6**, and 12-(3-vinylphenoxy)dodecylphosphonic acid **7**. (a) 4-Aminobenzenesulfonic acid or 4-methylaniline, HCl, NaNO₂, H₂O, rt, 1 h; NaOH 0°C to rt, 30 min; (b) Tetrakistriphenylphosphine palladium, (vinyl boronic acid) trimer [23], K_2CO_3, dimethoxyethane, H₂O, 89 °C, 16 h; (c) Tetrakistriphenylphosphine palladium, trivinylboronicacidanhydride-pyridine, K_2CO_3, dimethoxyethane, H₂O, 89 °C, 16 h; (d) 12-bromododecylphosphonic acid, K_2CO_3, EtOH, 83 °C, 16 h
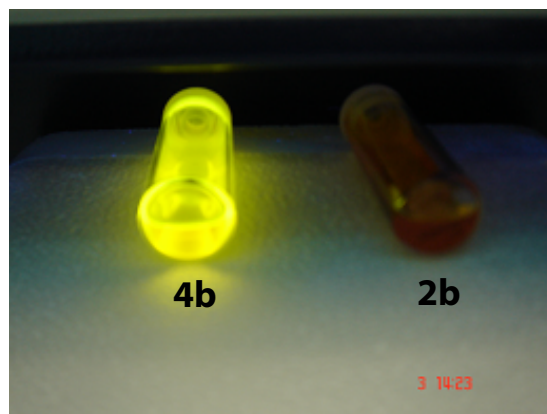
Figure 3.3: fluorescent cinnoline **4b** and **2b**, upon excitation at 366 nm.

Since this direct approach did not lead to our target compound **5**, a slightly longer route involving 2 more steps had to be developed (Scheme 3.4). The diazonated compounds **2a, 2b** were directly reduced with $Na_2S_2O_4$, which gives us the free amine **8** (55%) [24]. Before coupling the head to the phenol group, it is necessary to protect the amine group. At first pivaloyl was used as a protection group, but the formed amide was too stable to be selectively deprotected afterwards. Another protecting group was searched for and it was found that Boc seems to work in our case. From this point the amine was converted into tert-butyl 2-bromo-4-hydroxyphenylcarbamate **9** [25] with di-tert-butyl dicarbonate in order to protect it before the Pd^0-catalyzed cross-coupling reaction. All by-products were removed by column chromotography (83%). This time the Suzuki Pd^0-catalyzed cross-coupling was successful to introduce the vinyl group using trivinylboronicacidanhydride-pyridine reagent in good isolated yield 79%. The best deprotection protocol for an *N*-Boc-group employed TFA in dichloromethane at room temperature and yielded **5** [26]. The reaction usually proceeded within several minutes and was easy to monitor by TLC. The excess of TFA was removed after several co-evaporations with dichloromethane.
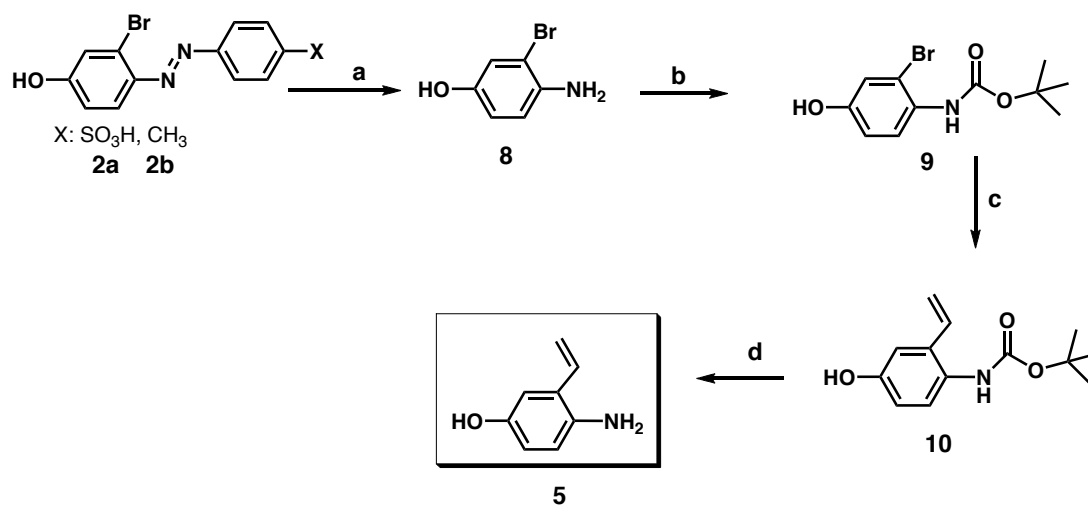
Scheme 3.4: Synthesis of **CP 5** (a) $Na_2S_2O_4$, H_2O, rt, 4 h. (b) Boc_2O, THF, rt, 12 h; (c) Tetrakistriphenylphosphine palladium, trivinylboronicacidanhydride-pyridine, K_2CO_3, dimethoxyethane, H_2O, 89 °C, 16 h; (d) 1:6 TFA:DCM, rt, 4 h.

Synthesis of Head Group (HG)

As it has been already mentioned we prefer an alkyl-phosphonic acid with 12 carbons because longer chains are difficult to synthesize and purify and a chain length of 12 carbons forms better SAMs due to van der Waals interactions than shorter chains. For the head-part synthesis, the starting materials are 1,12-dibromododecane and triethyl phosphite. The synthesis was carried out according to Michaelis-Arbuzov [8] [9] [10] which yields a mixture of two products and the reactant. All by-products, dodecane-1,12-diyldiphosphonic acid and 1,12-dibromododecane, were removed by column chromotography. After the synthesis of 12-bromododecylphosphonicacid-diethylester **11** (Scheme 3.5) two different reactions were carried out to liberate the free phosphonic acid, which is planned to be used as head group. In the first one, KI reacts with trimethylbromosilane to trimethylchlorosilane, which is more reactive. Deprotection of 12-bromododecylphosphonicacid-diethylester **11** was carried out at room temperature, which gave 12-iododecylphosphonic acid **12a** in 77% [27]. In the second reaction **11** was refluxed in HBr which gave **12b** with 36% yield.
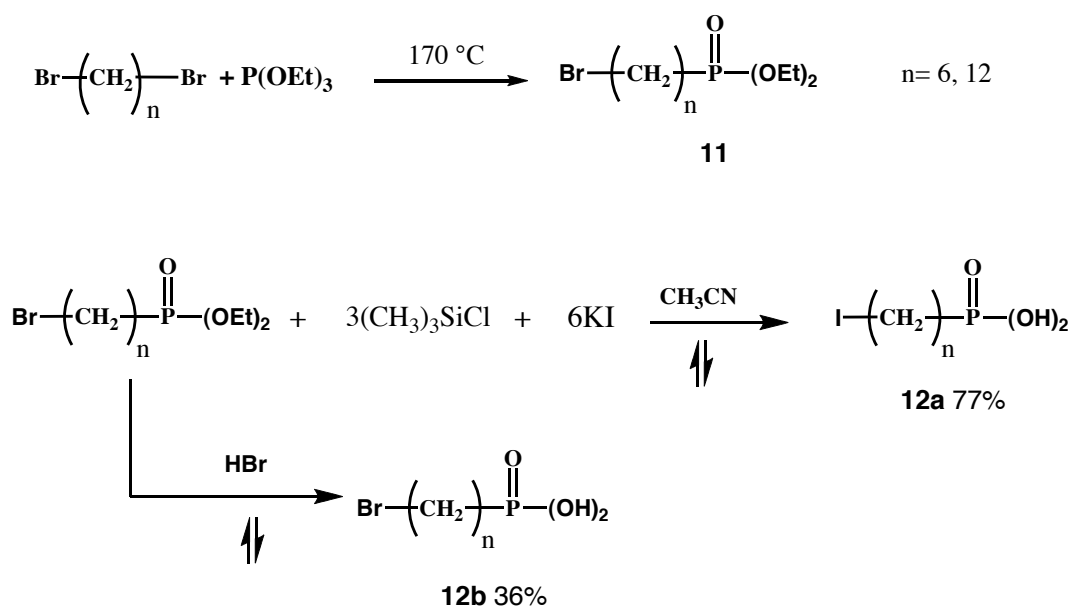
Scheme 3.5: Synthesis of head group with different lengths and deprotection of 12-bromododecylphosphonicacid-diethylester (**11**).

Coupling of Head Group (HG)

As head group we wanted to use a phosphonic acid. The head group-precursor **10** (tertbutyl 4-hydroxy-2-vinylphenylcarbamate) was coupled with **12a** (12-iodododecylphosphonic acid) in EtOH and to give **13** (12-(4-(tert-butoxycarbonylamino)-3-vinylphenoxy)dodecylphosphonic acid), which was purified by precipitation in hexane. During this step we figured out that there was also a side product **13a** (12-ethoxydodecylphosphonic acid) which was formed by the reaction of the solvent EtOH. This side product is difficult to remove, for example by column chromatography, because of free phosphonic acid, and can be a problem when self-assembling monomers on the substrates. In the next step, deprotection was carried out with TFA in dichloromethane at room temperature. The excess TFA was removed under reduced pressure and vacuum (94%). This synthetic sequence made **14** (12-(4-amino-3-vinylphenoxy)dodecylphosphonic acid) available on a scale of 200 to 300 miligrams within one week (Scheme 3.6).
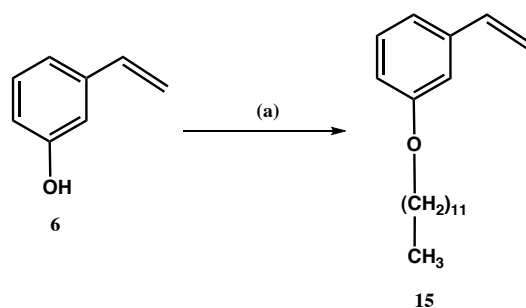
Scheme 3.7: Synthesis of 1-(dodecyloxy)-3-vinylbenzene (**15**), (a) 1-bromododecane, KOH, acetonitrile, 83 °C, 12 h.
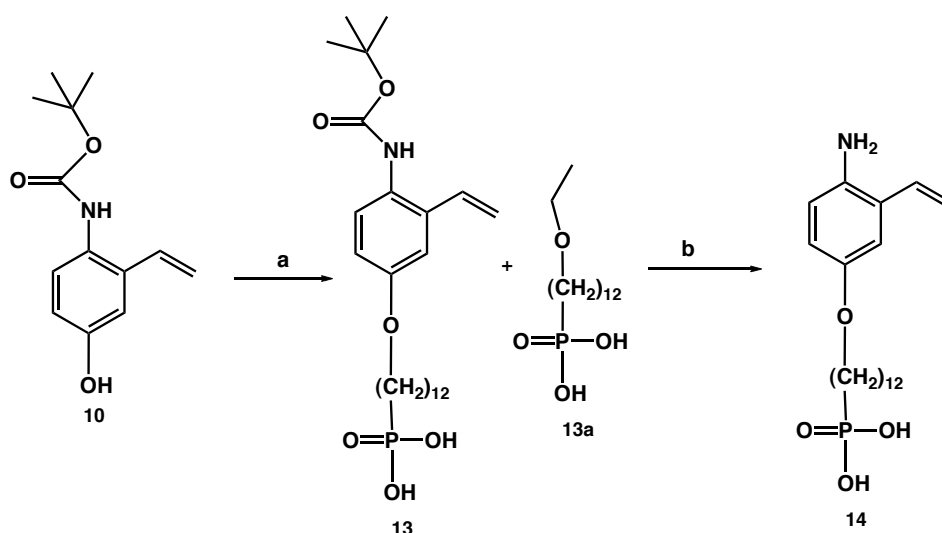
Scheme 3.6: Synthesis of 12-(4-amino-3-vinylphenoxy)dodecylphosphonic acid **14** (a) 12-iodododecylphosphonic acid, K_2CO_3, EtOH, 83 °C 16 h; (b) 6:1 TFA:DCM, rt, 4 h.

15 (1-(dodecyloxy)-3-vinylbenzene) was prepared as another spacer monomer (Scheme 3.7) in order to support self-assembly with the monomer molecule **7** or **14**. 1-bromododecane was reacted with **6** in acetonitrile and KOH was used as a base [28]. Using acetonitrile instead of EtOH as a solvent prevents the formation of the side product **13a**. The obtained yellowish oil 1-(dodecyloxy)-3-vinylbenzene **15** was purified by column chromatography (57%).
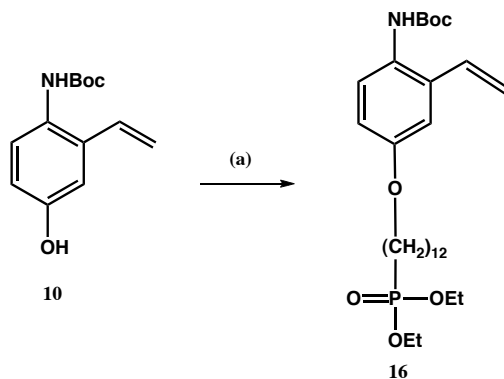
Scheme 3.8: Synthesis of tert-butyl-4-(12-(diethoxyphosphoryl)dodecyloxy)-2-vinylphenyl-carbamate **16**, (a) 12-bromododecylphosphonic acid-diethylester, K_2CO_3, acetonitrile, 83 °C, 16 h.

In order to solve the problem with the formation of the side product of **13a**, the synthetic protocol for the coupling was changed. Instead of 12-iodododecylphosphonic acid 12-bromododecylphosphonic acid-diethylester **11** was coupled to **10** in the presence of K_2CO_3 in acetonitrile at 83 °C for 16 h (Scheme 3.8). This compound can be purified by column chromatography on silica gel with petroleum ether / acetone / toluene (2:1:1) to afford tert-butyl-4-(12-(diethoxyphosphoryl)dodecyloxy)-2-vinylphenyl-carbamate **16** as an orange oil in high yield (93%).

The polymerization of these molecules will be discussed in the next chapter.

Coupling of Tail Group

We aim to produce well-ordered SAMs by van der Waals interaction with alkyl chains. Hence dodecanoate-NHS was coupled to 12-(4-amino-3-vinylphenoxy)dodecylphosphonic acid **14** in the presence of triethylamine in EtOH at room temperature (Scheme 3.9). Recrystallization from chloroform/hexane (1:1) and filtration of the product at 0 °C gave 12-(4-dodecanamido-3-vinylphenoxy)dodecylphosphonic acid **17** as, a brown solid (75%).

A second approach to tailoring the amine group was based on mimicking protein-resistant surfaces. This approach aims to eliminate non-specific adsorption. Poly(ethylene glycol) (PEG) has been extensively investigated for use in a

wide array of biomedical applications, and immobilization of PEG on surfaces has long been known to decrease protein adsorption. Of the many models proposed to explain this effect, steric stabilization and excluded volume are the most commonly cited [29] [30] [31] [32]. Therefore MPEG-SPA-2000 was coupled to 12-(4-amino-3-vinylphenoxy)dodecylphosphonic acid **14** in the presence of 4-methylmorpholine in DMSO at room temperature. Extraction with chloroform gave mPEG(ethanamido)-3-vinylphenoxy-dodecylphosphonic acid **18** as a brown solid (98%).
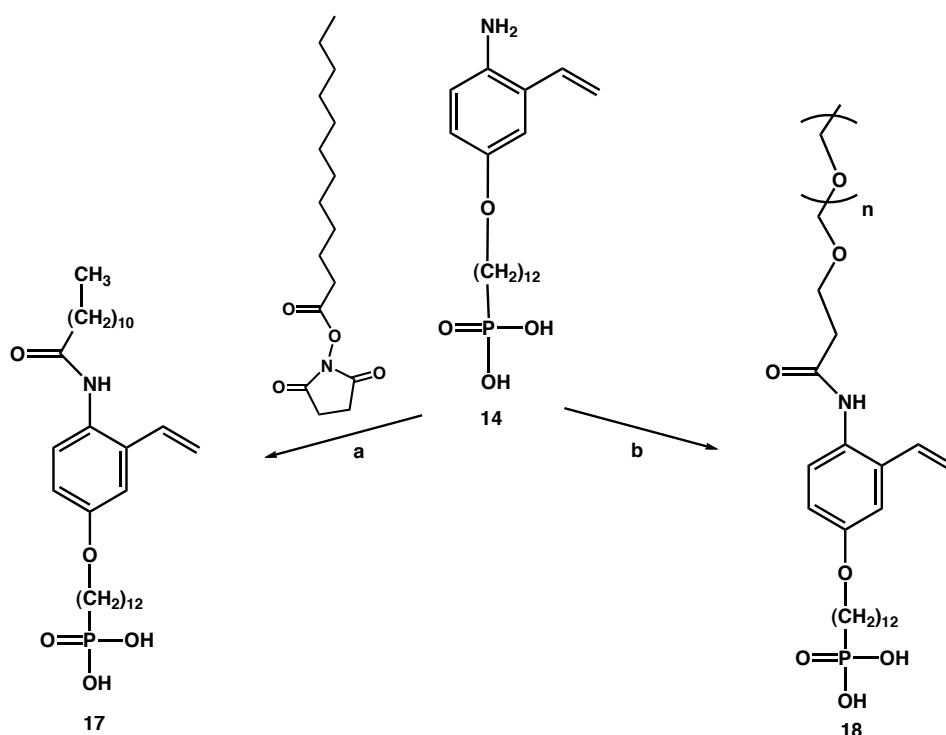
Scheme 3.9: Tail coupling, (a) 2,5-dioxopyrrolidin-1-yl dodecanoate, triethylamine, EtOH, rt ,12h; (b) MPEG-SPA-2000, 4-methylmorpholine, DMSO, rt, 12h.

The next step will be the functionalization of the tail group. Before functionalizing, the amine group boc-group was deprotected with TFA in dichloromethane at room temperature. The excess TFA was removed under reduced pressure and vacuum to give diethyl 12-(4-amino-3-vinylphenoxy)dodecylphosphonate **19** (93%) (Scheme 3.10). From this point it is planned to tailor the molecule before self-assembling, which will be discussed in chapter 3.3. Acetic anhydride was coupled to **19** with triethylamine and trifluoroacetic acid in dichloromethane

at room temperature for 16 h. The excess trifluoroacetic acid was evaporated under reduced pressure. The crude solid was purified by column chromatography on silica gel petroleum ether / acetone (1:1) yielding diethyl-12-(4-acetamido-3-vinylphenoxy)dodecylphsophonate **20** in 76% yield. In the next step diethyl ester groups need to first be silanated with trimethylbromosilane and then solvolyzed with water and methanol. **20** was silanated with trimethylbromosilane in dichloromethane at room temperature for 24 h. Trimethylbromosilane and dichloromethane were evaporated under reduced pressure and the resulting crude solid solvolyzed in MeOH / H_2O (95:5) at room temperature for 12 h. The MeOH / H_2O (95:5) was evaporated under reduced pressure to give 12-(4-acetamido-3-vinylphenooxy)dodecylphosphonic acid **21** as a white powder in 95% yield.
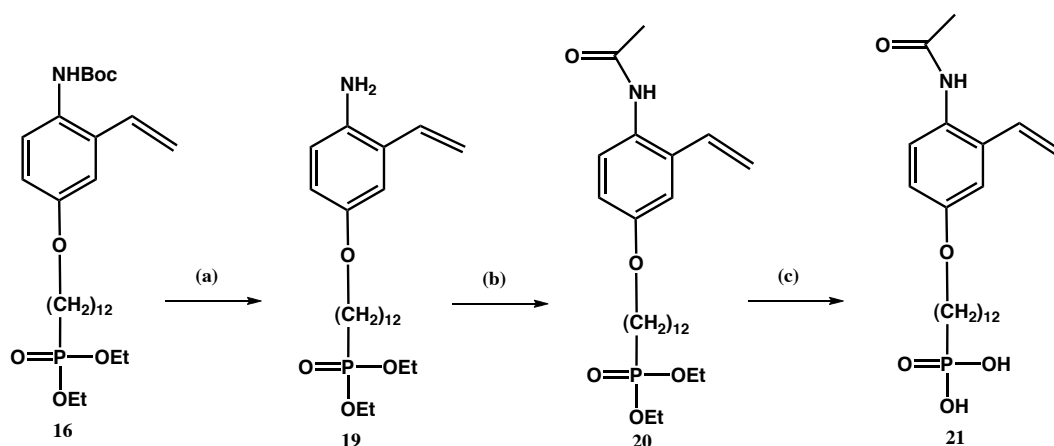
Scheme 3.10: Synthesis of the monomer (12-(4-acetamido-3-vinylphenooxy)dodecylphosphonic acid) **21**, (a) 6:1 TFA:DCM, rt, 4 h; (b) acetic anhydride, triethylamine, DCM, rt ,12 h; (c) trimethylbromosilane, DCM, rt, 24 h, MeOH:H_2O 95:5, rt, 12 h.

The silanation and solvolysis of tert-butyl-14-(12-(diethoxyphosphoryl) dodecyloxy) -2-vinylphenyl- carbamate **16** also was attempted in a one-step reaction. The problem was formation of hydrogen 12-(4-ammonio-3-vinylphenoxy)dodecylphosphonate **22** as a zwitter ion which was not soluble in most organic solvents (Scheme 3.11). Acetic anhydride was coupled to **22** with trimethylamine in DMSO at room temperature for 12 h. The crude solid was recrystallized from dimethoxyethane / petroleum ether and filtered. The yield for

12-(4-acetamido-3-vinylphenoxy)dodecylphosphonic acid **21** was relatively low after recrystallization (35%).
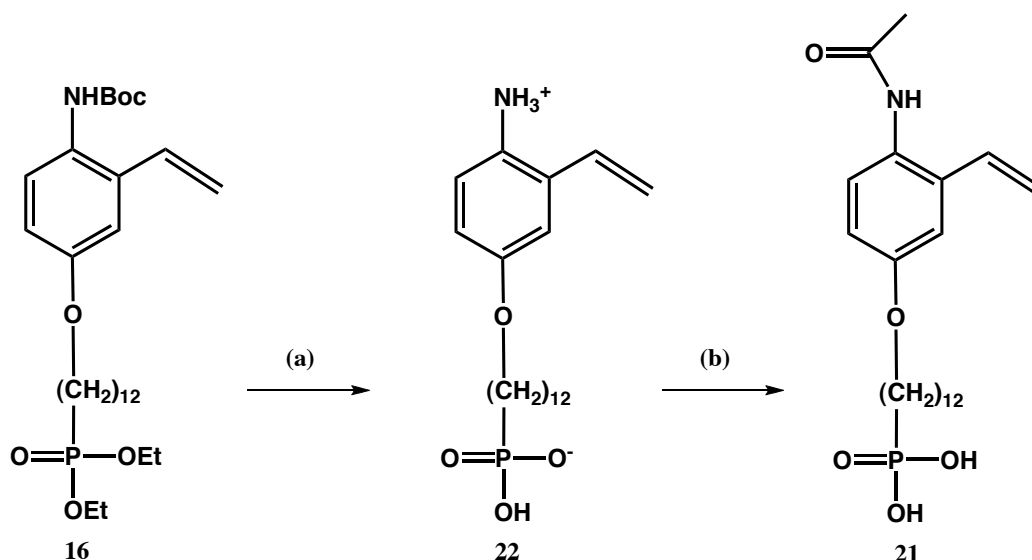
Scheme 3.11: Acetyl-coupling, (s) trimethylbromosilane, DCM, rt, 24 h, MeOH:H_2O 95:5, rt, 12 h; (t) acetic anhydride, triethylamine, DMSO, rt ,12 h.

Tail group functionalization carried out with MPEG-SPA-2000. MPEG-COOH 2000 was converted to acid chloride with oxalyl chloride in dichloromethane at room temperature 12 h. The excess oxalyl chloride and dichloromethane were removed under reduced pressure and vacuum. This highly reactive acid chloride was immediately coupled to **19** with triethylamine in dichloromethane at room temperature for 12 h. The resulting yellow crude solid was purified by dialysis in water for 48 h followed by freeze drying for 48 h to give a yellow solid (**23**) in 84% yield (Scheme 3.12). Diethyl-12-(4-PEG-3-vinylphenoxy)dodecylphosphonate **23** was silanated with trimethylbromosilane in dichloromethane at room temperature for 16 h and solvolyzed afterwards in MeOH / H_2O (95:5) at room temperature for 24 h. The obtained white crude solid purified by dialysis in water for 48 h and freeze dried for 48 h to give **18** in 56% yield.
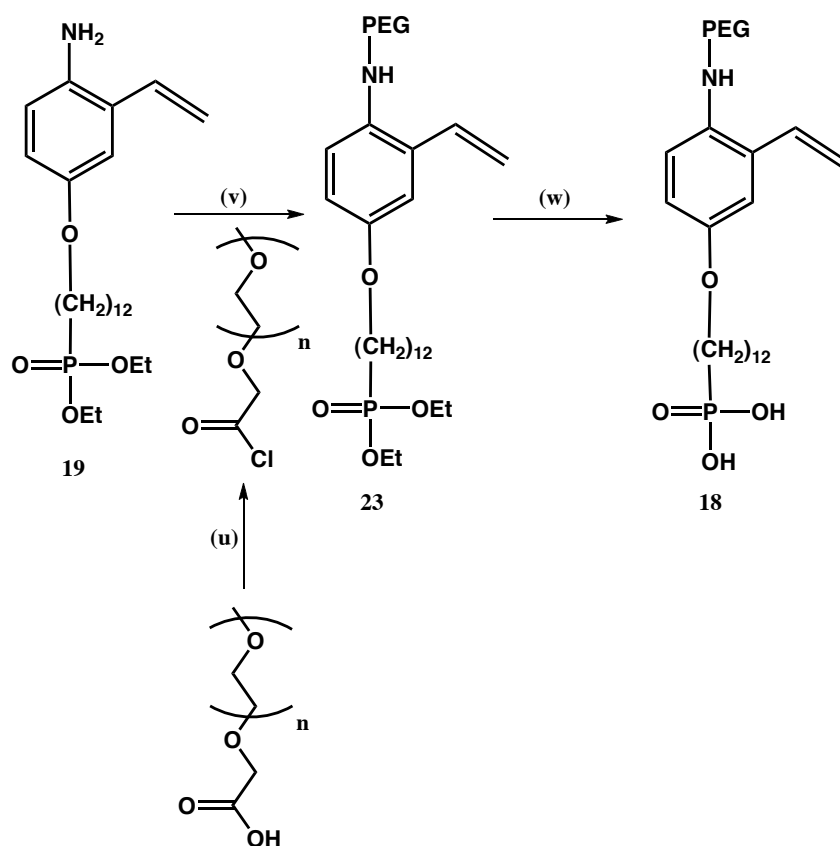
Scheme 3.12: Synthesis of PEG-coupled monomer **24**, (a) oxalyl chloride, DCM, rt, 4 h; (b) PEG-COCl, triethylamine, DCM, rt, 24 h; (c) trimethylbromosilane, DCM, rt, 24 h, MeOH:H$_2$O 95:5, rt, 12 h.

3.2 Synthesis of Polymer and Copolymer

The free radical polymerization was carried out with AIBN (2-2-azo-bis(isobutyronitrile)) in benzene. AIBN was used as a initiator after decomposing to 2-cyanoprop-2-yl radicals (Scheme 3.13).

3.2.1 Syntheses

Tert-butyl-4-(12-(diethoxyphosphoryl)dodecyloxy)-2-vinylphenyl-carbamate **16** was polymerized with AIBN in benzene at 85 °C for 24 h. Benzene was removed under
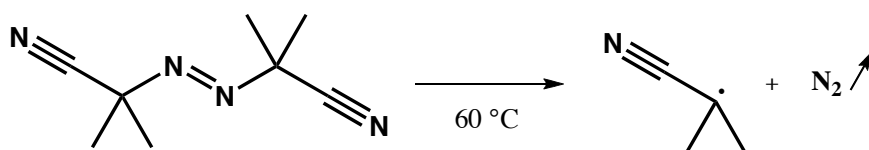
Scheme 3.13: Decomposition of AIBN to form 2-cyanoprop-2-yl radical.

reduced pressure. Deprotection of the Boc-aniline group and the diethylphosphonate group were performed in a similar way as for the monomeric compound **22** to give poly-2-ethyl-4-(12-phosphonododecyloxy)benzenaminium bromide **26** as a white powder in 75% yield.
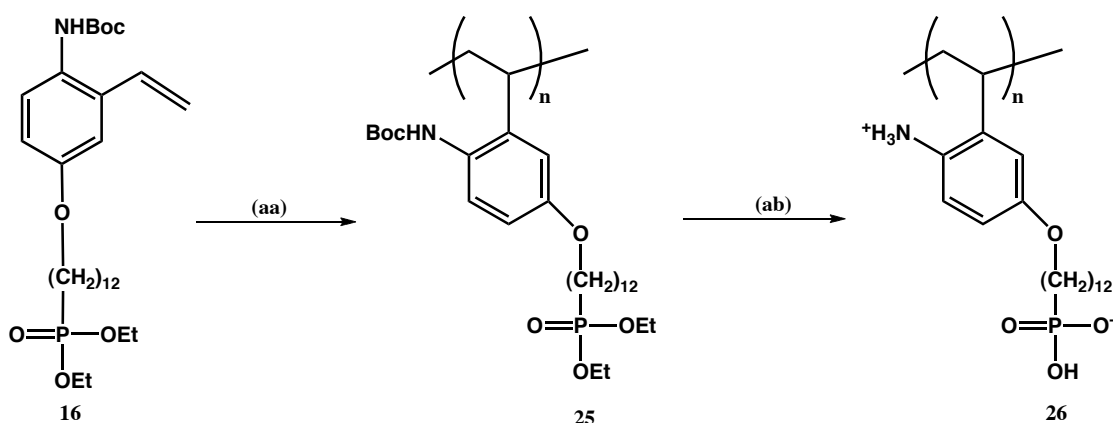
Scheme 3.14: Polymerization and solvolysis of tert-butyl-4-(12-(diethoxyphosphoryl)dodecyloxy)-2-vinylphenylcarbamate, (aa) AIBN, benzene, 85 °C, 16 h; (ab) trimethylbromosilane, DCM, rt, 24 h, MeOH:H$_2$O 95:5, rt, 12 h.

Since the center part of the molecule **17** has a styrene group and styrene polymerization is a well-known procedure, we decided do a copolymerization with styrene. Styrene and **17** were dissolved in benzene and copolymerized with AIBN at 85 °C for 16 h. The obtained yellow gel was recrystallized from benzene / hexane which gave **27** in 61% yield. Deprotection of the diethylphosphonate group was performed in a similar way as for the monomeric compound **22** to give poly(2-isopropyl-4-(12-phosphonododecyloxy)benzenaminium bromide-co-styrene) **28** as a white powder in 95% yield. PEG-NHS 5000 was coupled to **28** in the presence of

triethylamine in DMSO at room temperature for 12 h. According to 300 MHz
NMR spectroscopy it was difficult to recognize aromatic and alkyl groups rela-
tive to PEG-NHS 5000. The resulting white crude solid was dissolved partly in
H_2O, dialysed for 48 h and freeze dried for 48 h to give poly-12-(3-ethyl-4-(2-(2-
methoxyethoxy)ethanamido)phenoxy)dodecylphosphonic acid **29** in 92%.
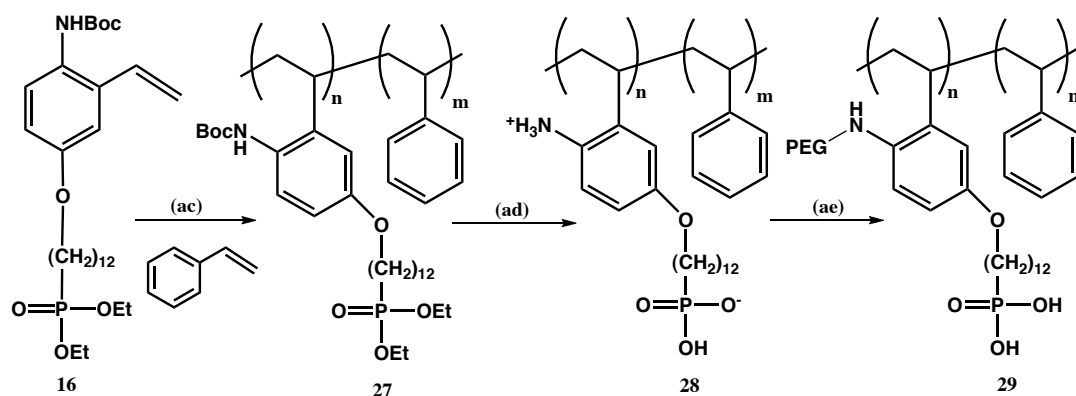
Scheme 3.15: Synthesis of phosphonic acid styrene-co-polymer, (ac) Styrene, AIBN, benzene, 85
°C, 16 h; (ad) trimethylbromosilane, DCM, rt, 24 h, MeOH:H_2O 95:5, rt, 12 h; (ae) m-PEG-NHS
5000, DMSO, triethylamine, rt, 12 h.

Besides styrene copolmer **27** we also planned an alternative copolymerization
with 1-(dodecyloxy)-3-vinylbenzene **15** which may help as a spacer on the TiO_2
after self-assembly.**15** was coupled to **17** with radical starter AIBN in benzene
at 85 °C for 36 h. The resulting oil was precipitated in MeOH / H_2O (4:1)
at 0 °C. Filtration gave poly-(tert-butyl 4-(12-(diethoxyphosphoryl)dodecyloxy)-
2-ethylphenylcarbamate-co-1-(dodecyloxy)-3-ethylbenzene **30** as sticky gel in 50%
yield.
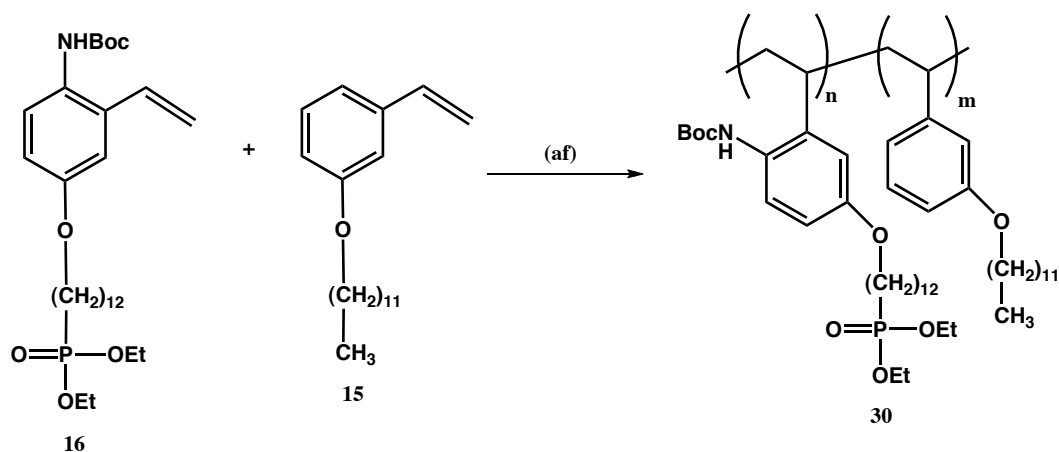
Scheme 3.16: Synthesis of poly-(tert-butyl 4-(12-(diethoxyphosphoryl)dodecyloxy)-2-ethylphenylcarbamate-co-1-(dodecyloxy)-3-ethylbenzene, (af) 1-(dodecyloxy)-3-vinylbenzene, AIBN, benzene, 85 °C, 36 h.

3.2.2 Characterization of Polymers

The synthesized polymers are characterized by different analytical methods. NMR was used to detect the vinyl group which has disappeared after polymerization. GPC has determined polymer molecular weight distribution. Following values were found for homopolymer **26** and copolymer **28** (Table 3.1). Elemental analysis has identified atomic percentages of the compounds and ratio of m,n which was found to be 1:1 in the copolymers.

Table 3.1: Polydispersity and M_w values for homopolymer **26** and copolymer **28**. Measurements were performed with a Viscotek GPC max VE 2001GPC solvent module and date were evaluated by Omnisec 4.0 software.

compound	poly dispersity	M_w
26	2.77	132.417
28	2.59	54.619

3.3 Adsorption of Monolayers on TiO$_2$

3.3.1 Self-assembly

As stated before, the alkane self-assembled monolayer system is very sensitive to contamination. Therefore, the solvents have to be of the highest quality, and free from any contamination that could compete with the assembling molecules. It is difficult to get contamination free samples because clean titanium oxide has a very high surface energy. It adsorbs easily compounds that are present in the environment. Different substrates were treated with different cleaning instruments for example plasma- and UV-cleaner to determine the best surface cleaning method for the self-assembly. Independent on the cleaning method used, UV or Plasma, traces of silicon were detected on almost all samples by XPS. Possible silicon sources may be due to presence of PDMS in laboratories or silicon dust coming from wafers cutting, but in also TiO$_2$ layers which are thinner than 10 nm. In the last case, the detected silicon comes from the substrate. In the same manner phosphorus and zinc have been detected by XPS on plasma cleaned samples which may be due to contamination inside the chambers or Zn(dttp)$_2$ contamination, a common lubricant for motor oils, in our case most probably coming from oil pumps which we use in the laboratories. Figure 3.5 shows two survey spectra of compound **21**, black line with zinc contamination (1020 and 1040 eV). Also sulfur has been detected only on plasma cleaned samples which may be due to contamination present at that time, a possible source could be old decomposing rubber tubes.

According to XPS measurements the detection limits of the contamination are around 1 %. The contamination that we were not able to detect is a small amount which should not interfere with the self-assembly process. A certain level of contamination can not be avoided, but some contaminants get replaced by the self-assembling molecules. Nevertheless, producing clean surfaces is a constant struggle in a surface chemistry laboratory.

Due to the above study, we followed the following cleaning procedure for our substrates. TiO$_2$ coated silicon wafers (1x1 or 4x2 cm) were first cleaned with isopropanol or EtOH in a sonicator 7 min then 30 min with UV or 4 min plasma and immediately measured by variable angle spectroscopic ellipsometry (VASE) to determine the oxide thickness. Compounds were dissolved in EtOH or H$_2$O and warmed up to 50° C in a water bath. Solutions were cooled down and filtered through
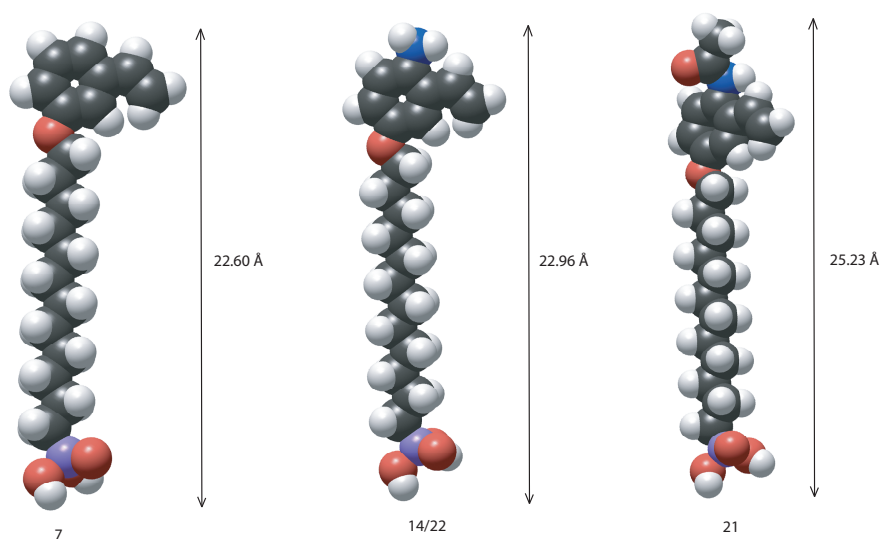
Figure 3.4: 3D Hyper Chem illustration of compounds **7**, **14**/**22** and **21**

a 0.22 μm filter. The samples were immersed in prepared monomer solutions for 16 to 48 h. Thickness of the films were measured again by VASE (table 3.2).

The length of the compounds was calculated using Hyper Chem 3D molecular modeling and compared with the measured thickness of the films in order to determine the position of the molecules on the surface. For SAMs obtained with **7** and **14** quite large deviations have been observed from sample to sample. Especially for **7** it turned out to be quite difficult to obtain reproducible SAMs. Also the thickness for SAMs of compound **7** is higher than the calculated value of 22.6 Å (Figure 3.4). A possible explanation for this behavior could be two layers on top of each other leading to a higher thickness. We also suspect for compound **22** that the synthetic side product **13a** adsorbs faster onto the surface than the desired compound **22**. This may be the explanation of lower reproducibility. The molecules **22** and **14** are more hydrophilic than the molecule **7** due to the aniline group which can be seen in average contact angle measurements (Table 3.2).
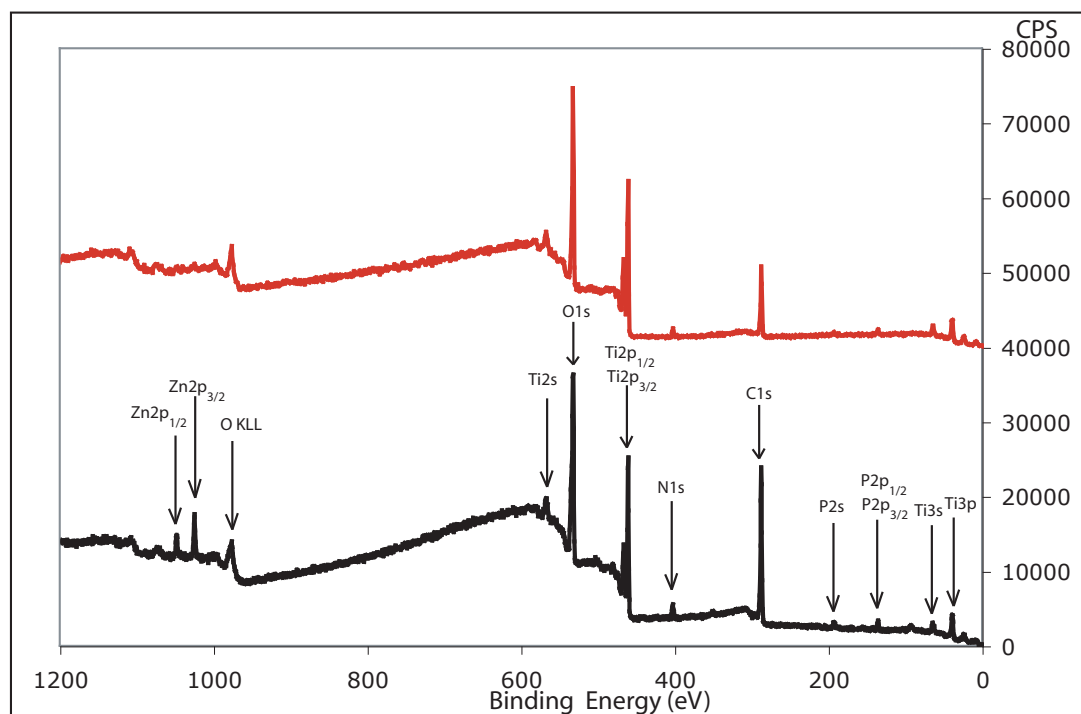
Figure 3.5: Survey spectra of compound **21** on TiO_2; black line with Zn contamination, red line without contamination

Table 3.2: Thickness of the SAMs with molecules **7**, **14**, **22** and **21**. The film thickness was determined by VASE M-2000F. (*) Synthesized according new coupling protocol, in the absence of side product (see chapter 3.1.2).

compound	thickness [Å]	average contact angle [°]
22	28.3 ± 0.6	65.7 ± 1.5
7	30.7 ± 6.2	79.3 ± 2.1
14	22.5 ± 3.5	66.3 ± 2.6
21	12.4 ± 0.8	57.0 ± 2.2
22*	20.5 ± 1.8	

Table 3.3: Elemental Analysis of compounds **22**, **7**, **22*** and **21** measured by Leco CHN-900

22	calculated %	found %	**7**	calculated %	found %
C	62.48	56.89	C	62.17	60.47
H	9.18	7.56	H	9.32	8.96
N	3.64	3.04	N	3.62	2.70
22*	calculated %	found %	**21**	calculated %	found %
C	62.25	61.71	C	64.84	64.90
H	8.31	8.63	H	9.21	9.36
N	3.30	3.30	N	2.91	2.96

The difference between the calculated and the found values (**7**, **22**) in the elemental analysis (Table 3.3) show that we do not have pure products but also side products **13a**. Especially large deviation for compound **22** is due to side product formation with solvent (EtOH). After the head group coupling protocol was changed the side product problem was solved. Compounds **21** and **22*** were synthesized according to the new head coupling protocol and the self-assembly study has been continued with these new molecules.

Table 3.4: Atomic concentrations of the SAMs compared to theoretically calculated values. The numbers are average values of at least three samples. XPS PHI 5700

	O %	N %	C %	P %
calculated	15.4	3.9	76.9	3.9
found				
22 series 1	19.1	1.6	75.2	4.2
22 series 2	17.6	1.5	76.5	4.3
	O %	N %	C %	P %
calculated	17.4	0	78.3	4.3
found				
7 series 1	14.2	0	81.8	3.6
7 series 2	16.2	0	79.6	3.6

Table 3.4 shows the atomic concentrations of the SAMs compared to theoretical values. Oxygen atomic concentration includes all the oxygen components except TiO_2. The low amount of nitrogen found in case of **22** proves our hypothesis, that **13a** coadsorbs on the surface. On the other hand in case of **7**, no nitrogen was expected.

The nitrogen concentration for compound **7** is much lower than compound **22** because the aniline group is on the top of compound **7**, whereas the ammonium group is at the bottom of compound **22** which is more difficult to detect by XPS.

XPS: The self-assembled monolayers for all investigated phosphonates were analyzed at 45° takeoff angle. The detailed spectra for O 1s, Ti 2p, C 1s and P 2p were resolved into their components using a fitting procedure as described below. The used parameters are presented in table 3.5.

O 1s: The main contribution to the O1s signal is originating from the oxygen in the substrate TiO_2 (binding energy 530.1 eV). We think the remaining oxygen contributions should originate at the substrate-SAM interface and can be assigned to P=O, C-O-C, P-O-Ti and Ti-O-H. The amount of oxygen from the substrate can be calculated and subtracted from the O1s signal. The remaining signal was modeled using three contributions, assigned to R-O-R at 533.2 eV, P-O-Ti and Ti-OH, which are assumed to have very similar binding energies and are fitted with peak centered at 531.6 eV, and the P=O at 530.9 eV. Some additional constraints had to be implemented in the fitting routine to get consistent results because the resolution of the O 1s peak does not allow us to distinguish between all these contributions. The area of the P=O component was assumed to be equal to the area of the C-O-C component and the binding energy of the P=O component is 0.80 eV higher than the binding energy of O1s TiO_2. The binding energy of C-O-C and P-O-Ti were found to be 3.00 eV and 1.46 eV higher than the O1s TiO_2 signal, respectively.

Ti 2p: The titanium signal was fitted with 2 components; Ti $2p_{1/2}$ at 464.43 eV and Ti $2p_{3/2}$ at 458.66 eV [Lit. http://srdata.nist.gov].

C 1s: The main part of the C1s signal originates from aliphatic and aromatic carbon with a binding energy of 285 eV. A shoulder at the higher binding energy of 286.5 eV originates from the C-O, C-N, and N-C-O groups connected to the benzene and the C-P group connected to the alkyl chain.

P 2p: The phosphorus signal was fitted as a doublet with P2p$_{3/2}$ at 133.0 ± 0.1 eV and P2p$_{1/2}$ with a binding energy difference of 0.84 eV and fixed area ratio of 2:1.

Compound 21

The samples were assembled according to the protocols presented above. After self-assembly of compound **21** the thickness of the films were determined by VASE (table 3.8).

Table 3.6: Atomic concentrations of the SAMs of compound **21** compared to theoretically calculated values. The numbers are average values of at least three samples (VG Theta Probe spectrophotometer). Oxygen atomic concentration does not include Ti-OH and TiO$_2$ component.

	O %	N %	C %	P %
calculated	17.3	3.6	75.9	3.5
found				
26 *hours*	15.3 ± 0.7	4.2 ± 0.8	77.5 ± 0.9	3.1 ± 0.1
72 *hours*	18.4 ± 0.6	4.1 ± 0.1	73.9 ± 0.6	3.7 ± 0.1

Table 3.7: XPS intensity ratios measured at 53 ° takeoff angle on a VG Theta Probe XPS machine. Interface Oxygen includes Ti-OH component.

Time	$Interface\ O/P$	$Ti-OH/P$	C/Ti
26 *hours*	12.0 ± 1.1	7.0 ± 1.1	3.0 ± 0.1
72 *hours*	5.8 ± 0.3	0.8 ± 0.3	2.8 ± 0.1

We calculated the excess oxygen per phosphonate group at the interface that must belong to Ti-OH (Table 3.7). There is clearly more Ti-OH for the self-assembly after 26 hours than the self-assembly after 72 hours. This is the first indication that for longer self-assembly time the phosphonate density is also larger, while the surface-bound water or hydroxyl groups become increasingly replaced. This effect is also supported by VASE measurements in table 3.8; the thickness of the SAMs after 72 hours are thicker than the SAMs after 26 hours. The effect of self-assembly time will be discussed in more detail in the coming chapter.

Table 3.5: XPS Binding energies and Fitting Parameters of compound **21** (Data measured on VG Theta Probe spectrophotometer)

	Binding Energy $(BE)[eV]$	Full Width at Half Maximum fwhm [eV]	constraints	Line Shape% Gauss−Lorentz and asymetry [Lit Casa]
$O1s$ $C - \mathbf{O} - C$	533.15 ± 0.01	1.48 ± 0.04	$BE = BE$ $(O1s\ TiO_2) + 3.00eV$	$GL(30)$
$O1s$ $P - \mathbf{O} - Ti$ $NC - \mathbf{O}$ $Ti - \mathbf{O} - H$	531.61 ± 0.01	1.63 ± 0.34	$BE = BE$ $(O1s\ TiO_2) + 1.46eV$	$GL(30)$
$O1s$ $P = \mathbf{O}$	530.95 ± 0.01	1.48 ± 0.04	$fwhm = fwhm$ $(O1s\ C\mathbf{O}C);$ $area = area$ $(O1s\ C\mathbf{O}C);$ $BE = BE$ $(O1s\ TiO_2) + 0.80eV$	$GL(30)$
$O1s$ TiO_2	530.15 ± 0.01	1.29 ± 0.04	$none$	$GL(30)$
Ti 2p$_{1/2}$	464.43 ± 0.1	2.16 ± 0.04	$none$	$GL(30)$
Ti 2p$_{3/2}$	458.66 ± 0.04	1.11 ± 0.01	$none$	$GL(30)T(3)$
$C1s$ $N - \mathbf{C} - O$	288.50 ± 0.1	1.38 ± 0.02	$fwhm = fwhm$ $(C1s\ ali - aro)$	$GL(30)$
$C1s$ $\mathbf{C}O$ $\mathbf{C}N$ $\mathbf{C}P$	286.50 ± 0.1	1.56 ± 0.05	$area = area$ $(C1s\ ali - aro) * 0.23$	$GL(30)$
$C1s$ aliphatic aromatic	285	1.38 ± 0.02	$none$	$GL(30)$
P 2p$_{1/2}$	133.85 ± 0.1	1.50 ± 0.11	$BE = BE$ $(P2p3/2) + 0.81eV;$ $area = area$ $(P2p3/2) * 0.5$	$GL(30)$
P 2p$_{3/2}$	133.04 ± 0.1	1.50 ± 0.11	$none$	$GL(30)$
$N1s$	400.41 ± 0.1	1.91 ± 0.1	$none$	$GL(30)$

Table 3.8: Thickness of the SAMs with molecule **21** after 26 and 72 hours. The film thickness was determined by VASE M-2000F

Time	[Å]
26 hours	12.21 ± 0.8
72 hours	14.89 ± 1.9

3.3.2 Attempted Polymerization of Pre-assembled 21

In this chapter we will describe different polymerization attempts after self-assembly of compound **21**. We tried two methods to prove polymerization directly on the surface, first one is the stability test at pH 2 and pH 9 and the second one is comparison of bulk monomer and polymer on the substrate which will be discussed in the following chapter.

Self-assembly, UV irradiation and stability tests (at pH 2 and pH 9) with compounds 21 and AHP (ammonium-12-hydroxydodecyl-phosphate)

The samples were assembled according to the protocols presented in chapter 3.3.1. After self-assembly of compounds **21** and **AHP** the thickness of the films were determined by VASE (table 3.9). The formed films were separately exposed to UV irradiation or polymerized with a radical initiator. UV irradiation was carried out at 366 nm under N$_2$-atmosphere at room temperature for 5 minutes and once with photo initiator Irgacure 2959 in EtOH (5 mg/1 ml) under N$_2$-atmosphere at room temperature for 5 minutes. Radical polymerization was attempted with AIBN-TEMPO (2,6-diethyl-2,6-dimethyl-1-(1-phenylethoxy)piperidin-4-one) under N$_2$-atmosphere in benzene at 80 °C for 12 h. Afterwards all the substrates were rinsed with appropriate solvent, blow-dried with nitrogen and the film thickness were measured by VASE. In the next step the substrates were dipped into HCl (pH 2) or NaOH (pH 9) solutions at room temperature for 12 hours, rinsed with water, blow-dried with nitrogen and the remaining film thickness measured again (Figure 3.6).

After UV irradiation and polymerization of compound **21** a large increase in thickness was observed on AIBN-TEMPO treated substrates (table 3.9). This thickness may originated from remaining radical initiator fragments on the substrate.

Solution of
surface-active
material

+

Substrate

Immersion time
48h

self-assembly

UV-irradiation
366 nm
5 min.
N_2

Irgacure 2959
UV-irradiation
366 nm
EtOH
5 min.
N_2

AIBN-TEMPO
radical polymerization
benzene
80° C
12 h
N_2

pH 2
at rt
12 h

pH 9
at rt
12 h

pH 2
at rt
12 h

pH 9
at rt
12 h

pH 2
at rt
12 h

pH 9
at rt
12 h
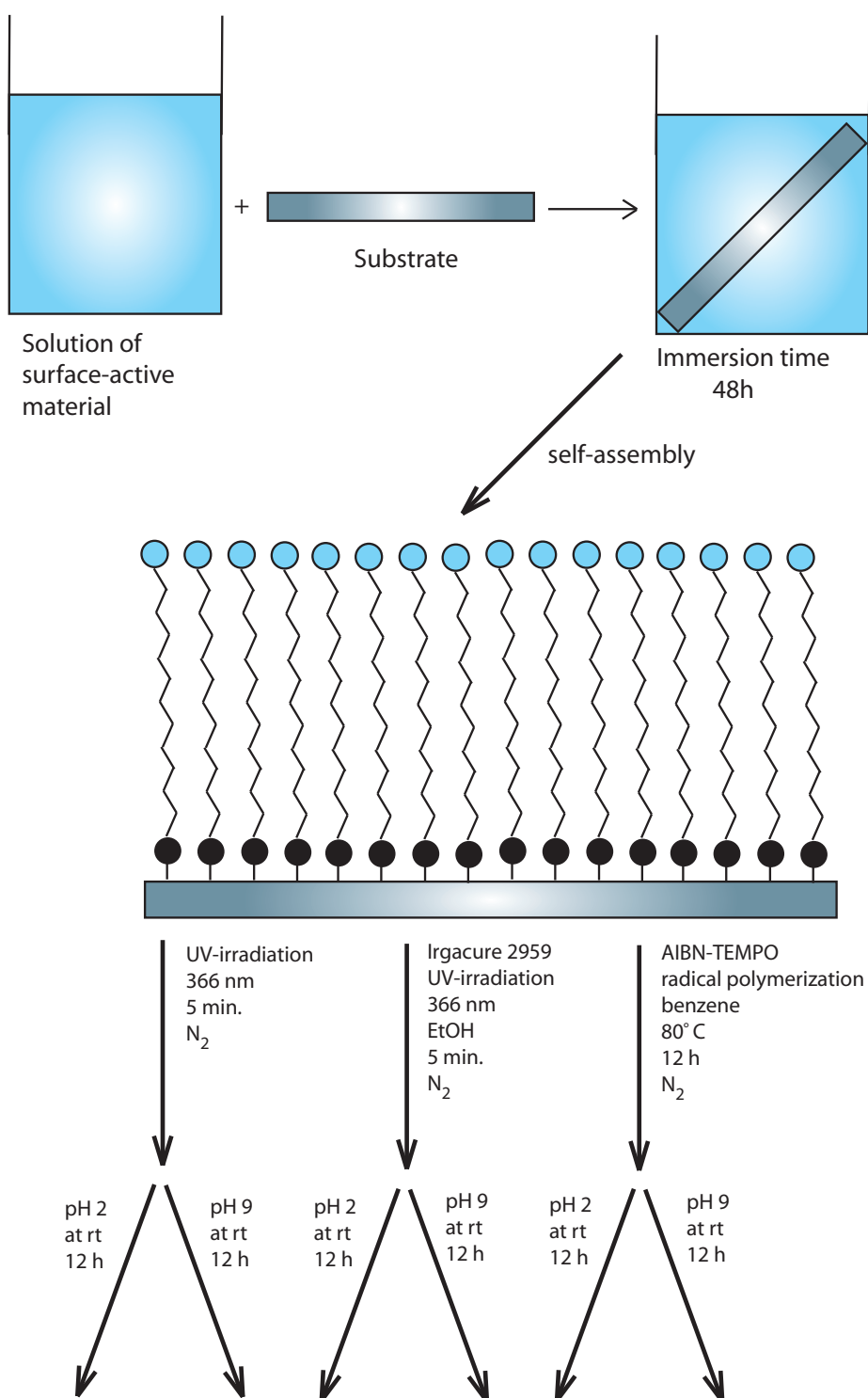
Figure 3.6: Flow chart of self-assembly, UV-irradiation at 366 nm, Irgacure 2959 UV-irradiation, AIBN-TEMPO radical polymerization and stability test at pH 2 and pH 9

After pH 2 treatment we did not observe a large change in film thickness, whereas after pH 9 treatment we observed a large decrease in film thickness for all of the samples. This decrease in film thickness showed that at pH 9 some P-O covalent bonds break and the molecules are removed from the surface. However, we do not expect any changes in SAMs thickness after polymerization. The change in thickness of compound **21** was compared with the thickness change of compound **AHP**, which does not has the possibility to polymerize and therefore should be removed much more easier, compared to polymerized **21** [will be submitted for publication].
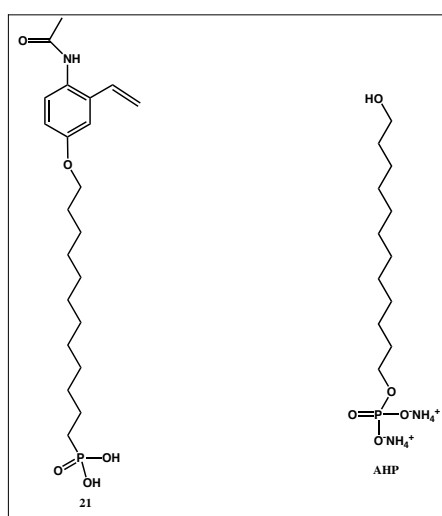
Figure 3.7: Structure of **21** and **AHP** (ammonium-12-hydroxydodecyl-phosphate)

Table 3.9: Average film thickness for compound **21** were measured before and after UV irradiation (254 and 366 nm) or radical polymerization. Stability tests at pH 2 and pH 9 were carried out at room temperature for 12 hours and film thicknesses were measured

	Thickness [Å]	attempt of polymerization	after pH 2	after pH9
21 SAMs	15.0 ± 1.5		21.9 ± 2.9	6.1 ± 4.4
AHP SAMs	18.9 ± 1.0		15.1 ± 0.6	3.4 ± 3.0
UV irradiation at 366 nm		15.5 ± 1.3	18.3 ± 3.2	2.7 ± 0.3
Irgacure 2959 UV irradiation		17.4 ± 1.8	16.2 ± 0.8	8.1 ± 1.6
AIBN-TEMPO polymerization		31.8 ± 6.5	19.9 ± 5.5	13.2 ± 4.6

As an additional comparison, polymer **28** was assembled according to the protocols presented in chapter 3.3.1. After self-assembly of compound **28** for 48 hours

the SAMs were again tested for their stability at pH2 and pH 9 (table 3.10). After
pH 2 treatment the SAMs lose some thickness, but the more important result is seen
after pH 9 treatment: with self-assembled copolymer there is still a remaining layer
thickness of 14.8 Å. The comparison with self-assembly of **21** (Table 3.9) proves the
higher stability of polymer **28** (Figure 3.10) on the surface.

Table 3.10: Thickness of the SAMs with polymer **28** after 48 hours, pH 2 and pH 9 treatment.
The film thickness was determined by VASE M-2000F

	Thickness [Å]	after pH 2 [Å]	after pH 9 [Å]
48 hours	28.8 ± 3.7	23.1 ± 1.2	14.8 ± 2.1

UV-irradiation of Monomers Directly on the Surface

In order to distinguish polymerization on surface we attempted to UV-irradiate
compounds **7** and **22**. The spectra show vinyl bands of the molecule at 1602 cm^{-1}
(Figure 3.8). Polymerization attempted by Stratagene UV Stratalinker 2400 on TiO$_2$
(8 nm) - gold (80nm) wafer with maximum energy (999 microjoule) at 254 nm. IR
measurements before and after UV exposure showed no change in absorbance at
the vinyl band (1602 cm^{-1}). This result proves that the polymerization attempts of
compounds **7** and **22** were not successful.
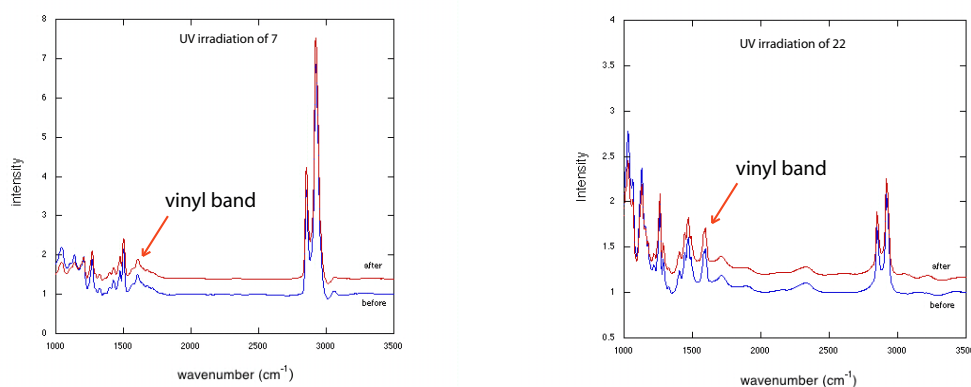
Figure 3.8: PM-IRRAS spectra in the vinyl band region of compound **7** and **22**. The spectra
shows UV irradiation of the bulk compounds at room temperature with 999 microjoule.

PM-IRRAS measurements of the SAMs of compound **22** were carried out on
TiO$_2$ (8 nm) covered gold (80 nm) substrates. The bands at 2920 cm^{-1} and 2850

cm^{-1} are assigned to the symmetric and anti-symmetric strecthing modes of the methylene groups. These bands show up at 2930 cm^{-1} and 2858 cm^{-1} (Figure 3.9) which show that alkyl chains are not well ordered [33] [34] [35].
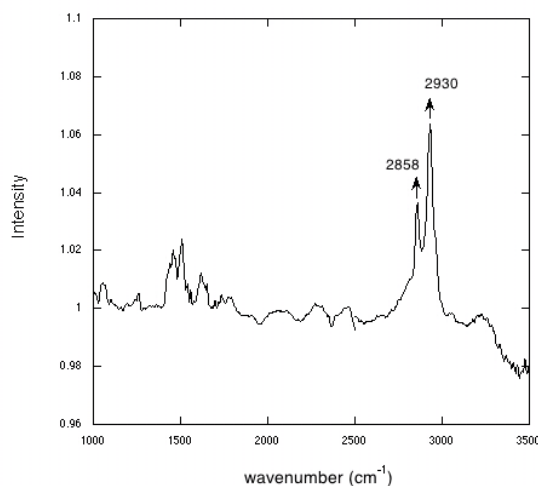
Figure 3.9: PM-IRRAS spectra of compound **22** after self-assembly.

Comparison of bulk monomer and polymer by PM-IRRAS

Another method to distinguish the polymerization on surface is comparison of bulk monomer and polymer on the substrate. We attempted to distinguish between polymerized **21** and monomeric **21** by PM-IRRAS. The two thick films of either **21** or **16** (homopolymer of **21**) were spin coated on gold substrates. The PM-IRRAS measurement of the two compounds is shown in Figure 3.10. Unfortunately, the band from the vinyl group at 1602 cm^{-1} is overlapped by strong aromatic bands which makes it very difficult to use this technique as a test method for polymerization of **21**.
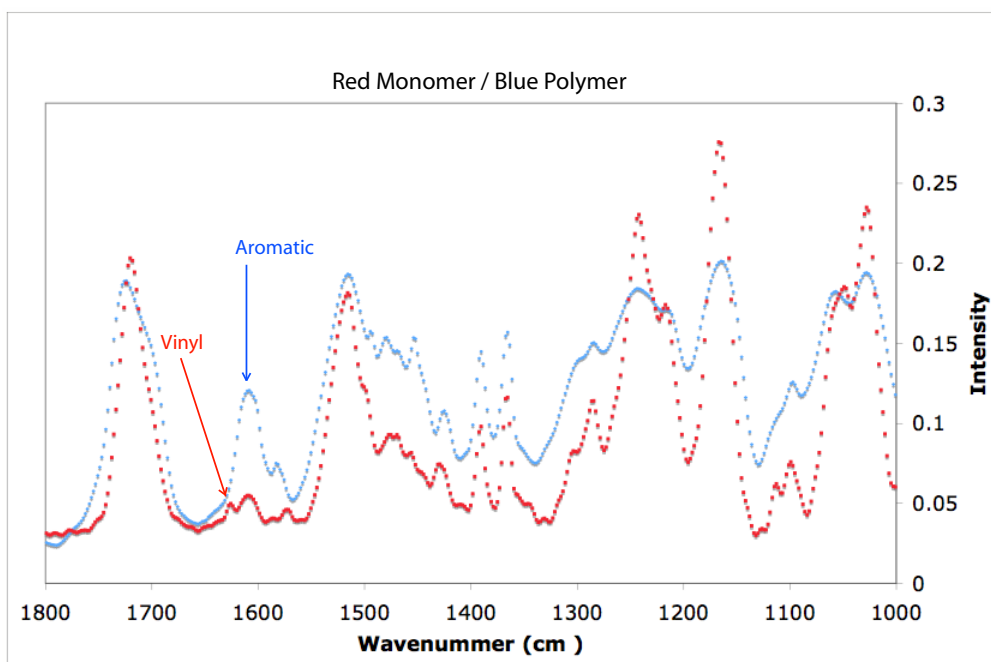
Figure 3.10: Comparison of bulk monomer and polymer on the substrate by PM-IRRAS

3.3.3   Adsorption of Phosphonic Acid Polymers and Phosphonic Acid Styrene Copolymer

Adsorption of compound 28

XPS:

The self-assembled monolayers for all investigated polymeric phosphonates were analyzed at 53° takeoff angle. The detailed spectra for O 1s, Ti 2p, C 1s and P 2p were resolved into their components using a fitting procedure as described in chapter 3.3.1. The used parameters are presented in table 3.11 (in comparison to **21** there is no NCO component at 288.50 eV for **28**).

Atomic concentrations of the SAMs were calculated and compared with theoretical values (Table 3.12). The found atomic concentrations of O and C are pretty close to calculated values, which shows us that we have successfully self-assembled polymer (**28**) on TiO_2 substrates. After self-assembly of compound **28** for 48 hours the thickness of the films were determined by VASE.

Table 3.11: XPS Binding energies and Fitting Parameters for compound **28** (Data measured on VG Theta Probe spectrophotometer)

	Binding Energy (BE)[eV]	Full Width at Half Maximum fwhm [eV]	constraints	Line Shape% Gauss−Lorentz and asymetry [Lit Casa]
O1s C − **O** − C	533.15 ± 0.01	1.48 ± 0.04	$BE = BE$ $(O1s\ TiO_2) + 3.00eV$	$GL(30)$
O1s P − **O** − Ti Ti − **O** − H	531.61 ± 0.01	1.63 ± 0.34	$BE = BE$ $(O1s\ TiO_2) + 1.46eV$	$GL(30)$
O1s P = **O**	530.95 ± 0.01	1.48 ± 0.04	$fwhm = fwhm$ $(O1s\ C\mathbf{O}C);$ $area = area$ $(O1s\ C\mathbf{O}C);$ $BE = BE$ $(O1s\ TiO_2) + 0.8eV$	$GL(30)$
O1s TiO$_2$	530.15 ± 0.01	1.29 ± 0.04	$none$	$GL(30)$
Ti 2p$_{1/2}$	464.43 ± 0.1	2.16 ± 0.04	$none$	$GL(30)$
Ti 2p$_{3/2}$	458.66 ± 0.04	1.11 ± 0.01	$none$	$GL(30)$
C1s **C**O **C**N **C**P	286.50 ± 0.1	1.56 ± 0.05	$fwhm = fwhm$ $(C1s\ ali - aro)$	$GL(30)$
C1s aliphatic aromatic	285	1.38 ± 0.02	$none$	$GL(30)$
P 2p$_{1/2}$	133.85 ± 0.1	1.50 ± 0.11	$BE = BE$ $(P2p3/2) + 0.84eV;$ $area = area$ $(P2p3/2) * 0.5$	$GL(30)$
P 2p$_{3/2}$	133.04 ± 0.1	1.50 ± 0.11	$none$	$GL(30)$
N1s	400.41 ± 0.1	1.91 ± 0.1	$none$	$GL(30)$

Table 3.12: Atomic concentrations of the SAMs of compound **28** compared to theoretically calculated values. The numbers are average values of at least three samples (VG Theta Probe spectrophotometer)

time	O %	N %	C %	P %
calculated	11.7	2.9	82.4	3.0
found 18 hours	13.9 ± 0.8	3.6 ± 0.2	79.0 ± 1.1	3.5 ± 0.2

Self-assembly of monomer 22*, homopolymer 26 and copolymer 28

The monolayer formation was the same as in the previous chapter. The formed films of compound **22*** were separately exposed to UV irradiation. UV irradiation was carried out at 254 and 366 nm under N_2-atmosphere at room temperature for 5 minutes and once with photo initiator Irgacure 2959 in EtOH (5 mg/1 ml) under N_2-atmosphere at room temperature for 5 minutes. Afterwards all the substrates were rinsed with appropriate solvent, blow-dried with nitrogen and the film thickness were measured by VASE. The aniline compound **22*** synthesized according to the new synthetic protocol (no side product **13a**) forms now very reproducible SAMs with a layer thickness very close to the calculated length of the molecules. The same is true for the copolymer **28**. In contrast, the homopolymer **26** does not form reproducibly thick layers. This is most probably due to steric repulsion and configuration of this polymer which hinders a nice assembly on the surface.

Table 3.13: Thickness of the SAMs with monomer (**22***) and polymers (**26**, **28**) after 20 hours. The film thickness was determined by VASE M-2000F

Compound	Thickness [Å]
22* Aniline SAMs	21.5 ± 1.5
26 Homopolymer SAMs	16.4 ± 9.0
28 Copolymer SAMs	23.3 ± 0.5

3.3.4   Influence of Adsorption Parameters: Concentration and Time for self-assembly

The self-assembly processes of alkyl thiols onto gold are known to be very fast. Thiols adsorb on the gold surface and are able to diffuse laterally. The lateral displacement allows for dense packing of the final monolayer. Phosph(on)ate SAMs are believed to grow in the form of islands [36]. The monolayers are then completed by coalescence of these islands.

Concentration vs. Thickness and Contact Angle

In this chapter we have studied the effect of the polymer concentration versus thickness and contact angle. Four different concentrations 0.025 to 0.25 x 10^{-3} mM were prepared in DMSO/H$_2$O (1:10 v:v) and self-assembled for 48 h.
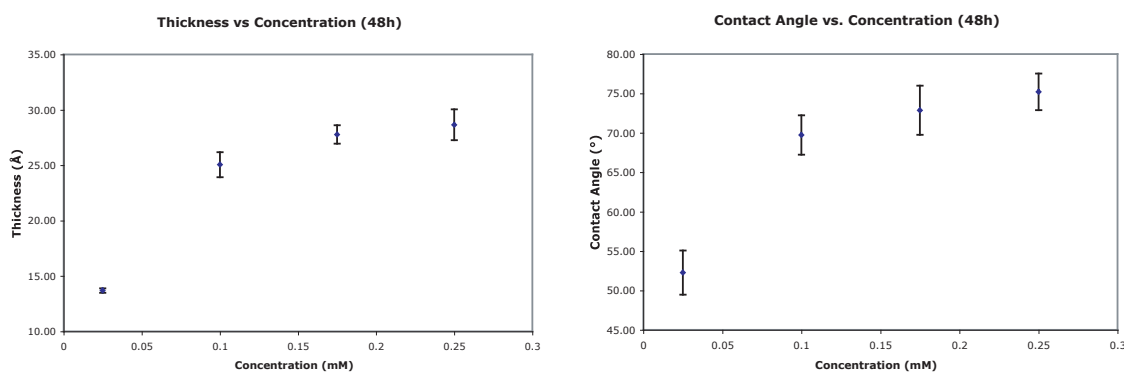

Figure 3.11: Thickness and contact angle vs. concentration of the SAMs with compound **28**. The film thickness was determined by VASE M-2000F. Contact angle was measured using Ramè-hart goniometer

The 0.025 mM solution of compound **28** showed lower coverage of the metal oxide by VASE and CA measurements. The wettability of 0.025 nM is relatively lower than, at other concentrations. According to VASE and contact angle measurments 0.025 mM is definitely too low in concentration for formation of a complete monolayer within 48 h (Figure 3.11).

Time vs. Thickness and Concentration

We continued with the study of the time needed for self-assembly of compound **28**. VASE measurement showed that the thickness of the adsorption is increasing within the first hours (Figure 3.12). As we stated in the previous chapter we observed an increase in film thickness between 26 h and 72 h (table 3.8). We believe that more surface-bound hydroxyl groups will be replaced by the adsorption of molecules and they interact with neighboring molecules, which decreases the final tilt angle of the molecules.
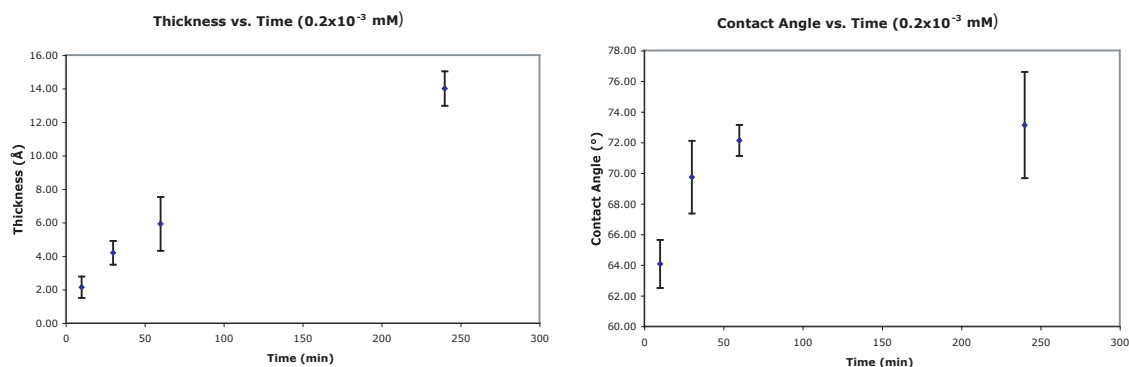
Figure 3.12: Thickness and contact angle vs. time of the SAMs with compound **28**. The film thickness was determined by VASE M-2000F. Contact angle was measured using Ramè-hart goniometer

Comparison of the results from the two methods demonstrate that both VASE and contact angle measurements can be used as sensitive methods to observe for SAM formation for compound **28**. From these data as well as other observations we think that the self-assembled monolayer method needs at least 0.1 mM concentration and 20 hours time to assemble on the surface.

3.3.5   Cinnolines

As stated in chapter 3.1.2 we have found two new compounds **4a** and **4b** which are highly luminescent. In literature we have found two similar molecules which were synthesized with different methods [20], [22], [21] (Scheme 3.17). Triphenyldiazenium was synthesized by electrochemistry and radical reaction whereas Benzo[c]cinnoline by photochemical cyclohydrogenation. In our case **4a** and **4b** were synthesized using a Pd-catalyzed Suzuki cross-coupling reaction [15] [16] [17] (Scheme 3.18, 3.19). The reagent used to introduce vinyl group is trivinylboronic acid anhydride pyridine [18]. This reaction is rather straightforward and can be easily be scaled up to large quantities.

We speculate that this reaction could be useful for the synthesis of large chromophores (Scheme 3.18) which could be used as organic light emiting diods (OLED), for example in displays (LCDs). Therefore it would be interesting to study if paladium-catalyzed reactions are possible with different substituents and different boronic acids for example to synthesize other cinnoline compounds under similar

Triphenyldiazenium

Benzo[c]cinnoline
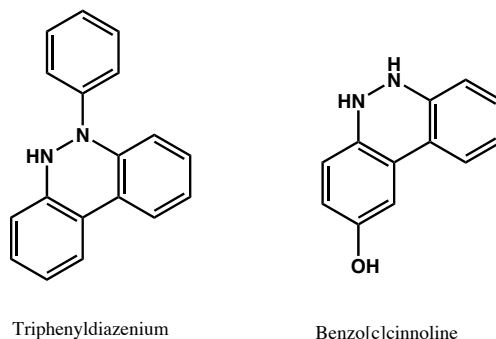
Scheme 3.17: Structure of two cinnolines that have been synthesized so far [20], [22], [21].
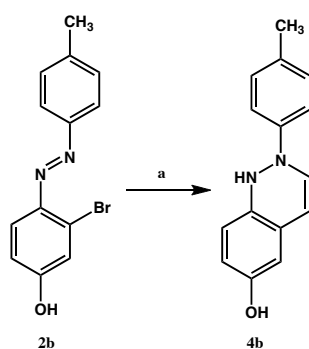
Scheme 3.18: Synthesis of 2-p-tolyl-1,2-dihydrocinnolin-6-ol. (a) (E)-3-bromo-4-(p-tolyldiazenyl)phenol **2b**, dimethoxymethane, tetrakistriphenylphosphine palladium, K$_2$CO$_3$, (vinyl boronic acid) trimer, H$_2$O, 89° C, 16h.
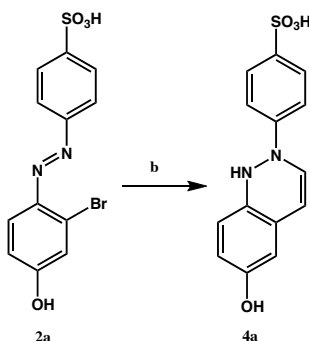
Scheme 3.19: Synthesis of 4-(6-hydroxycinnolin-2(1H)-yl)benzenesulfonic acid. (b) (E)-4-((2-bromo-4-hydroxyphenyl)diazenyl)benzenesulfonic acid **2a**, dimethoxymethane, tetrakistriphenylphosphine palladium, K$_2$CO$_3$, (vinyl boronic acid) trimer, H$_2$O, 89° C, 16h.

conditions with different types of boronic acids like phenylboronic acid (Scheme 3.19). If the generality of the reaction could be proved, it would be a method to synthesize a whole class of new highly conjugated molecules.
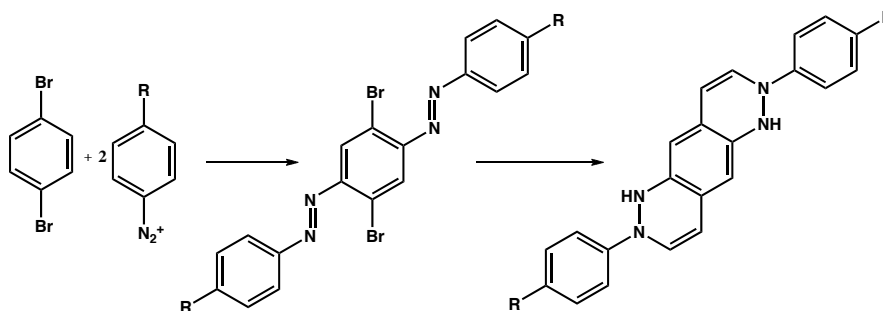
Scheme 3.20: Structure of possible chromophores which could be synthesized by the new developed Pd-cross coupling reaction.
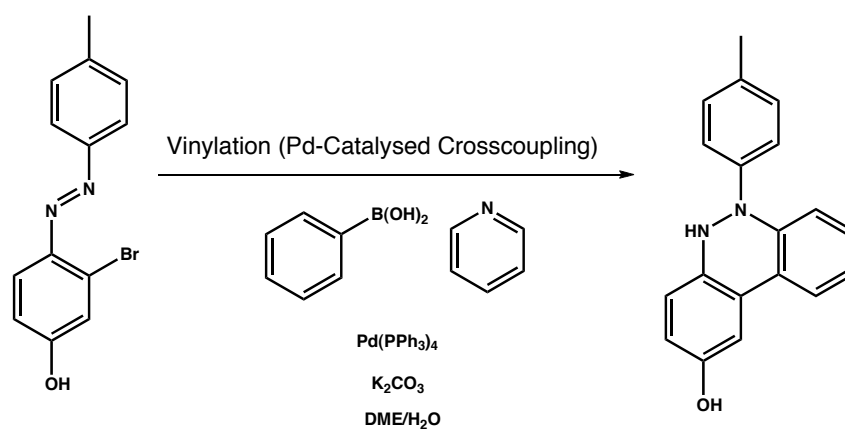
Scheme 3.21: Proposed synthesis of a new Benzo[c]cinnoline derivative using an aromatic borate

References

[1] Nuzzo, R. G. and Allara, D. L. Adsorption of Bifunctional Organic Disulfides on Gold Surfaces. *Journal of the American Chemical Society*, **105**(13), 4481–4483, 1983.

[2] Textor, M., Ruiz, L., Hofer, R., Rossi, A., Feldman, K., Hahner, G. and Spencer, N. D. Structural chemistry of self-assembled monolayers of octadecylphosphoric acid on tantalum oxide surfaces. *Langmuir*, **16**(7), 3257–3271, 2000.

[3] Brovelli, D., Hahner, G., Ruiz, L., Hofer, R., Kraus, G., Waldner, A., Schlosser, J., Oroszlan, P., Ehrat, M. and Spencer, N. D. Highly oriented, self-assembled alkanephosphate monolayers on tantalum(V) oxide surfaces. *Langmuir*, **15**(13), 4324–4327, 1999.

[4] Hofer, R., Textor, M. and Spencer, N. D. Alkyl phosphate monolayers, self-assembled from aqueous solution onto metal oxide surfaces. *Langmuir*, **17**(13), 4014–4020, 2001.

[5] Silverman, B. M., Wieghaus, K. A. and Schwartz, J. Comparative properties of siloxane vs phosphonate monolayers on a key titanium alloy. *Langmuir*, **21**(1), 225–228, 2005.

[6] Huang, N. P., Voros, J., De Paul, S. M., Textor, M. and Spencer, N. D. Biotin-derivatized poly(L-lysine)-g-poly(ethylene glycol): A novel polymeric interface for bioaffinity sensing. *Langmuir*, **18**(1), 220–230, 2002.

[7] Lee, H., Kepley, L. J., Hong, H. G. and Mallouk, T. E. Inorganic Analogs of Langmuir-Blodgett Films - Adsorption of Ordered Zirconium 1,10-Decanebisphosphonate Multilayers on Silicon Surfaces. *Journal of the American Chemical Society*, **110**(2), 618–620, 1988.

[8] Michaelis, A. *Ber*, **31**, 1048, 1898.

[9] Arbuzov, A. E. *J. Russ. Phys. Chem. Soc.*, **38**, 687, 1906.

[10] Arbuzov, A. E. *Chem. Lett.*, **II**, 1639, 1906.

[11] Hazard, R. and Tallec, A. Electrochemical Preparation of Nu-Hydroxyindoles .2. Controlled Potential Oxidation of Some "Alpha-(O-Hydroxyaminophenyl)Alkenes. *Bulletin De La Societe Chimique De France Partie Ii-Chimie Moleculaire Organique Et Biologique*, **1-2**, 121–125, 1974.

[12] Reiser, A. Positive-working photoresist for microlithography, 1999.

[13] Bahulayan, D., John, L. and Lalithambika, M. Modified clays as efficient acid-base catalyst systems for diazotization and diazocoupling reactions. *Synthetic Communications*, **33**(6), 863–869, 2003.

[14] Mu, F. R., Coffing, S. L., Riese, D. J., Geahlen, R. L., Verdier-Pinard, P., Hamel, E., Johnson, J. and Cushman, M. Design, synthesis, and biological evaluation of a series of lavendustin A analogues that inhibit EGFR and Syk tyrosine kinases, as well as tubulin polymerization. *Journal of Medicinal Chemistry*, **44**(3), 441–452, 2001.

[15] Chemler, S. R., Trauner, D. and Danishefsky, S. J. The B-alkyl Suzuki-Miyaura cross-coupling reaction: Development, mechanistic study, and applications in natural product synthesis. *Angewandte Chemie-International Edition*, **40**(24), 4544–4568, 2001.

[16] Miyaura, N. and Suzuki, A. Palladium-Catalyzed Cross-Coupling Reactions of Organoboron Compounds. *Chemical Reviews*, **95**(7), 2457–2483, 1995.

[17] Suzuki, A. Recent advances in the cross-coupling reactions of organoboron derivatives with organic electrophiles, 1995-1998. *Journal of Organometallic Chemistry*, **576**(1-2), 147–168, 1999.

[18] Kerins, F. and O'Shea, D. F. Generation of substituted styrenes via Suzuki cross-coupling of aryl halides with 2,4,6-trivinylcyclotriboroxane. *Journal of Organic Chemistry*, **67**(14), 4968–4971, 2002.

[19] Antonios, O. A. and James, W. C. Observation of Catalytic Intermediates in the Suzuki Reaction by Electrospray Mass Spectroscopy. *Journal of the American Chemical Society*, **116**(15), 6985–86, 1994.

[20] Cauquis, G. and Reverdy, G. Electrochemistry of Photochemical Cyclodehydrogenation of Triphenyldiazenium Cation. *Tetrahedron Letters*, **37**, 3267–3270, 1977.

[21] Lewis, G. E., Prager, R. H. and Ross, R. H. M. Benzo[C]Cinnoline Derivatives .7. Reactions of Benzo[C]Cinnoline and Chlorobenzo[C]Cinnolines with Lithium Dimethylamide. *Australian Journal of Chemistry*, **28**(11), 2459–2477, 1975.

[22] Wittig, G. and Schuhmacher, A. Uber Dihydrophenazonyl-Radikale. *Chemische Berichte-Recueil*, **88**(2), 234–246, 1955.

[23] Chen, C. Y., Dagneau, P., Grabowski, E. J. J., Oballa, R., O'Shea, P., Prasit, P., Robichaud, J., Tillyer, R. and Wang, X. Practical asymmetric synthesis of a potent cathepsin K inhibitor. Efficient palladium removal following Suzuki coupling. *Journal of Organic Chemistry*, **68**(7), 2633–2638, 2003.

[24] Fieser, L. F., Gates, M. D. and Kilmer, G. W. Quinonyl derivatives of fatty acids. *Journal of the American Chemical Society*, **62**, 2966–2970, 1940.

[25] Vigroux, A., Bergon, M. and Zedde, C. Cyclization-Activated Prodrugs - N-(Substituted 2-Hydroxyphenyl and Alpha-Hydroxypropyl)Carbamates Based on Ring-Opened Derivatives of Active Benzoxazolones and Oxazolidinones as Mutual Prodrugs of Acetaminophen. *Journal of Medicinal Chemistry*, **38**(20), 3983–3994, 1995.

[26] Rybtchinski, B., Sinks, L. E. and Wasielewski, M. R. Combining light-harvesting and charge separation in a self-assembled artificial photosynthetic system based on perylenediimide chromophores. *Journal of the American Chemical Society*, **126**(39), 12268–12269, 2004.

[27] Gaboyard, M., Hervaud, Y. and Boutevin, B. Synthesis and structural analysis of alkylphosphonic acids with a long hydrocarbon chain. *Phosphorus Sulfur and Silicon and the Related Elements*, **177**(4), 877–891, 2002.

[28] Watanabe, T., Hayashi, K., Yoshimatsu, S., Sakai, K., Takeyama, S. and Takashima, K. Studies of Hypolipidemic Agents .1. Synthesis and Hypolipidemic Activities of Alkoxycinnamic Acid-Derivatives. *Journal of Medicinal Chemistry*, **23**(1), 50–59, 1980.

[29] Harris, J. M. *Poly(ethylene glycol) chemistry: biotechnical and biomedical applications.* Plenum Press, New York, 1992.

[30] Jeon, S. I., Lee, J. H., Andrade, J. D. and Degennes, P. G. Protein Surface Interactions in the Presence of Polyethylene Oxide .1. Simplified Theory. *Journal of Colloid and Interface Science*, **142**(1), 149–158, 1991.

[31] Bjoerling, M. Interaction between Surfaces with Attached Poly(ethylene oxide) chains. *Macromolecules*, **25**, 3956–70, 1992.

[32] Morra, M. *Poly(ethylene oxide) Coated Surfaces in Water in Biomaterials Surface.* Chichester, 2001.

[33] Nuzzo, R. G., Korenic, E. M. and Dubois, L. H. Studies of the Temperature-Dependent Phase-Behavior of Long-Chain Normal-Alkyl Thiol Monolayers on Gold. *Journal of Chemical Physics*, **93**(1), 767–773, 1990.

[34] Macphail, R. A., Strauss, H. L., Snyder, R. G. and Elliger, C. A. C-H Stretching Modes and the Structure of Normal-Alkyl Chains .2. Long, All-Trans Chains. *Journal of Physical Chemistry*, **88**(3), 334–341, 1984.

[35] Snyder, R. G., Strauss, H. L. and Elliger, C. A. C-H Stretching Modes and the Structure of Normal-Alkyl Chains .1. Long, Disordered Chains. *Journal of Physical Chemistry*, **86**(26), 5145–5150, 1982.

[36] Stranick, S. J., Atre, S. V., Parikh, A. N., Wood, M. C., Allara, D. L., Winograd, N. and Weiss, P. S. Nanometer-scale phase separation in mixed composition self-assembled monolayers. *Nanotechnology*, **7**(4), 438–442, 1996.

Experimental Section

4.1 Materials and methods

4.1.1 Analysis

NMR spectroscopy:

Nuclear magnetic resonance spectra were recorded with a Bruker 300 or 500 MHz spectrometer with the corresponding solvent signals as internal standards. Chemical shifts are reported in parts per million (ppm). Values of the coupling constant, J, are given in Hertz (Hz). The following abbreviations are used in the experimental section for the description of ^{1}H-NMR spectra: singlet (s), doublet (d), triplet (t), multiplet (m), doublets of doublet (dd), broad singlet (bs). The chemical shifts of complex multiplets are given by means of the range of their occurrence. The deuterated solvents were purchased from Merck, Fluka or Acros.

Elemental analysis:

It was used a Leco CHN-900, CHS-932 and RO-478.

Melting point:

Melting points were measured by BÜCHI B-540.

Chromatographic Methods

Analytical TLC

Reactions were checked by TLC with TLC-ready charts by Merck (plastic sheets with silica gel Si 60) or TLC-ready charts by Macherey-Nagel (Polygram Alox N/UV$_{254}$, ready foils with 0.2 mm aluminium oxide with fluorescent indicator F254). detection was in UV light with wavelength $\lambda = 254$ or $\lambda = 366$ nm.

Preparative column chromotography:

The chromotography was run with Fluka flash silica gel (230-400 mesh ASTM).

Analytical GPC:

Measurements were performed with a Viscotek GPCmax VE 2001GPC solvent/sample module and data were evaluated by Omnisec 4.0 software.

4.1.2   Substrates

Si-wafer samples were purchased in the form of 6-inch wafers mounted on a polymeric foil that was used to support the cutting of the wafer to the desired size (Powatec, Cham Switzerland).

Preparation of TiO$_2$ Layers

Titanium metal surfaces spontaneously form a natural amorphous oxide film. Therefore, the adsorption takes place at the metal oxide. Titaniumdioxide films were deposited by a sputter-coating process on silicon wafers (PSI, Villigen, CH). In order to ensure that no contaminants are present at the interface between the Si-wafer and the subsequently thin sputter coating, the following three types of contamination had to be removed:

(1) Dust created during handling and removal of the Si-wafer from the polymeric foil support

(2) Glue residues on the backside of the Si-wafer

(3) Hydrocarbon contamination and absorbed water from the ambient atmoshere

Gold Coating

Before starting with gold coating, the wafers were sonicated for 10 minutes with toluene and dried with N_2-gas. Then they were cleaned with piranha solution and rinsed many times with water. Afterwards they were washed with ethanol, dried with N_2-gas and plasma treated. The formation of an 80 nm gold film was carried out by a physical vapor deposition process (BAL-TEC Multi Control System 010 MED 020 Coating Systems).

4.1.3   Cleaning of the Substrate Surfaces

All substrates were placed in a highly clean PTFE container and treated in an ultrasonic bath with 2-propanol for 10 minutes. It is very important to place the samples in a vertical position to remove microscopically small particles, such as silicon powder, during the sonication. Such small particles cannot be removed by simply blowing them away, not even with a strong gas stream. The samples were removed from 2-propanol and blow-dried in a nitrogen stream followed by an additional cleaning in a UV-ozone cleaner for 30 minutes or in an oxygen-plasma cleaner for 2 minutes, right before the assembly process.

Sonicator: Bandelin Model Sonorex super 10P

UV-1: Boekel Industries, Inc. UV Clean Model 135500

UV-2: OmniLAB UV-Ozone Photoreactor^{TM} Ultra Violet Products Model PR-100

Plasma-1:   Harrick Scientific Corp.   Ossining, New York Plasma Cleaner/Sterilizer Model PDC-002 (PIN 191-500)

Plasma-2: Harrick Plasma Cleaner/Sterilizer Model PDC-32G

Plasma-3:   Harrick Scientific Corp.   Ossining, New York Plasma Cleaner/Sterilizer Model PDC-002 (PIN 191-500)

Plasma-4: Harrick Plasma Cleaner/Sterilizer Model PDC-32G

4.1.4   Chemicals

All commercially available substances were purchased from Fluka, Aldrich, Merck, or Acros, and used without further purification.

4.2   Instruments

The following items of apparatus were used for specific parts of the work and have therefore been separated into different subchapters.

4.2.1   Apparatus for the Cleaning and Coating of the Substrates

The following instruments were used for specific parts of the work:

Ultrasonic Bath Sonication in general performed in a Ultrasonic bath Branso 5210 for 10 minutes.

UV-cleaner We used two different UV-cleaner in our experiments: UV-Ozone Cleaner Model 135500 Boekel Industries; Inc. in Laminar flow box Skan USA-180 for surface preparation & UV-Ozone Photoreaktor Ultra-Violet Products.

Oxygen plasma cleaner The apparatus used for the experiments are: Plasma Cleaner/Strilizer Harrick & Plasma Cleaner/Sterilizer Harrick PDC-32G.

4.2.2   Glassware and Tools Cleaning

All glass containers were cleaned with piranha acid (volume 7:3 H_2SO_4:H_2O_2), followed by extensively rinsing with ultrapure water until the water was pH-neutral to ensure that all organic and inorganic contaminations have been removed. In order to be sure that no soluble contaminants, which could compete with the molecular assembly steps, are present, all containers were then washed several times with 2-propanol and/or ethanol. Before and after every batch of sample cleaning and coating processes these containers were treated in an ultrasonic bath with 2-propanol and/or ethanol for 10 minutes.

4.2.3   Preparation of Self-assembly Solution

The alkyl phosp(on)ate self-assembled monolayer system is very sensitive to contamination. Therefore, the solvents have to be of the highest quality, and free from any hydrocarbon contamination that could compete with the assembling molecules.

4.2.4   Surface Characterization

In this chapter, methods for quantitative surface analysis with an information depth of a few nanometers are presented. These methods were used for surface characterization before and after coating with adsorbates such as alkyl phosphonate SAMs.

X-ray Photoelectron Spectroscopy (XPS)

XPS analysis was performed using a PHI 5700 spectrophotometer (Physical Electronics, Eden Prairie, MN) and a VG Theta Probe spectrophotometer (Thermo Electron Corporation, West Sussex, UK).

PHI 5700 spectrophotometer: It was equipped with a concentric hemispherical analyzer. Spectra were acquired at a base pressure of 10^{-9} mbar or below using a non-monochromatic Al-Kα source operating at 350 W and positioned 10 mm away from the sample. The instrument was run in the minimum-area mode using an aperture of 0.4 mm diameter. The CHA was used in the fixed-analyzer-transmission mode. Pass energies used for survey scans and detailed scans were 187.85 ad 46.95 eV, respectively for titanium Ti2p, carbon C1s, oxygen O1s, and phosphorus P2p. Under these conditions, the energy resolution (full width at half maximum height, fwhm) measured on silver Ag3d$_{5/2}$ is 2.7 ad 1.1 eV, respectively. Acquisition times were approximately 5 min for survey scans and 15 min (total) for high-energy-resolution elemental scans. These experimental conditions were chosen in order to have an adequate signal-to -noise ratio in a minimum time and to limit beam-indiced damage. Under these conditions, sample damage was negligible, and reproducible analyzing conditions were obtained on all samples. In addition, only one sample was introduced into the analyzing chamber at a time. The measurements were performed with a takeoff angle of 53° with respect to the surface plane. All recorded spectra were referenced to the aliphatic hydrocarbon C1s signal at 285.0 eV.

VG Theta Probe spectrophotometer: It was equipped with concentric hemispherical analyzer and two-dimensional channel plate detector with 112 energy and 96 angle channels. Spectra at different locations on the sample were acquired at a base pressure of 10^{-9} mbar or below using a monochromatic Al-Kα source with a spot size of 300 μm. The analyzer was used in the constant analyzer energy mode. Pass energies used for survey scans and detailed scans are 200 and 50 eV, respectively for titanium 2p, carbon C1s, oxygen O1s, and nitrogen 1s. Acquisition times were approximately 15 min for high-energy-resolution elemental scans and 5 min for survey scans. These experimental conditions were chosen in order to obtain an adequate signal-to-noise ratio in a minimum time and to limit beam-indiced damage. Under these conditions, sample damage was negligible. All recorded spectra were referenced to the hydrocarbon C 1s signal at 285.0 eV. Data were analyzed using the program CASA XPS.

Variable Angle Spectroscopic Ellipsometer (VASE)

The thickness of films were determined by VASE (M-2000F, L.O.T Oriel GmbH, Germany). Measurements were conducted under ambient conditions at three angles of incidence (65, 70 and 75°) in the spectral range of 250 - 1000 nm. Measurements were fitted with the WVASE32 analysis software using a multilayer model for an oxide layer on silicon and organic adlayer (monomer and polymer). The n and k values for the oxide layers were fitted, and the adlayer thickness for film was determined using the Cauchy model.

Contact Angle

Contact-angle measurements were carried out by means of a Ramè-hart, Inc. NRL C.A. Goniometer (Model No 100-00-230). All the reported values are the average of advancing contact angles at 5 different spots per sample.

Infrared Spectroscopy (PM-IRRAS)

PM-IRRAS measurements were carried out on a Bruker IFS66v Spectrometer equipped with a PMA50 photoelastic modulator accessory. The interferrogram from the spectrometer was modulated with a ZnSe Photoelastic modulator (Hinds Co) at

a frequency of 50 kHz and was analyzed with a lock-in amplifier (Stanford Research, USA) . Typically 1024 scans were acquired at 8 cm^{-1} resolution. In these measurements 80 nm gold and 8 nm TiO$_2$ coated silicon oxide wafers were used (4 x 2 cm). The sample chamber was continuously purged with dry air during the measurement. The resulting spectra were baseline corrected with a polynomial background using the instruments OPUS software (Bruker Optics). The spectra showed strong bands in the frequency region below 1000 cm^{-1} arising from the TiO$_2$ layer. However, the regions of interest in this study are free of any interfering features from the TiO$_2$ layer underneath.

4.3   Syntheses

4.3.1   Synthesis of Monomer
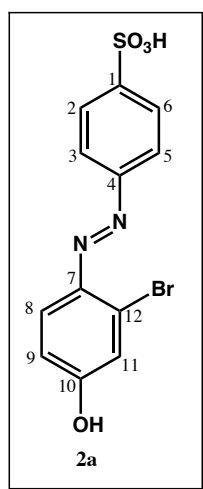
Figure 4.1: Structure of (E)-4-((2-bromo-4-hydroxyphenyl)diazenyl)benzenesulfonic acid **2a**.

Synthesis of (E)-4-((2-bromo-4-hydroxyphenyl)diazenyl) benzenesulfonic acid 2a. 4-Aminobenzenesulfonic acid (100 g, 0.58 mol) was suspended in 36 % hydrochloric acid (125 ml, 1.45 mol) and sodium nitrite solution (39.89 g, 0.58 mol in 300 ml water) was added dropwise at 0-5 °C. 3-bromophenol (100 g, 0.58 mol) was dissolved in sodium hydroxide solution (184 g, 4.62 mol in 500 ml water) and the previous solution containing 4-sulfobenzenediazonium was added slowly

to the orange bromophenol suspension. The reaction mixture was stirred at rt for 12h. The resulting orange suspension was made acidic with 150 ml 36 % hydrochloric acid to precipitate the product. Filtration at 0 °C gave (E)-4-((2-bromo-4-hydroxyphenyl)diazenyl)benzenesulfonic acid as an orange powder (151 g, 92 %).

^{1}H-NMR (500 MHz, CDCl$_3$) δ 7.82 (d, 2H, J=8.5 Hz, C^{3}H, C^{5}H), 7.66 (d, 1H, J=9 Hz, C^9), 7.28 (d, 2H, J=8 Hz, C^3, C^5), 7.20 (d, 1H, J=2.7 Hz, C^8), 6.81 (dd, 1H, J$_1$=2.7 Hz, J$_2$=9 Hz, C^{11}), 2.41 (s, 3H, CH$_3$) ppm.

^{13}C-NMR (125 MHz, CDCl$_3$) δ 158.33, 150.80, 143.87, 141.58, 129.76, 127.43, 123.11, 119.97, 115.35, 21.50 ppm.

EA C$_{12}$H$_9$N$_2$O$_4$SBr

Calculated: C: 40.35 H: 2.54 N: 7.84. Found: C: 38.00 H: 3.08 N: 6.35.

MP 302-306 °C.
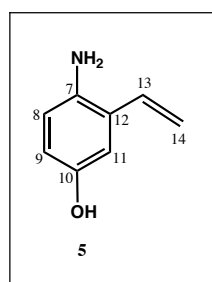
Figure 4.2: Structure of 4-Amino-3-vinylphenol **5**.

Synthesis of 4-Amino-3-vinylphenol 5. Tert-butyl 4-hydroxy-2-vinylphenylcarbamate **10** (50 mg, 0.21 mmol) was dissolved in dichloromethane / trifluoroacetic acid (9:1) (1.8:0.2 ml) and stirred at rt for 6h. Dichloromethane and trichloroacetic acid were evaporated under reduced pressure. Yellow crude solid was washed with diethyl ether and filtered to give lila solid (10 mg, 35%).
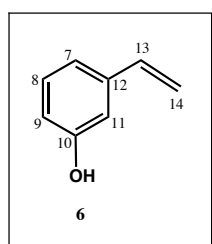
Figure 4.3: Structure of 3-vinylphenol **6**.

Synthesis of 3-vinylphenol 6. 3-Bromophenol (3 g, 17.3 mmol) was dissolved in dimethoxyethane. Tetrakistriphenylphosphine palladium (0.2 g, 0.017 mmol), potassium carbonate (4.77 g, 34.6 mmol), boric acid (1.38 g, 5.8 mmol) and water (15 ml) were added under N_2-atmosphere. The reaction mixture was stirred at reflux for 12 h, cooled and acidified with 2N HCl (100 ml). The mixture was extracted with diethyl ether (3 x 50 ml). The combined organic layers were dried over anhydrous $MgSO_4$ and concentrated under reduced pressure. The residue was purified by column chromatography on silica gel with petroleum ether / diethyl ether (10:1) resulting white-yellow oil (1.30 g, 63%).

^{1}**H-NMR** (500 MHz, MeOD) δ 7.11 (t, 1H, C^8), 6.86 (d, 1H, C^7), 6.85 (d, 1H, C^9), 6.68 (dd, 1H, C^{11}), 6.67-6.65 (dd, 1H, J=1.0, J=17.6 Hz, C^{13}), 5.70-5.67 (dd, 1H, J=1.2, J=17.4 Hz, C^{14}), 5.17-5.15 (dd, 1H, J=1.2, J=17.4 Hz, C^{14}) ppm.

^{13}**C-NMR** (125 MHz, MeOD) δ 155.61, 140.39, 138.24, 130.48, 118.85, 115.86, 113.77, 113.58 ppm.

EA C_8H_8O

Calculated: C: 79.97 H: 6.71. Found: C: 76.30 H: 6.77.
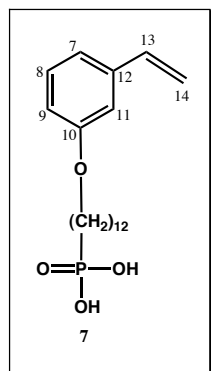
Figure 4.4: Structure of 12-(3-vinylphenoxy)dodecylphosphonic acid **7**.

Synthesis of 12-(3-vinylphenoxy)dodecylphosphonic-acid 7. 3-vinylphenol **6** (0.3 g, 2.5 mmol) was dissolved in EtOH (15 ml) and potassium carbonate (1.38 g, 10 mmol). The reaction mixture was heated to reflux and 12-iodododecylphosphonic acid was added. The reaction mixture was stirred at reflux for 12 h, cooled and acidified with 1N HCl (10 ml). The resulting mixture was extracted with diethyl ether (3 x 50 ml). The combined organic layers were dried over

anhydrous $MgSO_4$ and concentrated under reduced pressure. The yellow crude solid was dissolved in hexane (10 ml), dried over anhydrous $MgSO_4$ and concentrated under reduced pressure to give white powder (180 mg, 59%).

^{1}H-NMR (300 MHz, $CDCl_3$) δ 8.96 (bs, 2H, OH), 7.25 (t, 1H, C^8), 7.01 (d, 1H, C^7), 6.97 (d, 1H, C^{11}), 6.83 (dd, 1H, C^9), 6.76-6.66 (d, 1H, J=10.8, J=17.4 Hz, C^{13}), 5.79-5.73 (dd, 1H, J=17.4 Hz, C^{14}), 5.28-5.25 (d, 1H, J=10.8 Hz, C^{14}), 1.30 (m, 24H, CH_2) ppm.

^{13}C-NMR (75 MHz, $CDCl_3$) δ 159.4, 139, 136.9, 129.4, 118.7, 114.1, 112.2, 70.1, 67.9, 45.2, 32.7, 30.6, 30.4, 29.6, 29.4, 29.1, 26.9, 26.1, 22.1, 22.0 ppm.

EA $C_{20}H_{39}N_2O_4P$

Calculated: C: 65.20 H: 9.03. Found: C: 60.58 H: 9.22. The difference is due to the side product.

MP 73-76 °C.
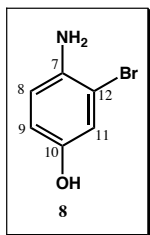
Figure 4.5: Structure of 4-Amino-3-bromo-phenol **8**.

Synthesis of 4-Amino-3-bromo-phenol 8.   (E)-4-((2-bromo-4 hydroxyphenyl) diazenyl)-benzenesulfonic acid **2a** (9.89 g, 0.027 mol) was suspended in H_2O (150 ml) and after 20 min. $Na_2S_2O_4$ [1,2,3] (4.82 g, 0.027 mol) was added. The orange color changed to light yellow. The reaction mixture was stirred at rt for 4 h after which diethyl ether (100 ml) was added. The mixture was extracted with diethyl ether (3 x 70 ml). The organic layers were washed with water, combined, dried over anhydrous $MgSO_4$ and concentrated under reduced pressure. 2.87 g (55%) beige solid.

^{1}H-NMR (300 MHz, D_2O-K_2CO_3) δ 6.75 (d, 1H, J=2.7 Hz, C^{11}) , 6.67 (d, 1H, J=8.7 Hz, C^8), 6.46 (dd, 1H, J_1=2.7 Hz, J_2=8.7 Hz, C^9) ppm.

^{13}C-NMR (75 MHz, D_2O-K_2CO_3) δ 155.3, 134.2, 120.2, 119.0, 118.0, 111.0 ppm.

EA $C_6H_6NO_4Br$

Calculated: C: 38.33 H: 3.22 N: 7.45 O: 8.51 Br: 42.50. Found: C: 38.28 H: 3.31 N: 7.44 O: 8.55 Br: 42.62.

MP 152-156 °C.
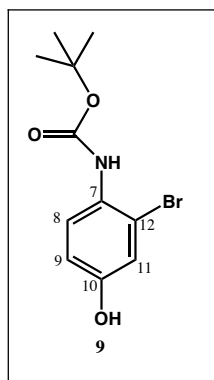
Figure 4.6: Structure of tert-butyl 2-bromo-4-hydroxyphenylcarbamate **9**.

Synthesis of tert-butyl 2-bromo-4-hydroxyphenylcarbamate 9. 4-Amino-3-bromo-phenol **8** (36 g, 0.19 mol) was dissolved in THF (100 ml) and di-tertbutyl-dicarbonate (45.92 g, 0.21 mol) [4] was added. The reaction mixture was stirred at rt for 12 h and concentrated under reduced pressure. Column chromatography of the crude product on silica gel with petroleum ether / acetone (4:1) gave tert-butyl-4-hydroxy-2-vinylphenylcarbamate **9** as a white solid (45.65 g, 83 %).

^{1}H-NMR (300 MHz, $CDCl_3$) δ 7.70 (d, 1H, J=9 Hz, C^8), 6.99 (d, 1H, J=2.7 Hz, C^{11}), 6.70 (dd, 1H, J_1=2.7 Hz, J_2=9 Hz, C_9), 6.63 (bs, 1H, OH), 1.53 (s, 9H, $(CH_3)_3$) ppm.

^{13}C-NMR (75 MHz, $CDCl_3$) δ 154.1, 153.3, 128.3, 124.3, 119.4, 116.3, 115.6, 81.4, 28.4 ppm.

EA $C_{11}H_{14}NO_3Br$

Calculated: C: 45.85 H: 4.90 N: 4.86 O: 16.66 Br: 27.73. Found: C: 45.93 H: 5.10 N: 4.77 O: 16.57 Br: 27.54.

MP 136-139 °C.
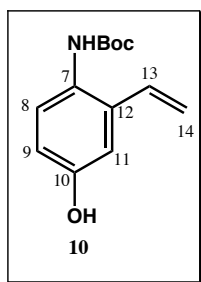
Figure 4.7: Structure of tert-butyl 4-hydroxy-2-vinylphenylcarbamate **10**.

Synthesis of tert-butyl 4-hydroxy-2-vinylphenylcarbamate 10. Tert-butyl 2-bromo-4-hydroxyphenylcarbamate **9** (20 g, 0.069 mol) was dissolved in DME (180 ml) and tetrakistriphenylphosphine palladium (0.8 g, 0.069 mmol), potassium carbonate (19.15 g, 0.139 mol), boric acid (5.55g, 0.023 mol) and water (60 ml) were added. The reaction mixture was stirred at reflux for 12 h, cooled and acidified with 2N HCl (150 ml). The mixture was extracted with diethyl ether (3 x 100 ml). The combined organic layers were dried over anhydrous $MgSO_4$ and concentrated under reduced pressure. The residue was purified by column chromatography on silica gel with petroleum ether / acetone (4:1) to give white-yellow solid (12.79 g, 79%).

^{1}H-NMR (300 MHz, $CDCl_3$) δ 7.25 (d, 1H, J=8.1 Hz, C^8), 6.84 (d, 1H, J=3, C^{11}), 6.81-6.72 (dd, 1H, J=11.2, J=17.4 Hz, C^{13}), 6.61 (dd, 1H, J=2.7, J=9.3 Hz, C^9), 6.17 (bs, 1H, OH), 5.64-5.58 (dd, 1H, J=1.2, J=17.4 Hz, C^{14}), 1.51 (s, 9H, $(CH_3)_3$) ppm.

^{13}C-NMR (75 MHz, $CDCl_3$) δ 154.3, 153.4, 133, 127.3, 126.1, 117.1, 116.2, 115.7, 112,8, 80.6, 28.4 ppm.

EA $C_{13}H_{17}NO$

Calculated: C: 66.36 H: 7.28 N: 5.95 O: 20.40. Found: C: 66.41 H: 7.34 N: 5.89 O: 20.34.

MP 149-153 °C.
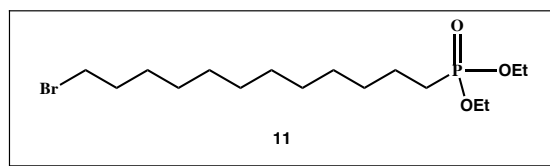
Figure 4.8: Structure of 12-bromododecylphosphonic acid-diethylester **11**.

Synthesis of 12-bromododecylphosphonic acid-diethylester 11. 1,12-dibromododecane (49.8 g, 0.152 mol) was heated to reflux and triethyl phosphite (25.21, 0.152 mol) was added drop-wise for 30 min. The yellow solution was stirred at 170 °C for 4 h. The crude product was purified by column chromatography on silica gel with petroleum ether / acetone (2:1) yielding **11** as a white oil (21.1 g, 36 %).

^{1}H-NMR (300 MHz, CDCl$_3$) δ 3.99 (m, 4H, CH$_2$), 3.31 (t, 2H, CH$_2$), 1.30-1.17 (m, 12H, CH$_2$) ppm.

^{13}C-NMR (75 MHz, CDCl$_3$) δ 61.3, 61.3, 33.9, 32.7, 30.8, 30.6, 30.4, 29.4, 29.3, 29.2, 28.9, 28.7, 28.1, 26.5, 24.6, 22.3, 22.2, 16.4, 16.3 ppm (Due to NMR active P).

EA C$_{16}$H$_{34}$O$_3$PBr

Calculated: C: 49.87 H: 8.89 O: 12.46 P: 8.04 Br: 20.74. Found: C: 49.99 H: 8.72 O: 12.57 P: 7.90 Br:20.17.

MP 136-140 °C.
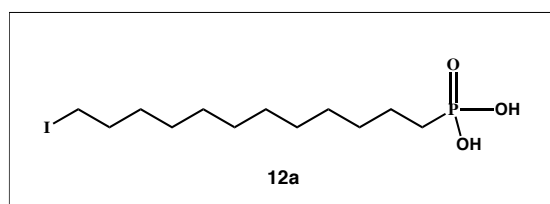
Figure 4.9: Structure of 12-iodododecylphosphonic acid **12a**.

Synthesis of 12-iodododecylphosphonic acid 12a. Potassium iodide (1.92 g, 11,5 mmol) was suspended in 12-bromododecylphosphonic acid-diethylester **11** (1.48 g, 3.84 mmol). Acetonitrile (3 ml) and trimethylchlorosilane (1.25 g, 11.5 mmol) were added under N$_2$-atmosphere to previous suspension and stirred over

night at reflux. Trimethylchlorosilane and acetonitrile were removed under reduced pressure. Recrystallization from chloroform and filtration of the product gave **12a** as a white powder (0.85 g, 60%)

^{1}H-NMR (300 MHz, CDCl$_3$) δ 7.38 (bs, 2H, OH), 3.21 (t, 2H, I-CH$_2$), 1.88-1.55 (m, 4H, CH$_2$), 1.38-1.28 (m, 20H, CH$_2$) ppm.

^{13}C-NMR (75 MHz, CDCl$_3$) δ 33.6, 30.5, 30.3, 30.1, 29.3, 29.2, 29.1, 28.9, 28.2, 27.6, 25.8, 25.2, 5.7 ppm (Due to NMR active P).

^{31}P-NMR (121 MHz, CDCl$_3$) δ 38.59 ppm.

EA C$_{12}$H$_{26}$O$_3$PI

Calculated: C: 38.31 H: 6.97 O: 12.76 P: 8.23 I: 33.73. Found: C: 39.35 H: 6.71.

MP 137-141 °C.
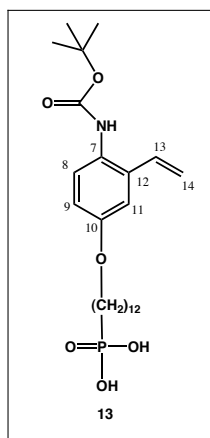
Figure 4.10: Structure of 12-(4-tert-butoxycarbonylamino)-3-vinylphenoxy)dodecylphosphonic acid **13**.

Synthesis of 12-(4-tert-butoxycarbonylamino)-3-vinylphenoxy) dodecylphosphonic acid 13. Potassium carbonate (0.47 g, 3.44 mmol), tert-butyl 4-hydroxy-2-vinylphenyl-carbamate **10** (0.2 g, 0.86 mmol) and EtOH (10 ml) were suspended, evacuated and heated to reflux (83 °C). 12-iodododecylphosphonic acid **12a** was added under N$_2$-atmosphere and stirred over night at reflux. The reaction mixture was acidified with 1N HCl (5 ml) and extracted with diethyl ether (3 x 100 ml). The combined organic layers were washed with H$_2$O, dried over anhydrous MgSO$_4$ and concentrated under reduced pressure. The yellow crude solid was dissolved in 10 ml diethyl ether and precipitated in hexane to give white solid **13** (0.24 g, 58 %).

^{1}**H-NMR** (300 MHz, CDCl$_3$) δ 7.50 (s, 1H, C^8), 6.96 (d, 1H, J=2.7, C^{11}), 6.85-6.76 (dd, 1H, J=11.2, J=18.6 Hz, C^{13}), 6.80 (dd, 1H, J=2.7, J=9.3 Hz, C^9), 6.17 (bs, 1H, NH), 5.69-5.64 (dd, 1H, J=1.2, J=18.6 Hz, C^{14}), 5.39-5.34 (dd, 1H, J=1.2, J=12 Hz, C^{14}) 4.06 (bs, 1H, OH), 3.91 (t, 2H, CH$_2$,) 1.50 (s, 9H, (CH$_3$)$_3$), 1.27-1.18 (s, 24H, CH$_2$) ppm.

^{13}**C-NMR** (75 MHz, CDCl$_3$) δ 68.3, 29.6, 29.4, 29.3, 29.1, 28.4, 26.0 ppm.

^{31}**P-NMR** (121 MHz, CDCl$_3$) δ 37.45 ppm.

EA C$_{29}$H$_{50}$NO$_6$P

Calculated: C: 64.54 H: 9.34 N: 2.60 O: 17.79. Found: C: 64.66 H: 9.45 N: 2.54 O: 17.85 P: 5.74.

MP: 83-86 °C.
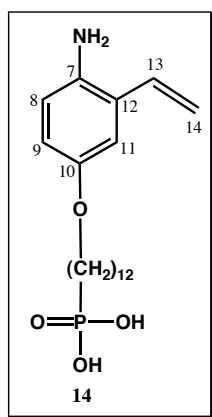
Figure 4.11: Structure of 12-(4-amino-3-vinylphenoxy)dodecylphosphonic acid **14**.

Synthesis of 12-(4-amino-3-vinylphenoxy)dodecylphosphonic acid 14. 12-(4-tert-butoxycarbonylamino)-3-vinylphenoxy)dodecylphosphonic acid **13** (0.1 g, 0.2 mmol) was dissolved in dichloromethane / trifloroacetic acid (6:1) (3:1 ml) and stirred at rt for 6h. Dichloromethane and trichloroacetic acid were evaporated under reduced pressure. Yellow crude solid was washed with diethyl ether and filtered which resulting yellow solid (74 mg, 94%).

^{1}**H-NMR** (300 MHz, CDCl$_3$) δ 6.69 (s, 1H, C^{11}), 6.76-6.67 (d, 1H, C^{13}), 6.76-6.67 (d, 1H, C^9), 5.58 (d, 1H, J=17.4 Hz, C^{14}), 5.53 (d, 1H, J=10.8 Hz, C^{14}), 3.90 (t, 2H, CH$_2$), 1.24-1.15 (m, 24H, CH$_2$) ppm.

^{13}**C-NMR** (75 MHz, CDCl$_3$) δ 161.0, 160.5, 159.4, 138.9, 136.9, 133.7, 129.4, 119.9, 118.6, 114.0, 112.1, 67.9, 31.9, 29.7, 29.7, 29.6, 29.6, 29.4, 29.4, 29.3 ppm.

^{31}**P-NMR** (121 MHz, CDCl$_3$) δ 23.98 ppm.

EA C$_{20}$H$_{34}$NO$_4$P

Calculated: C: 65.58 H: 9.63 N: 3.19 O: 14.56 P: 7.05. Found: C: 64.86 H: 10.23 N: 3.18 O: 14.83 P: 6.95.

MP: 143-148 °C.
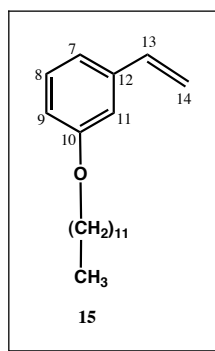
Figure 4.12: Structure of 1-(dodecyloxy)-3-vinylbenzene **15**.

Sythesis of 1-(dodecyloxy)-3-vinylbenzene 15. 3-vinylphenol **6** (0.74 g, 6.13 mmol) and KOH (1.37 g, 24.52 mmol) were dissolved in acetonitrile (8 ml). The solution was heated to reflux and 1-dodecylbromide was added. The mixture was stirred at reflux for 12 h, cooled and acidified with 2N HCl (10 ml). The reaction mixture was extracted with diethyl ether (4 x 50 ml). The combined organic phases were dried over MgSO$_4$, and the solvent was removed in vacuo. Chromatographic separation with silica gel as stationary phase and petroleum ether as mobile phase gave **15** as a yellow oil (998 mg, 57 %)

^{1}**H-NMR** (300 MHz, CDCl$_3$) δ 7.25 (d, 1H, C^{13}), 7.02 (d, 1H, C^7), 6.85 (dd, 1H, C^9), 6.78-6.67 (dd, 1H, C^8), 5.78 (d, 1H, C^{14}), 5.28 (d, 1H, C^{14}), 3.99 (t, 2H, CH$_2$), 1.83 (t, 2H, CH$_2$), 1.13 (s, 10H, CH$_2$), 0.93 (t, 2H, CH$_2$) ppm.

^{13}**C-NMR** (75 MHz, CDCl$_3$) δ 159.4, 138.9, 136.9, 129.4, 118.7, 113.9, 112.1, 67.9, 31.9, 29.7, 29.6, 29.3, 26.1, 22.7, 14.1 ppm.

EA C$_{20}$H$_{32}$O

Calculated: C: 83.27 H: 11.18 O: 5.55. Found: C: 83.42 H: 11.40 O: 5.53.
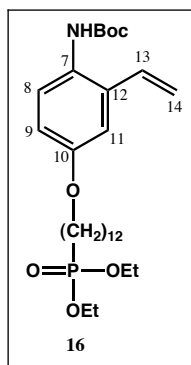
Figure 4.13: Structure of Tert-butyl-4-(12-(diethoxyphosphoryl)dodecyloxy)-2-vinylphenyl-carbamate **16**.

Synthesis of Tert-butyl 4-(12-(diethoxyphosphoryl)dodecyloxy)-2-vinylphenylcarbamate 16. Tert-butyl 4-hydroxy-2-vinylphenylcarbamate **10** (10.25 g, 0.044 mol) was dissolved in acetonitrile (150 ml) and potassium carbonate (24 g, 0.174 mol). The reaction mixture was heated to reflux and 12-bromododecylphosphonic acid-diethylester added. The reaction mixture was stirred at reflux for 12 h. The resulting reaction mixture was cooled, diethyl ether added, and filtered through celite. The filtrate was concentrated under reduced pressure. The residue was purified by column chromotography on silica gel with petroleum ether / acetone / toluene (2:1:1) gave yellow oil (21.97 g, 93%).

^{1}**H-NMR** (300 MHz, CDCl$_3$) δ 7.18 (m, 1H, J=7.5, J=17.4 Hz, C^{13}), 6.95 (d, 1H, J=3, C^8), 6.85-6.75 (dd, 1H, J=3, J=6 Hz, C^{11}), 6.8 (d, 1H, J=6 Hz, C^9), 6.21 (bs, 1H, NH), 5.68-5.63 (dd, 1H, J=1.2, J=17.4 Hz, C^{14}), 5.41-5.37 (dd, 1H, J=10.8, J=17.4 Hz, C^{14}), 4.1-4.02 (m, 4H, CH$_2$), 3.93 (t, 2H, J=6, CH$_2$), 1.49 (s, 9H, (CH$_3$)$_3$), 1.31-1.27 (m, 24H, CH$_2$) ppm.

^{13}**C-NMR** (75 MHz, CDCl$_3$) δ 156.2, 153.7, 132.3, 127.9, 124.8, 117.1, 115.0, 114.8, 114.5, 112.1, 80.2, 68.3, 30.7, 30.5, 29.5, 29.4, 29.3, 29.1, 28.3, 26.0, 25.1, 22.4, 22.3, 16.5, 16.4 ppm.

^{31}**P-NMR** (121 MHz, CDCl$_3$) δ 32.8 ppm.

EA C$_{29}$H$_{50}$NOP

Calculated: C: 64.54 H: 9.34 N: 2.60 O: 17.79 P: 5.74. Found: C: 64.66 H: 9.38 N: 2.61 O: 17.76 P: 5.77.
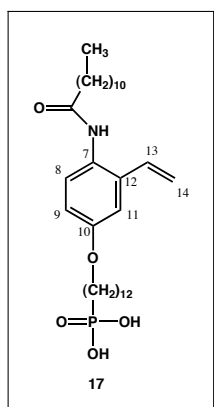
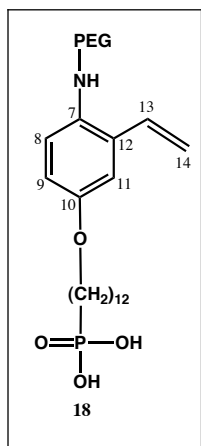*Figure 4.14:* Structure of 12-(4-dodecanamido-3-vinylphenoxy)dodecylphosphonic acid **17**.

Synthesis of 12-(4-dodecanamido-3-vinylphenoxy)dodecylphsophonic acid 17. 12-(4-amino-3-vinylphenoxy)dodecylphosphonic acid **14** and 2,5-dioxopyrrolidin1-yl were dissolved in DMSO in the presence of triethylamine and stirred over night at rt. The yellow solution was acidified with 2M HCl (5 ml) and resulting precipitation filtered. (97 mg, 69%)

^{1}H-NMR (300 MHz, DMSO-d6) δ 10,15 (bs , 1H, NH), 6.69 (m, 1H, C^8), 6.86 (s, 1H, C^{11}), 6.87-6.78 (q, 1H, C^{13}), 6.63 (d, 1H, C^9) 5.60 (d, 1H, J= 1.5, J=17.4 Hz, C^{14}), 5.14 (d, 1H, J=1.5, J=11.1 Hz, C^{14}), 3.85 (t, 2H, CH$_2$), 1.23-1.15 (m, 24H, CH$_2$) ppm.

^{13}C-NMR (75 MHz, DMSO-d6) δ 150.6, 132.6, 122.5, 117.1, 116.0, 113.1, 111.0, 67.8, 30.1, 29.9, 28.9, 28.8, 28.7, 28.6, 28.1, 27.0, 25.5, 22.7 ppm.

^{31}P-NMR (121 MHz, DMSO-d6) δ 26.70 ppm.

MP: 153-155 °C.

Figure 4.15: Structure of 12-(4-PEG-ethanamido)-3-vinylphenoxy)dodecylphosphonicacid **18**.

Synthesis of 12-(4-PEG-ethanamido)-3-vinylphenoxy) dodecylphosphonic acid 18. Diethyl-12-(4-PEG-ethanamido)-3-vinylphenoxy) dodecylphosphonate **23** was dissolved in dichloromethane and trimethylbromosilane was added. The reaction mixture was stirred at RT for 48 h. The solution was concentrated under reduced pressure. The white crude product was suspended in MeOH / H_2O (95:5) for 12 h. The white suspension was concentrated under reduced pressure. The crude product was purified by dialysis in deionized water (48 h) and lyophilization (48 h, at -50°C and 0.2 mbar) gave **18** as a white powder (105 mg, 53 %).

^{1}H-NMR (500 MHz, CDCl$_3$) δ 9.59 (s, 1H, NH), 8.07 (d, 1H, J=5.4, C[8]), 7.03 (d, 1H, J=3, C[11]), 6.83-6.77 (dd, 4H, J=7, C[9]), 6.69 (s, 1H, J=1.2, C[13]), 4.13 (s, 2H, CH$_2$), 3.72-3.64 (m, CH$_2$), 3.36 (t, 3H, CH$_3$), 1.73 (m, 9H, CH$_2$), 1.37-1.22 (m, 12H, CH$_2$) ppm.

^{13}C-NMR (125 MHz, Benzene-d6) δ 167.51, 155.44, 139.21, 128,5, 119.99, 68.05, 61.05, 39.16, 30.93, 30.24, 28.62, 28.43, 27.01, 25.89, 23.07 ppm.

^{31}P-NMR (202 MHz, DMSO-d6) δ 28.20 ppm.

EA $C_{109}H_{210}NO_{49}P$

Calculated: C: 55.72 H: 9.01 N: 0.60 O: 33.36 P: 1.32 (n=43). Found: C: 53.73 H: 8.97 N: 0.83 O: 33.11 P: 1.57.

MP: 46-49 °C.
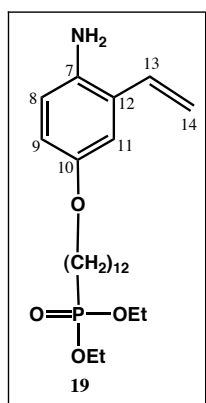
Figure 4.16: Structure of 4-(12-(diethoxyphosphoryl)dodecyloxy)-2-vinylbenzenaminium **19**.

Synthesis of diethyl 12-(4-amino-3-vinylphenoxy)dodecylphosphonate 19. Tert-butyl 4-(12-(diethoxyphosphoryl)dodecyloxy)-2-vinylphenylcarbamate **16** (0.5g, 0.93 mmol) was dissolved in a mixture of dichloromethane / trifloro acetic acid (18:3 v:v). The reaction mixture was stirred at RT for 12 h. The suspension was concentrated under reduced pressure to give a brown oil (0.62 g, 93%)

^{1}**H-NMR** (300 MHz, CDCl$_3$) δ 10.77 (bs, 3H, NH), 7.25 (d, 1H, J=2.7, C^8), 7.05 (d, 1H, J=2.7, C^{11}), 6.88-6.84 (dd, 1H, J=2.7, J=3 Hz, C^9), 6.83-6.76 (dd, 1H, J=11.2, J=17.4 Hz, C^{13}), 5.66-5.60 (dd, 1H, J=1.5, J=17.4 Hz, C^{14}), 5.33-5.29 (dd, 1H, J=11.2, J=17.4 Hz, C^{14}), 4.16-4.1 (m, 4H, CH$_2$), 4.02-3.98 (t, 2H, J=6, CH$_2$), 1.84-1.75 (m, 4H, CH$_2$), 1.39-1.29 (m, 24H, CH$_2$) ppm.

^{13}**C-NMR** (75 MHz, CDCl$_3$) δ 161, 160.5, 159.5, 133.7, 129.7, 124.7, 121.1, 120, 119.9, 117.3, 115.5, 114.6, 113.5, 113.1, 112.5, 68.3, 62.5, 62.4, 30.5, 30.3, 29.5, 29.4, 29.3, 29.2, 29.1, 29, 26, 25.8, 24.1, 22, 22.9, 16.3, 16.2 ppm.

^{31}**P-NMR** (121 MHz, CDCl$_3$) δ 34.3 ppm.

EA C$_{24}$H$_{42}$NO$_4$P

Calculated: C: 65.58 H: 9.63 N: 3.19 O: 14.56 P: 7.05. Found: C: 64.90 H: 10.23 N: 3.15 O: 14.83 P: 6.98.
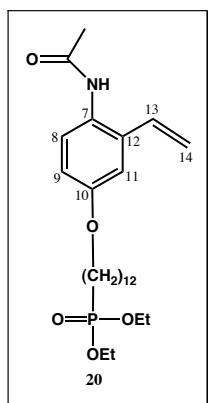
Figure 4.17: Structure of diethyl 12-(4-acetamido-3-vinylphenoxy)dodecylphosphonate **20**.

Synthesis of Diethyl-12-(4-acetamido-3-vinylphenoxy) dodecylphosphonate 20. Diethyl 12-(4-amino-3-vinylphenoxy)dodecylphosphonate **19** (0.4g, 0.93 mmol) was dissolved in dichloromethane (2 ml) and acetic anhyride (0.095 g, 0.93 mmol) and triethyl amine (0.376 g, 3.72 mmol) were added. The reaction mixture was stirred at rt for 12 h. The solution was concentrated under reduced pressure. The residue was purified by column chromotography on silica gel with petroleum ether / acetone (1:1) to give a white solid (0.34 g, 76%).

[1]**H-NMR** (300 MHz, CDCl$_3$) δ 7.54 (d, 1H, J=8.7, C[8]), 7.01 (d, 1H, J=2.7, C[11]), 6.88-6.84 (dd, 1H, J=2.7, J=3 Hz, C[9]), 6.85-6.76 (m, 1H, C[13]), 5.73-5.67 (dd, 1H, J=0.6, J=17.1 Hz, C[14]), 5.69-5.53 (dd, 1H, J=0.6, J=10.6 Hz, C[14]), 4.20-4.04 (m, 4H, CH$_2$), 3.99-3.93 (t, 2H, J=6.6, CH$_2$), 2.24 (s, 3H, CH$_3$) 1.84-1.75 (m, 4H, CH$_2$), 1.39-1.29 (m, 24H, CH$_2$) ppm.

[13]**C-NMR** (75 MHz, CDCl$_3$) δ 168.83, 158.78, 157.09, 133.06, 132.32, 131.89, 129.79, 127.28, 126.65, 117.07, 114.75, 114.49, 111.95, 111.45, 68.27, 668.16, 61.36, 61.31, 30.64, 30.57, 30.50, 29.45, 29.43, 29.32, 29.22, 29.18, 29.05, 26.19, 25.98, 25.92, 23.81, 22.37, 22.33, 20.59, 17.54, 16.54, 16.41.

[31]**P-NMR** (121 MHz, CDCl$_3$) δ 32.86 ppm

EA C$_{26}$H$_{44}$NO$_5$P

Calculated: C: 64.84 H: 9.21 N: 2.91 O: 16.61 P: 6.43. Found: C: 64.90 H: 9.36 N: 2.96 O: 16.59 P: 6.45.

MP 68-71 °C
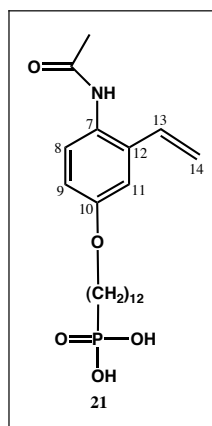
Figure 4.18: Structure of 12-(4-acetamido-3-vinylphenoxy)dodecylphosphonic acid **21**.

Synthesis of 12-(4-acetamido-3-vinylphenoxy)dodecylphosphonic acid 21. Hydrogen-12-(4-ammonio-3-vinylphenoxy)dodecylphosphonate **22** (0.4 g, 1.04 mmol) was dissolved in dimethyl sulfoxide (5 ml) and acetic anydride (0.1 g, 1.04 mmol) and triethyl amine (0.42 g, 4.16 mmol) were added. The reaction mixture was stirred at rt for 24 h and 2N HCl (10 ml) was added. The resulting precipitate was filtered and dried under reduced pressure. The residue was dissolved in 1,2-dimethoxyethane (3 ml) and precipitated from petroleum ether. Filtration afforded 12-(4-acetamido-3-vinylphenoxy)dodecylphosphonic acid **22** beige solid (162 mg, 37 %).

[1]**H-NMR** (300 MHz, DMSO-d6) δ 7.17 (s, 1H, NH), 7.2 (d, 1H, J=9, C[8]), 7.12 (d, 1H, J=3 C[11]), 6.86.6.82 (dd, 1H, J=3 J=9 Hz, C[9]), 6.85-6.76 (m, 1H, J=11.1, J=17.4 C[13]), 5.84-5.78 (dd, 1H, J=11.1, J=17.4 Hz, C[14]), 5.35-5.28 (dd, 1H, J=1.2, J=11.1 Hz, C[14]), 3.90-3.88 (t, 2H, J=6, CH$_2$), 2.02 (s, 3H, CH$_3$), 1.46-1.23 (m, 24H, CH$_2$) ppm.

[13]**C-NMR** (75 MHz, DMSO-d6) δ 169.1, 156.96, 133.76, 132.88, 128.71, 128.63, 116.06, 114.91, 114.82, 110.55, 68.04, 30.64, 30.43, 29.47, 29.35, 29.17, 28.93, 27.13, 25.98, 23.43, 23.23. 23.17 ppm.

[31]**P-NMR** (121 MHz, DMSO-d6) δ 26.77 ppm.

[1]**H-NMR** (500 MHz, MeOD δ 7.17(d, 1H, J=9, C[8]), 7.11 (d, 1H, J=3 C[11]), 6.87-6.86 (dd, 1H, J=2.8 J=6.9 Hz, C[9]), 6.86-6.79 (m, 1H, J=17.53, J=11,1 C[13]), 5.77-5.73 (dd, 1H, J=1, J=17.47 Hz, C[14]), 5.40-5.30 (dd, 1H, J=1, J=11 Hz, C[14]), 4-3.98 (t, 2H, J=6.4, CH$_2$), 2.14 (s, 3H, CH$_3$), 1.38-1.30 (m, 24H, CH$_2$) ppm.
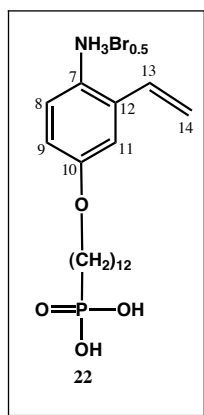
^{13}**C-NMR** (125 MHz, MeOD) δ 172.78, 159.27, 136.06, 133.66, 129.49, 128.59, 116.21, 115.68, 111.97, 69.24, 31.85, 31.72, 30.68, 30.54, 30.48, 30.39, 30.31, 28.65, 27.55, 27.15, 23.92, 22.79 ppm.

^{31}**P-NMR** (202 MHz, MeOD) δ 31.49 ppm..

EA $C_{22}H_{35}NO_5P$

Calculated: C: 62.25 H: 8.31 N: 3.30 O: 18.85 P: 7.30. Found: C: 61.71 H: 8.63 N: 3.30 O: 18.85 P: 7.20.

MP 96-100 °C.

Figure 4.19: Structure of Hydrogen-12-(4-ammonio-3-vinylphenoxy)dodecylphosphonate **22**.

Synthesis of Hydrogen-12-(4-ammonio-3-vinylphenoxy)dodecyl phosphonate 22. Tert-butyl 4-(12-(diethoxyphosphoryl)dodecyloxy)-2-vinylphenyl carbamate **16** (1 g, 1.85 mmol) was dissolved in dichloromethane (1 ml) and trimethylbromosilane was added. The reaction mixture was stirred at RT for 48 h. The solution was concentrated under reduced pressure. The crude brown product was suspended in MeOH / H_2O (95:5) for 12 h. The white suspension was concentrated under reduced pressure to give white solid (0.62 g, 89 %).

^{1}**H-NMR** (300 MHz, DMSO-d6) δ 6.99 (d, 1H, J=2.7, C^8), 6.87-6.78 (m, 1H, J=3.9, J=17.4 C^{13}), 6.84 (d, 1H, J=8.7 Hz, C^{11}), 6.76-6.72 (m, 1H, J=2.7, J=17.4, C^9), 5.77-5.70 (dd, 1H, J=0.9, J=17.1 Hz, C^{14}), 5.32-5.25 (dd, 1H, J=0.9, J=2.7 Hz, C^{14}), 3.91-3.86 (t, 2H, J=6, CH$_2$), 1.46-1.23 (m, 24H, CH$_2$) ppm.

^{13}**C-NMR** (75 MHz, CDCl$_3$) δ 158.4, 132.7, 130.1, 124.9, 121.5, 118.8, 115.4, 115.1, 114.6, 111.7, 67.8, 30.1, 29.9, 28.9, 28.8, 28.6, 28.5, 27.9, 26.9 25.4, 22.7, 22.6 ppm.
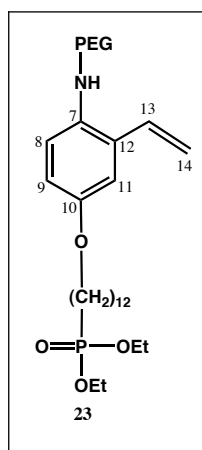
^{31}**P-NMR** (121 MHz, DMSO-d6) δ 26.64 ppm.

EA C$_{40}$H$_{70}$N$_2$O$_8$P$_2$Br

Calculated C: 56.60 H: 8.31 N: 3.30 O: 15.08 P: 7.30 Br: 9.41. Found: C: 56.78 H: 8.32 N: 3.25 O: 15.32 P: 7.31 Br: 9.60.

MP 148-155 °C.

4.3.2   Synthesis of Polymer and Copolymer

Figure 4.20: Structure of Diethyl-12-(4-PEG-ethanamido)-3-vinylphenoxy)dodecylphosphonate **23**.

Synthesis of Diethyl-12-(4-PEG-ethanamido)-3-vinylphenoxy)dodecyl phosphonate 23. Polyethylene glycol 2000 monomethyl ether (50 g, 25 mmol) was dissolved in KOH (35 g, 625 mmol,) then KMnO$_4$ (15.8 g, 100 mmol) was added drop-wise for 30 min. at rt and stirred 4 h at rt. The reaction mixture was filtered through Celite and 37% HCl (50 ml) was added. The colorless solution was concentrated under reduced pressure and extracted with CHCl$_3$ (300, 200, 100 ml), filtered and concentrated under reduced pressure which gave a white solid (46.35 g, 93 %). Recrystallization from CHCl$_3$ / Et$_2$O and filtration of the product at rt gave MPEG-COOH as a white solid (26.8 g, 63 %). MPEG-COOH (1 g, 0.5 mmol) was

dissolved in dichloromethane and oxayl chloride was added. After 12 h stirring at rt oxaly chloride and dichloromethane were evaporated under reduced pressure. **19** (219 mg, 0.5 mmol) was dissolved in dichloromethane and TEA was added. PEG-COCl was dissolved in dichloromethane and added to the previous reaction mixture. The resulting solution was stirred for 12 h at rt. Dicholoromethane and TEA were evaporated under reduced pressure. The crude product was purified by dialysis in deionized water (48 h) and lyophilization (48 h, at -50°C and 0.2 mbar) to give **23** yellow solid (1012 mg, 84 %).

MPEG-COOH: ^{1}**H-NMR** (300 MHz, CDCl$_3$) δ 4.13 (d, 2H, J=6, CH$_2$), 3.63-3.62 (m, CH$_2$), 3.32 (t, 3H, CH$_3$) ppm.

^{13}**C-NMR** (75 MHz, CDCl$_3$) δ 72.0, 71.8, 70.54, 68.90, 58.90 ppm.

EA C$_{89}$H$_{178}$O$_{46}$

Calculated: C: 53.87 H: 9.04 O: 37.09. Found: C: 53.51 H: 9.03 O: 37.27.

Diethyl-12-(4-PEG-ethanamido)-3-vinylphenoxy)dodecyl phosphonate 23: ^{1}**H-NMR** (300 MHz, CDCl$_3$) δ 8.56 (s, 1H, NH), 7.59 (d, 1H, J=9, C^8), 7.03 (d, 1H, J=3 C^{11}), 6.88-6.82 (dd, 1H, J=6 J=9 Hz, C^9), 6.87-6.74 (m, 1H, J=1.2, J=17.4 C^{13}), 5.74-5.68 (dd, 1H, J=1.2, J=17.4 Hz, C^{14}), 5.41-5.35 (dd, 1H, J=1.2, J=11.2 Hz, C^{14}), 4.17 (s, 2H, CH$_2$), 3.70-3.62 (m, CH$_2$), 3.39 (t, 3H, CH$_3$), 1.38-1.31 (m, 9H, CH$_2$), 1.29 (s, 6H, CH$_2$) ppm.
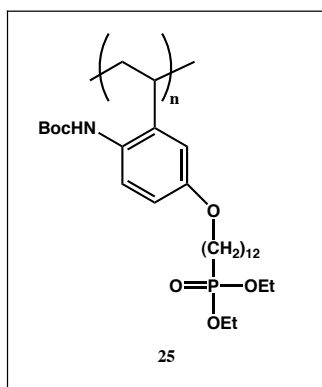
^{13}**C-NMR** (75 MHz, CDCl$_3$) δ 168.50, 157.05, 132.76, 132.11, 126.73, 126.07, 116.92, 114.50, 111.90, 71.89, 71.32, 70.75, 70.66, 70.64, 70.62, 70.60, 70.56, 70.52, 70.48, 70.23, 68.21, 61.35, 61.30, 58.98, 30.50, 29.51, 29.35, 29.33, 29.25, 29.05, 25.99, 16.46, 16.41 ppm.

^{31}**P-NMR** (121 MHz, CDCl$_3$) δ 32.78 ppm.

EA C$_{113}$H$_{218}$NO$_{49}$P

Calculated: C: 56.41 H: 9.13 N: 0.58 O: 37.09 P: 1.29 (n=43). Found: C: 56.25 H: 9.10 N: 0.72 O: 32.66 P: 1.48.

GPC M$_w$: 3.220, PD: 1.11

Figure 4.21: Structure of Poly-diethyl-12-(4-(3,3-dimethylbutanamido)-3-ethylphenoxy) dodecylphosphonate **25**.

Synthesis of Poly-diethyl-12-(4-(3,3-dimethylbutanamido)-3-ethylphenoxy) dodecylphosphonate 25. Tert-butyl 4-(12-(diethoxyphosphoryl) dodecyloxy) 2-vinylphenyl carbamate **16** (1 g, 1.86 mmol) was dissolved in benzene (1 ml) and AIBN was added. The reaction mixture was evacuated, degassed and stirred over night at 85 °C. Benzene was evaporated under reduced pressure. (0.75 g, 75%).

^{1}H-NMR (500 MHz, DMSO-d6) δ 7.62 (dd, 1H, Ar-H), 7.41 (br, 1H, NH), 6.92 (dd, 1H, Ar-H), 6.81 (d, 1H, Ar-H), 4.01-3.90 (br, 6H, CH$_2$), 1.7-1.62 (br, CH$_2$), 1.40-1.31 (br, CH$_2$) ppm.
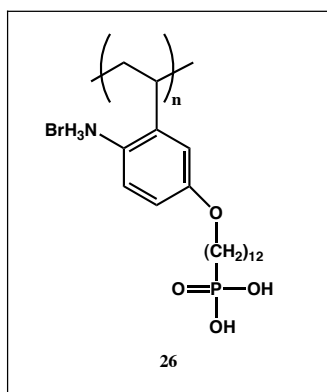
^{13}C-NMR (125 MHz, DMSO-d6) δ 166.94, 158.22, 131.69, 128.62, 124.26, 115.39, 67.76, 29.25, 25.37, 22.72, 13.85, 10.77 ppm.

^{31}P-NMR (121 MHz, DMSO-d6) δ 32.95 ppm.

EA C$_{30}$H$_{54}$NO$_6$P

Calculated: C: 64.84 H: 9.79 N: 2.52 O: 17.79 P: 5.74. Found: C: 63.40 H: 9.18 N: 2.73 O: 17.90 P: 5.77.

GPC M$_w$: 132.417, PD: 2.77

Figure 4.22: Structure of Poly-2-ethyl-4-(12-phosphonododecyloxy)benzenaminium bromide **26**.

Synthesis of Poly-2-ethyl-4-(12-phosphono dodecyloxy) benzenaminiumbromide 26 Diethyl-12-(4-(3,3-dimethyl butanamido)-3-ethylphenoxy) dodecylphosphonate **25** (0.294 g, 0.55 mmol) was dissolved in dichlormethane (1ml) and evacuated. Trimethylbromosilane (0.17 ml, 1.1 mmol) was added under N_2-atmosphere and stirred over night at rt. Dichloromethane and excess trimethylbromosilane was evaporated under reduced pressure. The resulting orange crude solid was dissolved in MeOH / H_2O (95:5) for 12 h. The pink suspension was concentrated under reduced pressure to give white solid (0.24 g, 57 %).
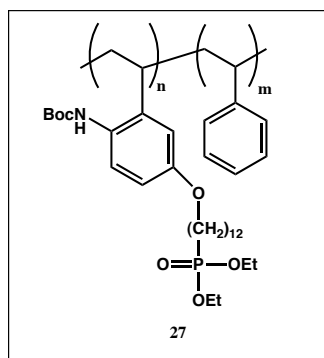
^{1}H-NMR (300 MHz, Benzene-d6) δ 7.90-7.60 (bs, 1H, NH), 7.20 (br, 2H, Ar-H), 6.98-6.79 (dd, 1H, Ar-H), 6.78 (br, 4H, Ar-H), 4.1 (br, 4H, CH$_2$), 4.04 (br, 2H, CH$_2$),1.80 (br, 8H, CH$_2$), 1.57 (br, 12H, CH$_2$), 1.39 (br, 16H, CH$_2$) ppm.

^{13}C-NMR (125 MHz, CDCl$_3$) δ 127.89, 125.65, 114.85, 112.10, 68.31, 61.31, 30.69, 30.56, 29.63, 29.33, 29.13, 28.33, 26.25, 26.11, 25.13, 22.42, 22.38, ppm.

^{31}P-NMR (121 MHz, Benzene-d6) δ 31.99 ppm.

EA $C_{40}H_{70}N_2O_8P_2Br$

Calculated: C: 56.60 H: 8.31 N: 3.30. Found: C: 57.71 H: 8.38 N: 3.35.

Figure 4.23: Structure of poly-(tert-butyl 4-(12-(diethoxyphosphoryl)dodecyloxy)-2-ethylphenylcarbamate-co-styrene) **27**.

Synthesis of poly-(tert-butyl 4-(12-(diethoxyphosphoryl)dodecyloxy) 2-ethylphenylcarbamate-co-styrene) 27. Tert-butyl 4-(12 (diethoxyphosphoryl) dodecyloxy) 2-vinylphenyl-carbamate **16** (0.5 g, 0.93 mmol) and styrene (0.19 g, 1.86 mmol) were dissolved in benzene (0.5 ml) and AIBN was added. The reaction mixture was stirred over night at 85 °C. The resulting yellow gel was precipitated in hexane at 0 °C and filtered. (0.37 g, 61%).

[1]**H-NMR** (300 MHz, DMSO-d6) δ 7.25-7.03 (br, 4H, Ar-H), 6.80-6.39 (br, 4H, Ar-H), 3.76 (br, 2H, CH_2), 1.49 (br, 2H, CH_2), 1.26 (br, 4H, CH_2), 1.19 (br, 12H, CH_2) ppm.
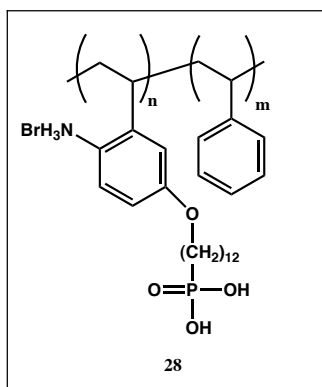
[13]**C-NMR** (75 MHz, DMSO-d6) δ 128.7, 100.0, 68.2, 29.60, 23.2, 23.1 ppm.

[31]**P-NMR** (121 MHz, DMSO-d6) δ 27.82 ppm.

EA $C_{37}H_{58}NO_6P$ (n/m=1)

Calculated: C: 69.02 H: 9.08 N: 2.18. Found: C: 70.59 H: 9.01 N: 2.15.

GPC M_w: 54.619, PD: 2.59

Figure 4.24: Structure of poly(2-isopropyl-4-(12-phosphonododecyloxy)benzenaminium bromide-co-styrene))phenylcarbamate **28**.

Synthesis of poly (2-isopropyl-4-(12-phosphonododecyloxy)benzen aminium bromide-co-styrene) 28. Poly-(tert-butyl 4-(12-(diethoxy phosphoryl) dodecyloxy)-2-ethylphenylcarbamate-co-styrene) **27** (0.37 g, 0.37 mmol) was dissolved in dichlormethane (1ml). Trimethybromosilane (0.12 ml, 0.89 mmol) was added under N_2-atmosphere and stirred over night at rt. Dichloromethane and excess trimethylbromosilane was evaporated under reduced pressure. The resulting orange crude solid was dissolved in MeOH / H_2O (95:5) for 12 h. The pink suspension was concentrated under reduced pressure to give white solid (0.2 g, 95 %).
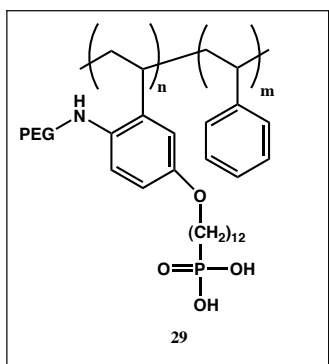
^{1}**H-NMR** (300 MHz, DMSO-d6) δ 7.30 (br, 24H, Ar-H), 6.55 (br, 20H, Ar-H), 3.76 (br, 6H, CH_2), 1.25 (br, CH_2), 1.23 (br, CH_2) ppm.

^{13}**C-NMR** (75 MHz, DMSO-d6) δ 128.7, 127.7, 100, 68.2, 29.6, 23.2, 23.1 ppm.

^{31}**P-NMR** (121 MHz, DMSO-d6) δ 28.02 ppm.

EA $C_{28}H_{42}NO_4PBr_{0.5}$

Calculated: C: 63.75 H: 8.02 N: 2.65 O: 12.13 P: 5.87 Br: 7.57. Found: C: 63.95 H: 7.85 N: 2.44.

Figure 4.25: Structure of poly-hydrogen-12-(4-ammonio-3-(4-phenylbutan-2-yl)phenoxy) dodecylphosphonate **29**.

Synthesis of poly-PEG-(2-isopropyl-4-(12-phosphonododecyloxy)-benzenaminium bromide-co-styrene) 29. Poly(2-isopropyl-4-(12-phosphono dodecyloxy)benzenaminium bromide-co-styrene) **28** (20 mg, 0.037 mmol) and PEG-NHS-5000 (0.037 mmol, 184 mg) were dissolved in DMSO (4 ml) and TEA was added. The crude product was purified by dialysis in deionized water (48 h) and lyophilization (48 h, at -50°C and 0.2 mbar) gave **29** white solid (188 mg, 92 %).

^{1}**H-NMR** (300 MHz, DMSO-d6) δ 7.15-7.04 (br, 4H, Ar-H), 6.68-6.34 (br, 4H, Ar-H), 4.02 (s, 2H, CH$_2$), 3.75 (m, 2H, CH$_2$), 3.52 (br, CH$_2$), 3.44 (br, CH$_2$), 1.25 (br, CH$_2$), 1.23 (br, CH$_2$) ppm.
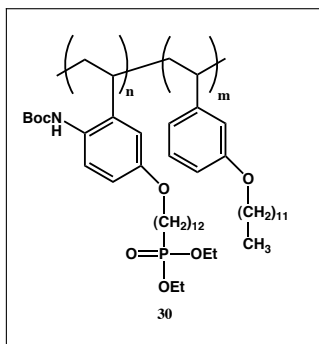
^{13}**C-NMR** (75 MHz, DMSO-d6) δ 171.62, 72.31, 71.25, 70.08, 69.76, 69.56, 67.62, 60.19, 58.02 ppm.

^{31}**P-NMR** (121 MHz, DMSO-d6) δ 9.88 ppm.

EA C$_{277}$H$_{540}$NO$_{129}$P

Calculated: C: 55.63 H: 9.10 N: 0.23. Found: C: 55.50 H: 9.08 N: 0.42.

Figure 4.26: Structure of poly-(tert-butyl 4-(12-(diethoxyphosphoryl)dodecyloxy)-2-ethylphenylcarbamate-co-1-(dodecyloxy) 3 ethylbenzene **30**.

Synthesis of poly-(tert-butyl 4-(12-(diethoxyphosphoryl)dodecyloxy)-2-ethylphenylcarbamate-co-1-(dodecyloxy)-3-ethyl benzene 30. 1-(dodecyloxy) 3-vinylbenzene **15** (0.21 g, 0.74 mmol), tert-butyl-4-(12-(diethoxy phosphoryl) dodecyloxy)-2-vinylphenyl-carbamate **16** (0.2 g, 0.37 mmol) and AIBN were dissolved in benzene. The mixture was stirred over night at 85 °C. The resulting solution was precipitated in MeOH / H_2O (4:1) at 0 °C and filtered which gave poly-(tert-butyl 4-(12-(diethoxyphosphoryl)dodecyloxy)-2-ethylphenylcarbamate-co-1-(dodecyloxy)-3-ethylbenzene **30** as sticky gel (204 mg, 50%).

^{1}H-NMR (300 MHz, Benzol-d6) δ 7.54 (s, 1H, Ar-H), 7.22 (s, 1H, Ar-H), 7.18 (s, 1H, Ar-H), 7.01(s, 1H, Ar-H), 6.90 (br, Ar-H), 6.53 (br, Ar-H), 4.12 (m, 4H, CH_2), 3.77 (t, CH_2), 1.84 (br, 3H, CH_2), 1.65 (br, 3H, CH_2), 1.50 (br, 12H, CH_2) ppm.
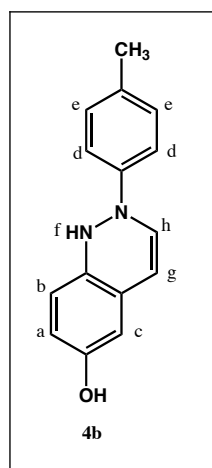
^{13}C-NMR (75 MHz, Benzol-d6) δ ppm.

^{31}P-NMR (121 MHz, Benzol-d6) δ 31.92 ppm.

EA $C_{49}H_{87}NO_7P$ (n/m=1)

Calculated: C: 70.64 H: 10.52 N: 1.68. Found: C: 73.58 H: 10.32 N: 1.14.

4.3.3 Cinnolines

**Figure 4.27:** Structure of 2-p-tolyl-1,2-dihydrocinnolin-6-ol

Synthesis of 2-p-tolyl-1,2-dihydrocinnolin-6-ol

(E)-3-bromo-4-(p-tolyldiazenyl)phenol **2b** (1.5 g, 5.2 mmol) was dissolved in DME (25 ml) and tetrakistriphenylphosphine palladium (59 mg, 0.052 mmol), potassium carbonate (1.42 g, 10.3 mmol), boric acid (410 mg, 1.72 mmol) and water (7 ml) were added. The reaction mixture was stirred at reflux for 12 h, cooled and acidified with 2N HCl (20 ml). The mixture was extracted with diethyl ether (3 x 50 ml). The combined organic layers were dried over anhydrous $MgSO_4$ and concentrated under reduced pressure. (0.51 g, 42%).

^{1}H-NMR (300 MHz, CDCl$_3$) δ 7.93 (d, 1H, J=7.5, C^c), 7.70 (d, 1H, J=9.6, C^b), 7.57 (d, 2H, J=8.1,C^d), 7.35 (d, 2H, J=8.1, C^e), 7.22 (dd, 1H, J=2.4 J=9.9, C^a), 7.16 (d, 1H, J=7.5, C^h), 6.33 (d, 1H, J=2.4, C^g), 3.45 (s, CH$_3$) ppm.

^{13}C-NMR (75 MHz, CDCl$_3$) δ 141.53, 132,48, 130.89, 122.03, 108.74, 21.21, 17.57 ppm.

MP 232-238 °C.
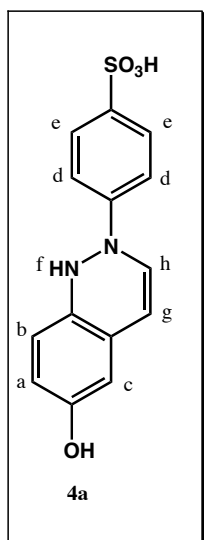
Figure 4.28: Synthesis of 4-(6-hydroxycinnolin-2(1H)-yl)benzenesulfonic-acid

Synthesis of 4-(6-hydroxycinnolin-2(1H)-yl)benzenesulfonic-acid

(E)-4-((2-bromo-4-hydroxyphenyl)diazenyl)benzenesulfonic acid **2a** (0.5 g, 1.4 mmol) was dissolved in DME (3 ml) and tetrakistriphenylphosphine palladium (16 mg, 0.014 mmol), potassium carbonate (386 mg, 2.8 mmol), boric acid (112 mg, 0.47 mmol) and water (3 ml) were added. The reaction mixture was stirred at reflux for 12 h, cooled and acidified with 2N HCl (5 ml). The mixture was extracted with diethyl ether (3 x 20 ml). The combined organic layers were dried over anhydrous $MgSO_4$ and concentrated under reduced pressure. The residue was purified by column chromatography on silica gel with MeOH / ethylacetate (1:2) to give white-yellow solid (353 mg, 90%).

^{1}H-NMR (500 MHz, K_2CO_3-D_2O) δ 8.70 (d, 1H, J=6.6, C^c), 8.01 (d, 2H, J=7.2, C^d), 7.97 (d, 2H, J=6.3,C^e), 7.95 (d, 1H, C^b), 7.79 (d, 1H, J=6.3, C^a), 7.31 (d, 1H, J=9.3, C^h), 6.65 (s, 1H, C^g) ppm.

^{13}C-NMR (125 MHz, K_2CO_3-D_2O) δ 167.73, 145.68, 143.97, 136.45, 133.41, 133.35, 127.85, 122.94, 1211.69, 109.14ppm.

MP > 400 °C.

Summary and Outlook

5.1 Summary

The aim of the present work was to accomplish a synthetic contribution for the self-assembly of monomeric and polymeric phosphonates. A modular synthetic concept had to be developed, which includes the synthesis of the head group, the center piece and the tail group. The head group binds to the substrate surface. The center piece has three important groups: the hydroxyl group which couples to the head group, the vinyl group will be the polymerizable group and the amino group can be selectively coupled to the end-functionalized terminating groups. A set of alkyl phosphonates for self-assembly were synthesized with the new synthetic strategy. According to the data measured by NMR and elemental analysis, the purities of **14** and **21** were very high. By polymerization and solvolysis of compound **16** we obtained poly-2-ethyl-4-(12-phosphonododecyloxy)benzenaminium bromide **26**. Copolymerization of **16** with styrene gave poly-(2-isopropyl-4-(12-phosphonododecyloxy)benzenaminium bromide-co-styrene) **28**. After self-assembly of the compounds we determined that for longer self-assembly time the phosphonate density is also larger, while the surface-bound water or hydroxyl groups become increasingly replaced.

Alkyl phosphonates have been shown to adsorb onto titanium oxide (TiO_2) surfaces forming a monolayer with direct, coordinative complexation of the phosphonate head-group onto titanium oxide surface. This direct coordination is believed to be one of the reasons for the stability of the phosphonate adlayer on TiO_2 surfaces.

Alkyl phosphonates are able to build up spontaneously organized monomolecular layers on titanium oxide surfaces. The coverage of the surface is completed within 16 hours, whereas the final organization of the films needs more than 48 hours. These molecular films play an important role in altering surface properties, including stability and wettability, even when the films are very thin on a molecular dimension. On the other hand, organized assemblies of organic species formed on solid surfaces exhibit unique functions controlled by the interaction between the adsorbed species and the solid surfaces.

Two methods were attempted to distinguish polymerization on the surface. The first method was the comparison of bulk monomer and polymer by PM-IRRAS. Two thick films of polymerized **21** and monomeric **21** were compared by PM-IRRAS. Unfortunately, the band from vinyl group at 1602 cm^{-1} is overlapped by strong aromatic bands which makes it very difficult to use this technique as a test method for polymerization of **21**. The second method was the comparison of the SAMs thickness of **21** after UV- irradiation and pH 9 treatment. The large decrease in film thickness for all the samples showed that we were probably not polymerizing on the surface. Whereas polymer self-assembly with **28** at the same conditions (pH 9) had a higher stability of polymer on the surface due to multisite attachment.

5.2   Outlook

A set of monomers and polymers as carriers for further functionalization is now accessible. The next step could be the investigation of application areas. Further investigation should lead to a better understanding of the influence that minor changes in surface order have on adlayer properties such as resistance to recontamination or stability on contact with solutions of different compositions.

One open question in this thesis is if other possibilities for polymerization can be studied and developed. Due to lack of knowledge of polymer behavior on the surface. The polymers we have worked on have molecular of weight 50000.

One of the most interesting aspects of research in biomaterials lies in the development of biosensing devices (biosensors). Titanium has been considered as the metallic biomaterials of choice, a field where is a need to control surface modifications of the oxide layer. Another active research used is the field of bone implants.

The interaction between the metal surface of the biomaterial and the newly formed bone tissue is known to be critical for the success of the implant settings.

Although there are many different approaches to self-assembly being carried out at present, everybody currently working in the field seems to agree on how useful self-assembling systems can be. The ultimate goals would surely be systems approaching the same complexity as living ones. But even in the near future there could be many applications forthcoming i.e. self-healing materials, self-assembling circuits or self-replicating nano-devices.

Acknowledgements

Maybe the best part of my thesis is the fact that I had the possibility to meet a lot of interesting people from different scientific, cultural and personal backgrounds, who have been around me during my PhD and supported me in achieving my goals by whatever means they could.

This work would not have been possible without the help and support of many people. It is my pleasure to express my gratitude to all the people who supported me during my PhD.

Firstly, I would like to thank Prof. Dr. Nicholas D. Spencer for having me in his group, giving me the oppurtunity to perform this thesis and for giving me the chance to go to conferences in Switzerland and abroad. He has created a truly unique environment for doing a doctorate. The way he is able to bring out the best of each student or colleague by giving him or her all the freedom, advice and support they need, while accepting the differences of each individual without judging them I have never experienced before. It is his truly humane and kind style of management which has influenced the whole atmosphere in the group where everybody is always trying to help each other, enjoy working together and share a common high standard of scientific quality. So I want to finally thank him again for the trust he gave me in fulfilling an interesting and interdisciplinary thesis.

Professor Marcus Textor I thank for the oppurtinity to work in the surface group, his remarks, interest and support in my work.

Dr. Stefan Zürcher has been a constant help, thanks to positive attitude, critical and motivating discussions and continous interest in my work including the correction of the thesis.

Thank you to Dr. Samuele Tosatti for supervision and helping me in surface part of my work.

This thesis could not have been defended here without Prof. Dieter Schlüter, who accepted being a co-examiner and Prof. Walter Steurer representing the department of materials.

All the members of our lab, LSST, are thanked very highly for sharing great time together, enabling to work in a helpful and comfortable environment. Being part of the LSST family was a great pleasure. Being afraid of forgetting someone, I will not mention any names.

Personal computer support was kindly provided by Tomas Bartos. LaTeX support was performed mainly by Martin Halter and Christian Brunner. Brigitta de Chapeaurouge coordinated the administrative issues. Thanks to all.

Sara Morgenthaler, my office mate for answering every kind of questions that I have asked to her over the last four years.

Hakan Atasoy and Edis Kasemi. The combination of friendship and corporate scientific intelligence did produce some very fruitful results.

Also I would like to thank volleynight players for reaching to quarter finals last december.

I further had help from external labs. GPC-analysis were performed by Martin Colussi, while Doris Sutter measured ^{13}C-NMR. Martin Elsener did great jobs with his machine which I gratefully acknowledge. I also want to thank Dr. Ömer Kut for supporting me during my PhD.

Josephine Baer gets a great thank you and a hug as well for helping me out with paperwork, for infinite patience and support during my writing.

Finally I want to thank my family Hatice Durmaz, Ismet Durmaz and Pinar Durmaz, for their care, support and love from childhood until know. Tesekkürler

Personal

Name:	Firat Durmaz
Date of Birth:	April 6, 1974
Nationality:	Turkish
Present Address:	Bucheggstr. 119
	CH-8057 Zürich
	Switzerland

Education and Practical Experience

2003 – 2006	Doctoral student at the Laboratory for Surface Science and Technology, Department of Materials, Swiss Federal Institute of Technology (ETH) Zürich. "A Modular Approach to Functional Self-assembled Monolayers".
2002	Diploma in Materials Science at Polymer Chemistry, Department of Materials, Swiss Federal Institute of Technology (ETH) Zürich "Synthese und Charakterisierung neuer Blockcopolymere auf der Basis von Polyethylenglykol".
1999-2002	Studies of Chemistry at Swiss Federal Institute of Technology (ETH) Zürich. Graduation with the degree of Dipl. Chemiker ETH
1993-1996	Bosphorus University Istanbul, Turkey

1986-1993   Secondary- and highschool education Kültür College, Turkey

Presentations and Publications

Presentations

2005 230th American Chemical Society (ACS) National Meeting (poster presentation)
F. Durmaz, S. Zürcher, N. D. Spencer
ACS, August 2005, Washington, USA

2005   Nanoscale Surface Self-Assembly (poster presentation)
F. Durmaz, S. Zürcher, N. D. Spencer
EUCHEMS conference, June 2005, Sigtuna, Sweden

2004   Interfaces, Chemistry (poster presentation)
F. Durmaz, S. Zürcher, N. D. Spencer
Gordon conference, August 2004, Meriden NH, USA

2004   Polymer Sciences in Switzerland (poster presentation)
F. Durmaz, S. Zürcher, N. D. Spencer
Polymer Group of Switzerland (PGS), November 2004, Zürich, Switzerland

2003   Functional Polymeric Surfaces in Biotechnology (poster presentation)
F. Durmaz, S. Zürcher, N. D. Spencer
Biosurf V, September 2003, Zürich, Switzerland

Publications

D. Spori, **F. Durmaz**, S. G. P. Tosatti, V. Nagaiyanallur, N. D. Spencer, S. Zürcher, *Study of the Chain-Length Dependence of Self-Assembled Alkyl Phosphates on Titanium Oxide. Using XPS, VASE, PM-IRRAS and CA.*(will be submitted for publication)